Forecasting the Impact of Storm Waves and Sea-Level Rise on Midway Atoll and Laysan Island within the Papahānaumokuākea Marine National Monument—A Comparison of Passive Versus Dynamic Inundation Models

Open-File Report 2013–1069

U.S. Department of the Interior
U.S. Geological Survey

FRONT COVER: Photograph showing the impact of a large wave on the south shore of Laysan Island, with endangered Laysan teal in the foreground (USGS photograph by M. Reynolds).

Forecasting the Impact of Storm Waves and Sea-Level Rise on Midway Atoll and Laysan Island within the Papahānaumokuākea Marine National Monument—A Comparison of Passive Versus Dynamic Inundation Models

By Curt D. Storlazzi, Paul Berkowitz, Michelle H. Reynolds, and Joshua B. Logan

Open-File Report 2013–1069

U.S. Department of the Interior
U.S. Geological Survey

U.S. Department of the Interior
KEN SALAZAR, Secretary

U.S. Geological Survey
Suzette M. Kimball, Acting Director

U.S. Geological Survey, Reston, Virginia: 2013

For more information on the USGS—the Federal source for science about the Earth, its natural and living resources, natural hazards, and the environment—visit *http://www.usgs.gov* or call 1–888–ASK–USGS

For an overview of USGS information products, including maps, imagery, and publications, visit *http://www.usgs.gov/pubprod*

Suggested citation:
Storlazzi, C.D., Berkowitz, P., Reynolds, M.H., and Logan, J.B., 2013, Forecasting the impact of storm waves and sea-level rise on Midway Atoll and Laysan Island within the Papahānaumokuākea Marine National Monument—a comparison of passive versus dynamic inundation models: U.S. Geological Survey Open-File Report 2013-1069, 78 p.

Contents

Figures

Tables

Appendixes

This page intentionally left blank

Forecasting the Impact of Storm Waves and Sea-Level Rise on Midway Atoll and Laysan Island within the Papahānaumokuākea Marine National Monument—A Comparison of Passive Versus Dynamic Inundation Models

By Curt D. Storlazzi[1] Paul Berkowitz[2], Michelle H. Reynolds[3], and Joshua B. Logan[1]

Abstract

Two inundation events in 2011 underscored the potential for elevated water levels to damage infrastructure and affect terrestrial ecosystems on the low-lying Northwestern Hawaiian Islands in the Papahānaumokuākea Marine National Monument. The goal of this study was to compare passive "bathtub" inundation models based on geographic information systems (GIS) to those that include dynamic water levels caused by wave-induced set-up and run-up for two end-member island morphologies: Midway, a classic atoll with islands on the shallow (2–8 m) atoll rim and a deep, central lagoon; and Laysan, which is characterized by a deep (20–30 m) atoll rim and an island at the center of the atoll. Vulnerability to elevated water levels was assessed using hindcast wind and wave data to drive coupled physics-based numerical wave, current, and water-level models for the atolls. The resulting model data were then used to compute run-up elevations using a parametric run-up equation under both present conditions and future sea-level-rise scenarios. In both geomorphologies, wave heights and wavelengths adjacent to the island shorelines increased more than three times and four times, respectively, with increasing values of sea-level rise, as more deep-water wave energy could propagate over the atoll rim and larger wind-driven waves could develop on the atoll. Although these increases in water depth resulted in decreased set-up along the islands' shorelines, the larger wave heights and longer wavelengths due to sea-level rise increased the resulting wave-induced run-up. Run-up values were spatially heterogeneous and dependent on the direction of incident wave direction, bathymetry, and island configuration. Island inundation was modeled to increase substantially when wave-driven effects were included, suggesting that inundation and impacts to infrastructure and terrestrial habitats will occur at lower values of predicted sea-level rise, and thus sooner in the 21st century, than suggested by passive GIS-based "bathtub" inundation models. Lastly, observations and the modeling results suggest that classic atolls with islands on a shallow atoll rim are more susceptible to the combined effects of sea-level rise and wave-driven inundation than atolls characterized by a deep atoll rim.

[1] U.S. Geological Survey, Pacific Coastal and Marine Science Center, 400 Natural Bridges Drive, Santa Cruz, CA 95060, USA
[2] Hawaii Cooperative Studies Unit, University of Hawaii at Hilo, Hawaii National Park, HI 96718, USA
[3] U.S. Geological Survey, Pacific Island Ecosystems Research Center, PO Box 44, Hawaii National Park, HI 96718, USA

Introduction

A number of recent studies (Grinsted and others, 2009; Jevrejeva and others, 2009; Merrifield and others, 2009; Milne and others 2009) suggest that not only is global sea-level rise (SLR) occurring and accelerating in response to global climate change, but that rapid, meter-scale SLR due to ice sheet collapse has occurred in the past (Blanchon and others, 2009). Furthermore, syntheses by Grinsted and others (2009) and Nicholls and Cazenave (2010) suggest that global mean sea level in 2100 may exceed the average projection by the Intergovernmental Panel on Climate Change (2007) of approximately 60 cm above 2000 levels, with some studies suggesting extreme (although less likely) rises as high as 200 cm in that time frame (Vermeer and Rahmstorf, 2009; Pfeffer and others, 2008; Rahmstorf, 2007). Beyond the year 2100, or perhaps sooner according to some scientists, rapid collapses of the Greenland and West Antarctic ice sheets could lead to a SLR of many meters (Overpeck and others, 2006). Although coral reefs can accrete into the accommodation space provided by sea-level rise over geologic time scales, published vertical reef-flat accretion rates for exposed fringing reefs (1–4 mm/yr; see Buddemeier and Smith, 1988; Montaggioni, 2005) are as much as an order of magnitude smaller than the rates of SLR projected for the years 2000–2100 (8–16 mm/yr; see Grinsted and others, 2009; Nicholls and Cazenave, 2010). It is therefore likely that projected SLR will outpace potential new vertical reef-flat accretion, resulting in a net increase in water depth over exposed reef flats on the order of 0.5–2.0 m during the 21st century.

Satellite observations from 1993 to 2010 (Leuliette, 2012) show global SLR occurring at almost double the rate cited in the Intergovernmental Panel on Climate Change (2007) report, and above-average rates have been observed in the Northwestern Hawaiian Islands (fig. 1). Rising sea levels have the potential to exacerbate the impacts of storms and wave action on coastlines and coral reefs by reducing wave-energy dissipation, primarily by reducing wave breaking at the reef crest and increasing the water depth relative to hydrodynamic roughness over the reef flat (see, for example, Storlazzi and others, 2011). By reducing wave-energy dissipation at the reef crest and over the reef flat, SLR will cause larger waves to directly affect the coastline and potentially drive coastal erosion. These larger waves at the shoreline increase the potential for marine inundation that can extend inland considerable distances. The maximum vertical extent of wave-driven inundation is primarily a function of the wave height, wavelength, and coastal slope. Because storm wave heights and wavelengths vary in time and space, and coral reefs are spatially heterogeneous, wave- and SLR-induced inundation will vary spatially and temporally. This variation is particularly large for Pacific Ocean islands and atolls that are exposed to waves in excess of 5 m high numerous times each year (U.S. Army Corps of Engineers, 2011). On low-lying atolls that typify much of the central and western Pacific Islands, a small rise in sea level may cause large horizontal migrations of the shoreline, impacts to terrestrial infrastructure, loss of critical terrestrial nesting and foraging habitat, or even complete inundation of the atoll islands.

Although there have been a number of efforts to investigate how reefs may respond to SLR (for example, Ogston and Field, 2010; Field and others, 2011; Storlazzi and others, 2011), there has been little information presented on how infrastructure and natural resources of atoll islands may be affected by changes in sea level. Studies to date that describe SLR threats to atolls (for example, Baker and others, 2006; Krause and others, 2012) have generally used passive inundation models to simulate flooding of the islands (fig. 2). These passive models, often referred to as “bathtub” models, do not project the cumulative effects of SLR and storm-driven

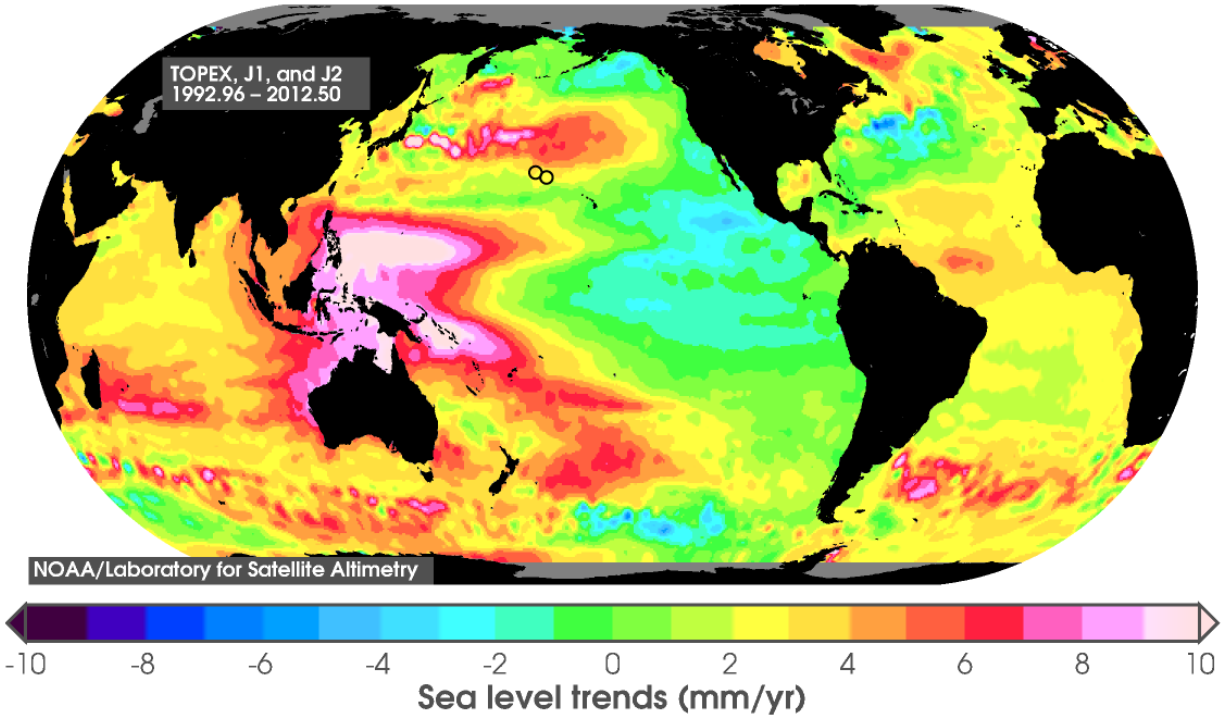

Figure 1. Map showing observed trends in sea level between 1993 and 2010 (Leuliette, 2012). Note the high rates (>5 millimeters per year, displayed in reds and pinks) observed in the central and western North Pacific Ocean, near the northwest end of Papahānaumokuākea Marine National Monument. The locations of Midway and Laysan are denoted with black circles.

waves on the adjacent terrestrial landforms, infrastructure, and natural resources. Although passive inundation represents an important element of SLR, islands are likely to be affected by a broader, more complex, and interrelated set of processes, including the following: loss of land due to erosion; island migration, breaching, and segmentation; wetland drowning, accretion, or migration; saltwater intrusion; and increased frequency of storm flooding (Gesch and others, 2009). The unique characteristics of a particular location affect the relative importance of each of these processes. More comprehensive modeling techniques that consider sediment transport, morphological changes to the island, currents, stratified and density-driven flows, and salt-water intrusion require additional data, including substrate analyses, grain size, current measurements, and detailed hydrodynamic roughness (Deltares, 2012).

This study explores the combined effect of SLR and storm-induced wave events for Laysan Island and Midway Atoll's Sand, Spit, and Eastern Islands within the Northwestern Hawaiian Islands. Wave and water-level model simulations under the present conditions and four SLR scenarios were used to map inundation and provide estimates of potential impacts to infrastructure and natural resources. These dynamic SLR model estimates that include wave-driven set-up and run-up are compared to passive SLR estimates to understand the relative importance of these processes on inundation and impacts to terrestrial habitats on Laysan Island and Midway Atoll's Sand, Spit, and Eastern Islands. By providing information on the range of forcing parameters (for example, SLR scenario, wave climate) that may threaten habitats, wildlife, and infrastructure, this study will help managers to prepare for possible climate-change scenarios and extreme weather events.

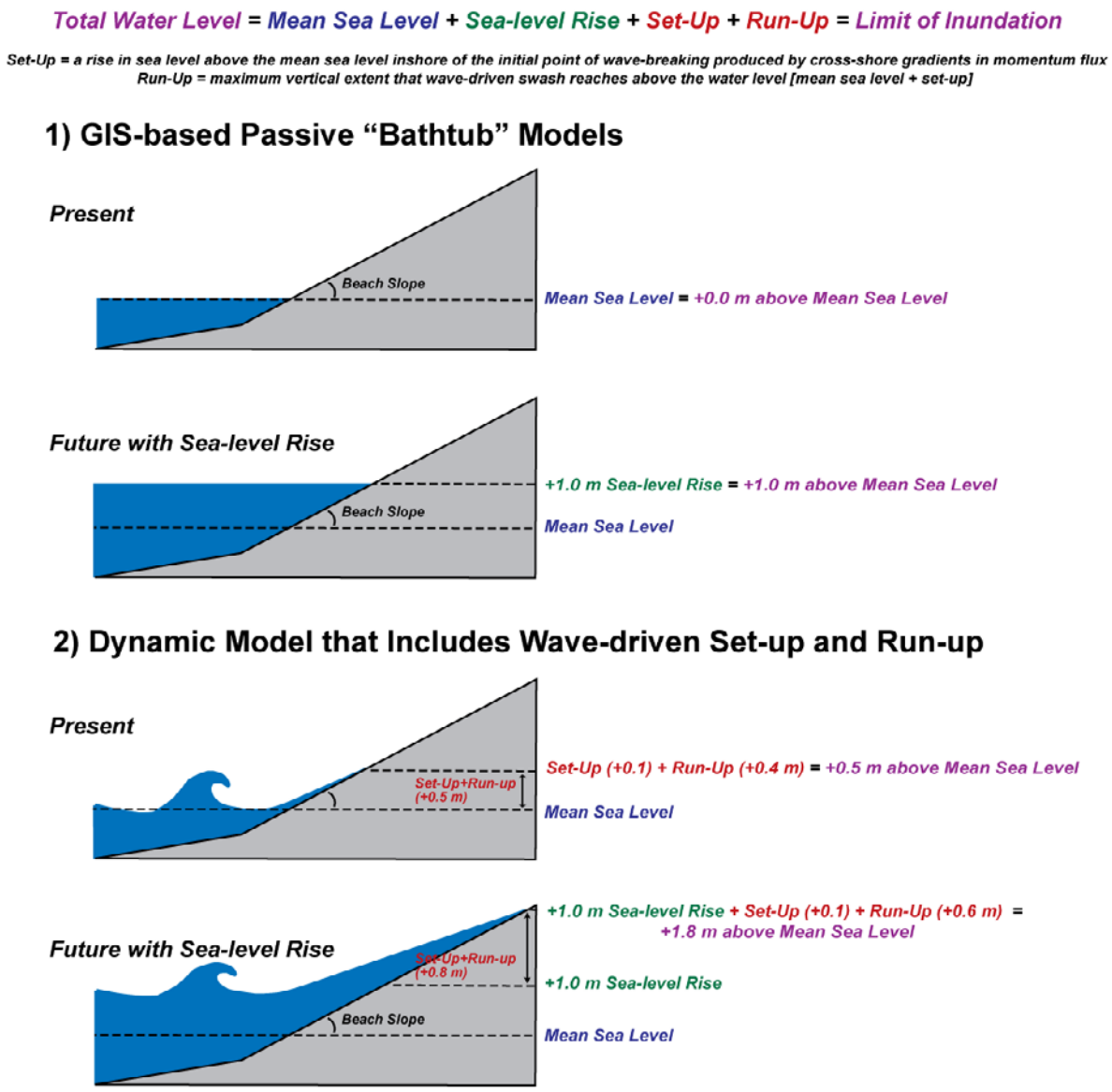

Figure 2. Schematic diagram comparing passive inundation models (also known as "bathtub" models; top panel) with dynamic wave-driven inundation models that incorporate wave-driven water levels (bottom panel). Most SLR models employ passive inundation modeling techniques, while the dynamic inundation model presented here includes wave-driven water levels.

Study Area

Laysan Island and Midway Atoll's Sand, Spit, and Eastern Islands are part of the Northwestern Hawaiian Islands (NWHI) and lie in the Papahānaumokuākea Marine National Monument (PMNM). PMNM is the largest conservation area in the United States and incorporates small islands, atolls, submerged banks, and reefs (fig. 3). The diverse ecosystems of the NWHI support 21 breeding seabirds and 17 terrestrial breeding species listed as endangered, threatened, or species of concern by the U.S. Fish and Wildlife Service, State of Hawaii, or International Union for Conservation of Nature (Krause and others, 2012).

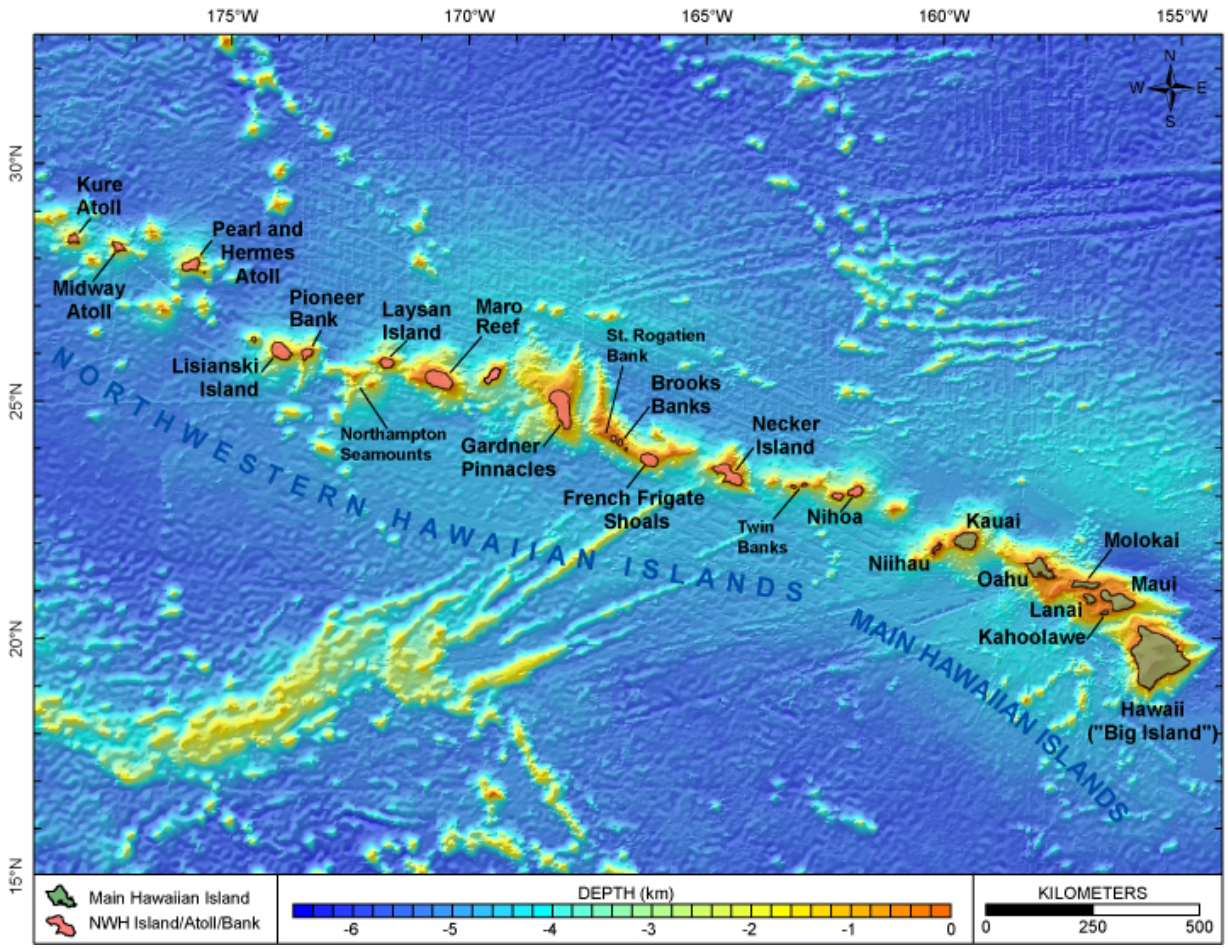

Figure 3. Map of the Northwestern Hawaiian Islands (NWH) in the Papahānaumokuākea Marine National Monument. Midway Atoll at the northwestern end of the island chain is located between Kure and Pearl and Hermes Atolls; Laysan is in the middle of the Northwestern Hawaiian Islands between the Northhampton Seamounts and Maro Reef. Image from the Pacific Islands Benthic Habitat Mapping Center (2011). The location where the U.S. Army Corps of Engineers' Wave Information System (2011) wave hindcast data were generated (28°00'N, 174°00'W) would be under the second "e" in the label for "Hermes Atoll."

Midway (28˚11–16' N and 177˚18–25' W) is a coral atoll situated between Kure Atoll to the west-northwest and Pearl and Hermes Atoll to the east-southeast. Midway Atoll comprises three islands: Sand (mean and maximum elevations = 3.2 m and 11.7 m, respectively), Spit (mean and maximum elevations = 1.5 m and 2.4 m, respectively), and Eastern (mean and maximum elevations = 2.6 m and 7.5 m, respectively). Sand and Eastern Islands have been significantly altered by human activity since the early 1900s (McDermond and Morgan, 1993). Under the jurisdiction of the United States since 1903, Midway has been occupied since the Commercial Pacific Cable Company began constructing cable houses and residences (Bryan, 1938). As a national defense facility, the islands experienced significant development, including seawalls, a harbor, piers, runways and other paved surfaces, dredge and fill operations, species introductions, and numerous buildings constructed from the 1930s to 1990s. In 1993 the Midway

Naval Air Station was decommissioned, and in 1996 jurisdiction over Midway was transferred to the U.S. Department of Interior as a National Wildlife Refuge (Speulda-Drews, 2010).

Laysan Island (25˚41–54' N and 171˚36–53 W) is situated between Lisianski Island to the west-northwest and Maro Reef to the east-southeast. Laysan is the second largest land mass in the Northwestern Hawaiian Islands and has mean and maximum elevations of 3.9 m and 10.4 m, respectively. Laysan lies approximately 1,600 km northwest of Honolulu and 700 km southeast of Midway Atoll. Laysan contrasts sharply with the lower lying open and closed atolls in the region, having substantially more emergent land (412.0 hectares [ha], including the hypersaline lake basin) than most islands within the monument, the largest natural lake in the Hawaiian Islands, and less lagoon/insular shelf habitat (approximately 57 km^2 of habitat less than 100 m water depth) than any nearby island or atoll. Guano miners in the early 1900s introduced rabbits and other mammals to Laysan Island, devastating the flora and fauna (Olson, 1996). Laysan has been protected as a bird reserve since 1909, introduced mammals have been extirpated, and the island has no infrastructure besides a small field camp.

Methods

The potential impact of SLR and inundation from ocean surface gravity waves (wind waves and swell) on Laysan Island and Midway Atoll's Sand, Spit, and Eastern Islands were investigated quantitatively using a suite of physics-based, numerical wave and water-level models driven by historical hindcast data and projected values of SLR.

Oceanographic and Meteorological Forcing Data

There are a very large number of potential combinations of storm sources, so deep-water storm waves generated by specific storms were not modeled in this study. Rather, a number of simulations of varying wave height and wave period were developed around the primary wave sources for the area (North Pacific swell, trade-wind waves, and South Pacific swell). There is a lack of wave buoys with long records for the areas of interest. Accordingly, hourly U.S. Army Corps of Engineers' Wave Information System (2011) model hindcast wind and wave data from 1981 to 2004 for a location (28°00'N, 174°00'W) approximately 330 km east of Midway and 375 km northwest of Laysan were used. These data sets were analyzed for end-member (top 5 percent) storm conditions based on the 24 years of available Wave Information System (WIS) hourly hindcast data, using methodology presented by Storlazzi and Wingfield (2005) and Storlazzi and Reid (2010). The top 5 percent of monthly data was chosen because it represents those conditions exceeded 36 hours per month and most likely to coincide with a high tide and thus be representative of maximum water-level conditions that would be experienced in a given year. These different sets of conditions constrained the combinations of deep-water wave heights, wave periods, and wave directions above which possible damage to infrastructure and natural resources may occur under historical wind and wave forcing conditions. Existing forecasts of how the wind and wave climate in the study areas of the northern Pacific Ocean may be affected by climate change (Caires and others, 2006; Mori and others, 2010) are not in firm agreement on the seasonality and magnitude of the resulting change. Because of such lack of agreement, this study does not take into account any possible future change in the wind and wave climate. Because of the large range of conditions and SLR scenarios, the data presented here are constrained to the two end-members: North Pacific winter conditions and summer conditions (which include the time periods when the islands are exposed to trade-wind waves and South Pacific swell). The conditions that typified the spring and fall seasons fell between these two end-members.

Wave and Water-Level Models

The WIS hindcast deep-water ocean surface gravity waves (wind waves and swell) and winds were used as boundary conditions to drive simulations of storm waves and water levels at Sand, Spit, Eastern, and Laysan Islands using the Deltares Delft3D hydrodynamic model. Delft3D simulates currents and water levels via the Delft3D-FLOW module, which is coupled to the third-generation SWAN wave model using the Delft3D-WAVE module. The SWAN model is based on discrete spectral action balance equations, computing the evolution of random, short-crested waves (Holthuijsen and others, 1993; Booij and others, 1999; Ris and others, 1999). Physical processes such as bottom friction and depth-induced breaking, and nonlinear quadruplet and triad wave-wave interactions are included. Wave propagation, growth, and decay from deep-water sources and in situ wind-wave growth are solved periodically throughout the model grid. The SWAN model has been shown to accurately model the propagation and breaking of waves over Pacific coral reefs (Lowe and others, 2009; Hoeke and others, 2011; Storlazzi and others, 2011). The results of the SWAN wave simulations, such as significant wave height (H_s), peak spectral period (T_p), mean wave direction (θ_{wave}), wind speed (U_w), mean wind direction (θ_{wind}), and mass fluxes (wave-driven water levels such as set-up, the additional elevation of the water level due to the effects of transferring wave-related momentum to the surf zone) are stored on the grid, with the wave-driven water levels coupled between the SWAN model and Delft3D-FLOW module, thus providing updated water levels over which to compute the updated wave fields.

Most of the standard Delft3D model settings were used. The SWAN model space had a frequency range of 0.05–1.00 Hz in 24 frequency bins over 36 (10°) directional bins. Processes incorporated in the model included radiation stress forcing, wave set-up, depth-induced breaking using the Battjes and Janssen (1978) formulation ($\alpha = 1.0$, $\gamma = 0.78$), nonlinear triad interactions, wind-wave growth, and whitecapping using the Komen and others (1984) formulation. Wave propagation in spectral space included both refraction and frequency shift. Based on the results presented in Hoeke and others (2011), a wave hydraulic roughness length scale of 0.1 m was used for the entire model domains in the Madsen and others (1988) formulation for bottom friction. The Delft3D-FLOW module that was coupled with the SWAN wave model was run with open water-level boundaries with a reflection parameter of 0 s^2 and the boundaries defined by astronomic forcing. Because the goal was to determine the influence of wave-driven forcing over the course of wave events that generally occur on time scales of 12–24 hours, the contribution from subdiurnal tidal constituents was deemed not important, and thus the simulations were run with sea level set to zero and with the vertical datum of the grids defined by mean higher water (MHW). To do this, the astronomical forcing had an M2 tidal amplitude and phase of 0 m and 0°, respectively, and the water level was adjusted for the SLR simulation by defining an A0 tide amplitude (0.00 m, +0.50 m, +1.00 m, +1.50 m, and +2.00 m) with 0° phase. The background horizontal eddy viscosity was set at 1 m^2/s, free wall roughness slip conditions were used, the stress formulation due to waves followed the Fredsoe (1984) methodology, and a uniform Madsen and others (1988) wave hydraulic roughness length scale of 0.1 m was used, following Hoeke and others (2011). The results from the larger, outer domains for both the SWAN and Delft3D-FLOW modules that covered the entire atolls were used as boundary input into the finer scale, smaller sized domains in the SWAN and Delft3D-FLOW modules around the atoll islands.

Modeled Water Surfaces and Wave-Driven Total Water Levels

The SWAN model was used to generate input parameters for computations of wave run-up (the maximum vertical reach of wave uprush on a shore). The SWAN output parameters include

wave height, wavelength, and wave-induced set-up (for example, a rise in mean water level inshore of the initial point of wave breaking). For each grid cell, these parameters were extracted for present sea level (+0.00 m) and four future SLR scenarios (+0.50 m, +1.00 m, +1.50 m, and +2.00 m), as defined on the basis of studies and projections from the Intergovernmental Panel on Climate Change (2007), Grinsted and others (2009), and Nicholls and Cazenave (2010) and similar to the prescribed scenarios for the 2009 sea-level risk assessment for Department of Defense (DoD) coastal installations (for example, Mickler, 2009). Using the extracted wave height and wavelength data, wave run-up heights were computed with the methodology of Stockdon and others (2006). For each computational grid cell, the wave-induced set-up, wave-driven run-up heights, and SLR values were combined into total water elevations and then projected on the islands' slopes along shore-normal transects.

Topography and Bathymetry

As input to the wave inundation models, seamless nested topographic/bathymetric grids of differing scales were created. The larger, outer atoll grids covered a broad area surrounding the entire atoll to water depths of 3,000 m and had coarser spatial resolutions or grid cell sizes, and the finer grids encompassed the islands plus the surrounding waters and had higher spatial resolution. Midway Atoll's grid had 451 (east-west) x 401 (north-south) cells at 50-m resolution (fig. 4), the Sand Island grid had 420 (east-west) x 350 (north-south) cells at 20-m resolution, and the Spit and Eastern Islands' grid had 325 (east-west) x 225 (north-south) cells at 20-m resolution (fig. 5). Laysan atoll's grid had 501 (east-west) x 351 (north-south) cells at 100-m resolution (fig. 6), and the Laysan Island grid had 258 (east-west) x 333 (north-south) cells at 20-m resolution (fig. 7).

For Midway Atoll, a 1/3 arc-second (~10 m) integrated bathymetric–topographic digital elevation model (DEM) had been compiled previously by Grothe and others (2010) as boundary information to model tsunami generation, propagation, and inundation. For Laysan, extensive preprocessing was required to generate integrated bathymetric–topographic DEMs from a wide range of data sources and formats, including the following: bathymetric gridded data from the Pacific Island Benthic Habitat Mapping Center (2011), synthesized grids from IKONOS satellite imagery (in depths of <16 m) and multibeam sonars (in depths of 20–5,000 m); raster and electronic navigational charts from the Office of Coast Survey (2011); bare-earth 1-m DEM data derived from photogrammetric methods by PhotoSat Information Ltd. (2010, unpublished); and a digitized coastline based on a May 18, 2010, WorldView-2 satellite photo from DigitalGlobe Inc. (2010, unpublished). When two or more data sources covered the same area, the less reliable sources were excluded from analysis. In general, older navigational chart data were used only to fill in data gaps in the newer IKONOS-derived and multibeam sonar data. After converting all depths and elevations to a common datum, the two grids were generated using geostatistical kriging techniques (Childs, 2004) in ArcGIS (Environmental Systems Research Institute, 2010). For more detailed maps of the islands' topography based on airborne lidar surveys, please see Krause and others (2012).

The methodology and bathymetric grids presented here reflect the current state of the reefs without future reef accretion. Reef accretion was not included in this study because no data exist for the study areas and published vertical reef flat accretion rates for reef flats exposed to open-ocean storm waves (1–4 mm/yr; see Buddemeier and Smith, 1988; Montaggioni 2005) such as Laysan and Midway are very small compared with the rates of projected SLR until 2100. (including wave set-up and run-up) assigned to coastal points spaced 20 m apart. For each SLR scenario, wave-driven inundation was projected inland from each coastal point along shore-

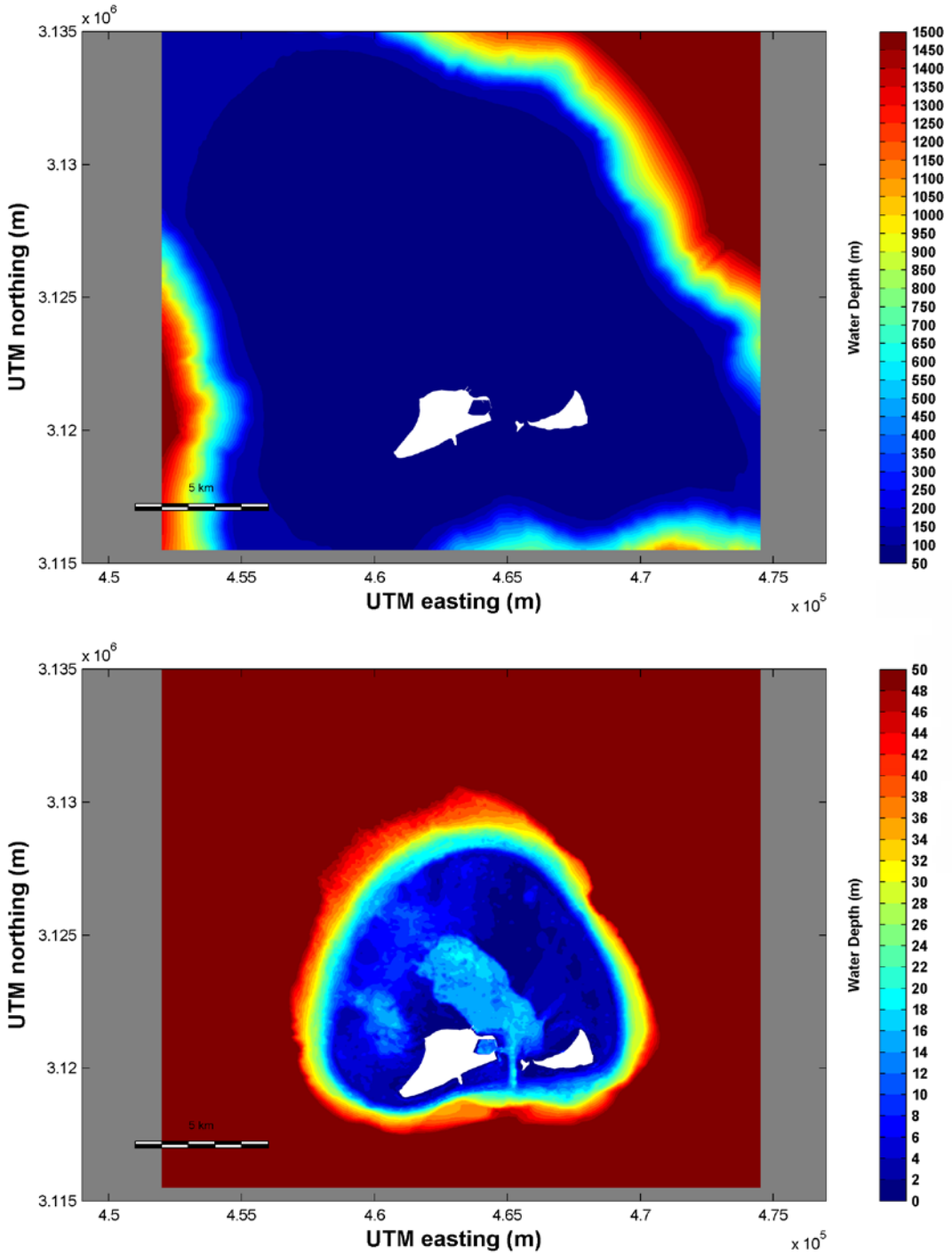

Figure 4. Maps showing the large-scale, coarse-resolution bathymetric grid of Midway used in the Delft3D hydrodynamic model. The top image shows the bathymetry of the entire atoll by focusing on a greater depth range; the bottom image shows the bathymetry of the atoll's top by focusing on a shallower depth range.

normal transects oriented in a direction perpendicular to coastal segments drawn as regression lines based on the location of each coastal point and its 10 nearest neighbors (5 to each side). Orthogonal transects were defined to run in the direction of the negative reciprocal of the

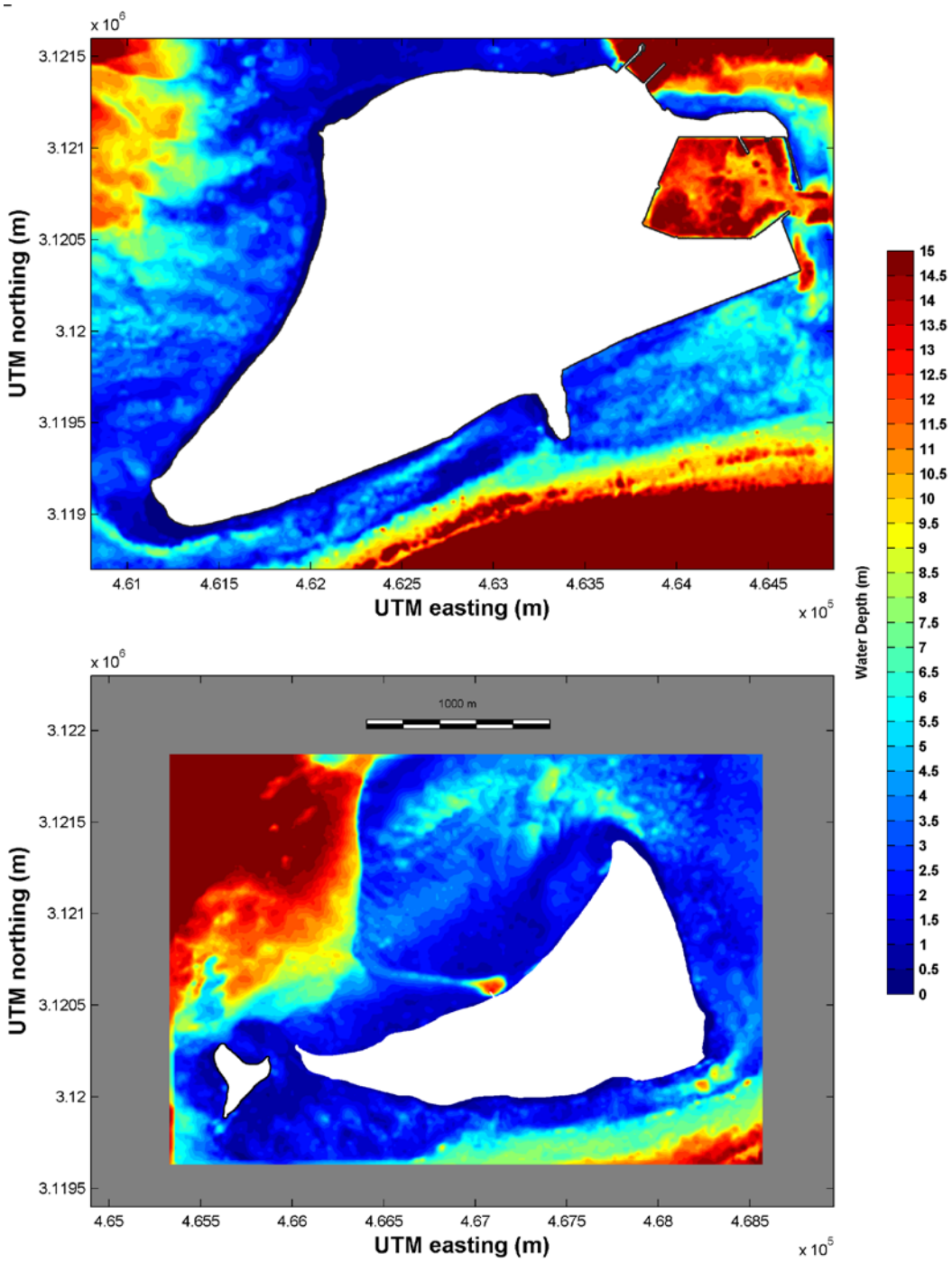

Figure 5. Maps showing the small-scale, fine-resolution bathymetric grids surrounding Sand, Spit, and Eastern Islands used in the Delft3D hydrodynamic model. The top image shows the bathymetry surrounding Sand Island; the bottom image shows the bathymetry surrounding Spit and Eastern Islands.

regression slope. For each scenario, the combined SLR and wave-driven inundation heights were projected orthogonally upslope from each coastal point until land elevations exceeded combined water heights, with the highest point reached on each shore-normal transect representing the high

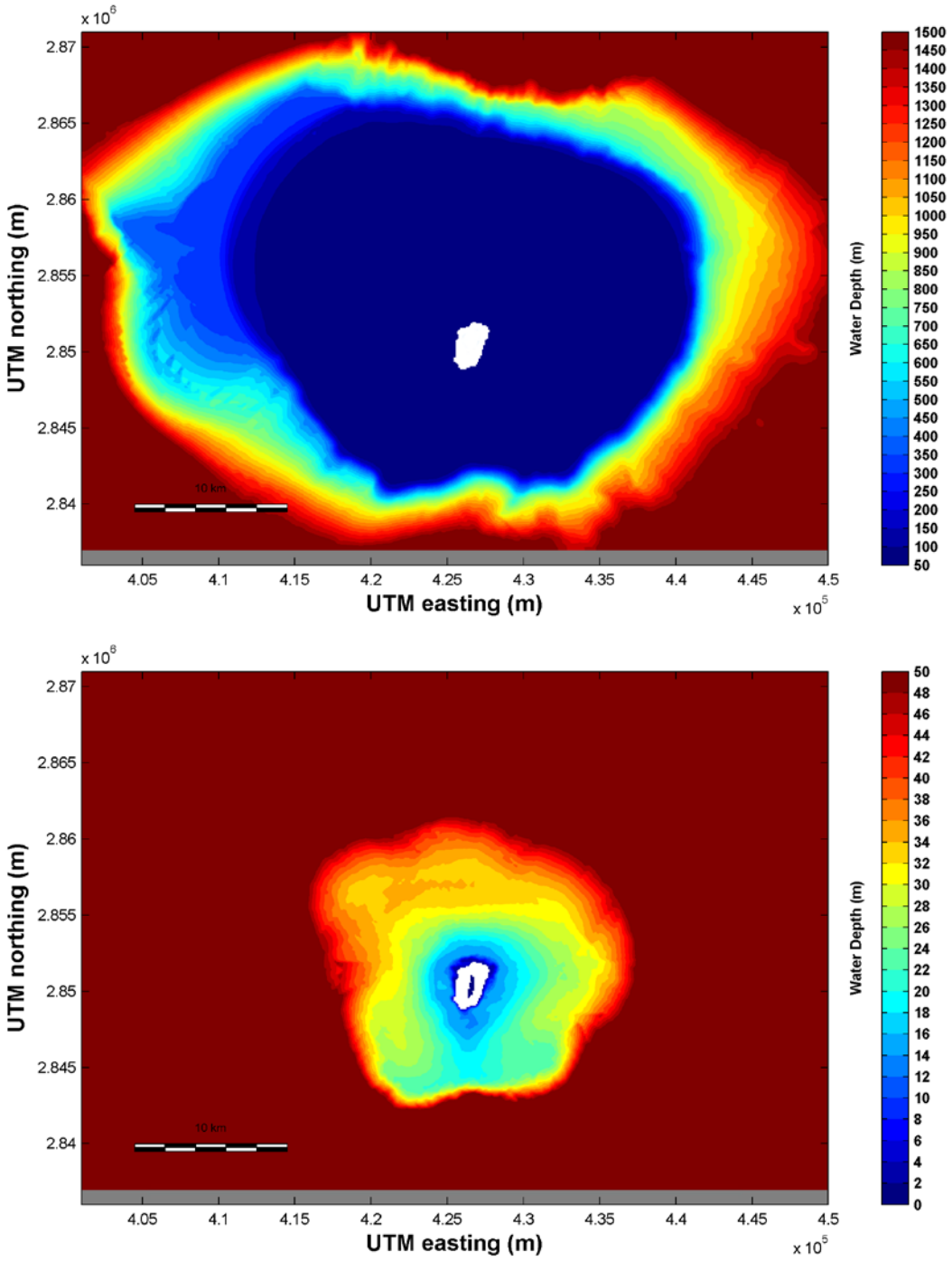

Figure 6. Maps showing the large-scale, coarse-resolution bathymetric grid of Laysan used in the Delft3D hydrodynamic model. The top image shows the bathymetry of the entire atoll by focusing on a greater depth range; the bottom image shows the bathymetry of the atoll's top by focusing on a shallower depth range.

water mark. The extent of inundation was then delineated by connecting the high water marks from adjacent transects on each of the four islands.

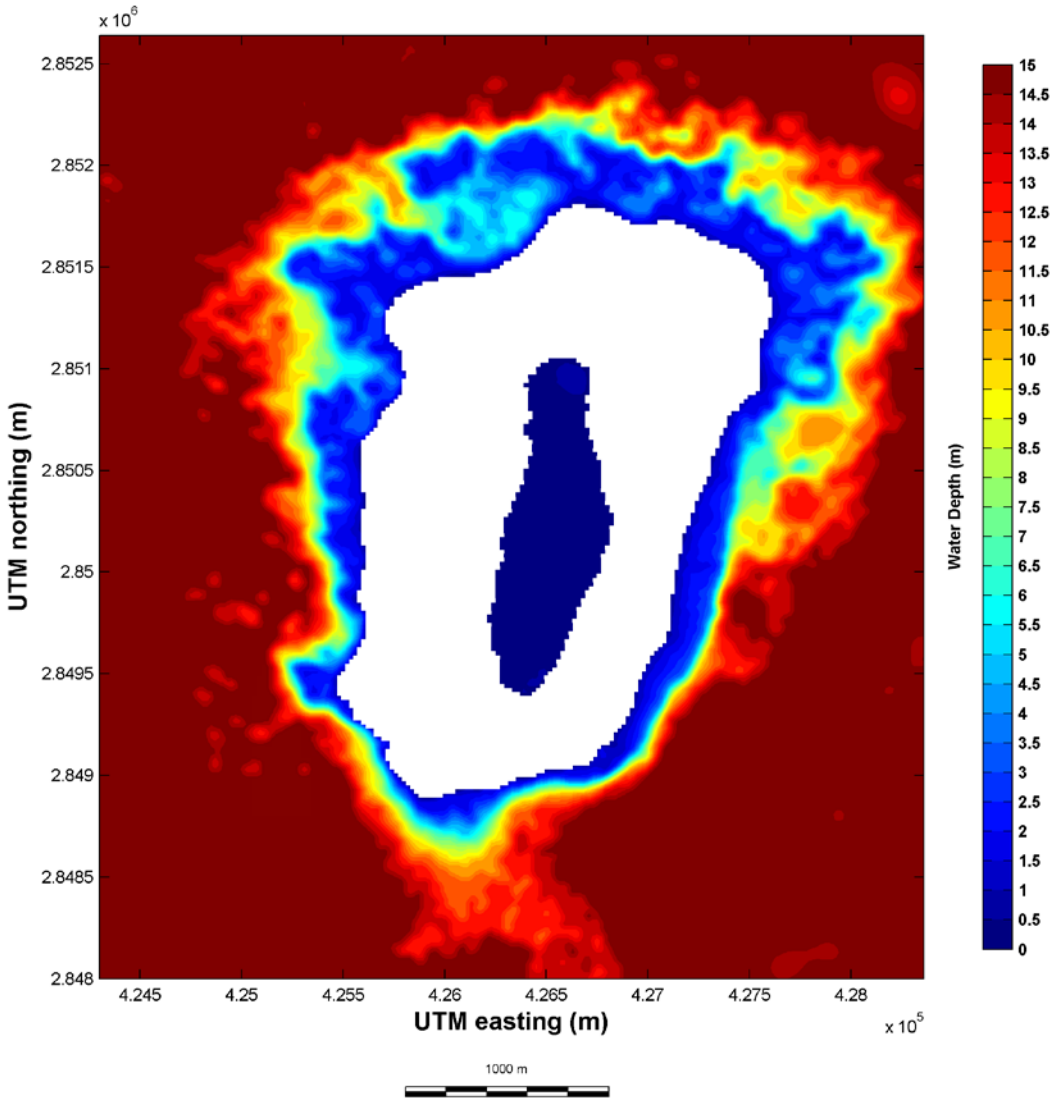

Figure 7. Map showing the small-scale, fine-resolution bathymetric grid surrounding Laysan Island used in the Delft3D hydrodynamic model.

Inundation Mapping

In order to map inundation on the islands, the modeled SLR and wave-driven water-level surface (20-m grid format) was linked to the atoll islands' coastlines using nearest neighbor techniques (Environmental Systems Research Institute, 2010), with the nearest inundation values

As a refinement to the above method, to model inundation of the three major depressions on Laysan, water was modeled to flow into these basins if they were adjacent to inundated transects, hydrologically connected, and at lower elevations than the inundated transects. While the models produce run-up elevations, they do not estimate run-up volumes; therefore, the volume of run-up that is likely to flow into adjacent topographic depressions is unknown. Thus in depicting the extent of inundation for SLR scenarios on Laysan, the initial inundation patterns were mapped as wave inundation propagates onshore, representing a transient state before run-up volumes flow laterally into adjacent depressions. Based on the long average duration of storms (>6 hours) and high frequency of swash motions (order ~5–360 times/hour) relative to hydraulic

conductivities (<0.0001 m/s; Hunt and Peterson, 1980), it was assumed that on the time-scale of storm-wave-driven inundation events, infiltration is approximately nonexistent. Thus the maximum extent of inundation was delineated as if run-up volumes were unlimited and no infiltration occurred. This allowed seawater to fill Laysan's topographic lows (terrestrial basins in the islands' DEMs) during storm events.

For both the passive and dynamic wave-modeling approach, inundation extents were analyzed and mapped within an ArcGIS framework for all five SLR scenarios (+0.00 m, +0.50 m, +1.00 m, +1.50 m, and +2.00 m). The passive approach represents a reference level and depicts the amount of inundation due to SLR only, while the dynamic approach considers the additional effect of wave-driven set-up and run-up from the average of the top 5 percent winter and summer events in the U.S. Army Corps of Engineers (2011) data set. As mentioned above, all inundation maps depict flooding under the worst-case daily scenario (for example, at mean high water [MHW], defined as the average of all high water heights over a 19-year National Tidal Datum Epoch, the period of time that includes most tidal variation due to lunar and solar forces).

Land Cover and Habitat Delineation

Land cover on Midway Atoll was classified using WorldView-2 satellite imagery collected during 2011; Laysan Island's land cover was classified using WorldView-2 satellite imagery from 2010. To classify satellite imagery digitally, the IsoCluster unsupervised classification tool in ArcGIS (Environmental Systems Research Institute, 2010) was used; this tool classifies pixels based on color, texture, tone, pattern, and associated information (Xie and others, 2008). Where field mapped land cover data were available from the U.S. Fish and Wildlife Service (USFWS), these were incorporated (USFWS unpublished data, 2007; Cornett and others, 2008; Boyd and others, 2009; Kristof and others, 2011).

Remotely sensed and field mapped land cover on Midway Atoll and Laysan Island was classified into categories, including six vegetation classes (tree/shrub, mixed shrub, grass/herbaceous cover, vine/ground cover, partially vegetated overgrown runways, and wetland vegetation), four unvegetated areas (bare ground, hard pan, beach, and wetland), and human infrastructure (including active runways, roads, and structures). Not all land cover classes appear on the different ecosystems of each island, and species composition may vary within land cover vegetation classes between islands. Definitions for land cover classes are provided in table 1, which lists some, but not all, of the dominant plant species identified in each land cover class. Plant species were described from Wagner and others (2012) and multiple botanical reviews for Midway Atoll (Starr and Martz, 1999; Klavitter, 2006; Starr and others, 2006; Starr and others, 2008) and Laysan Island (USFWS, written commun., 1999; Kristof and others, 2011). A rigorous quantitative accuracy assessment of the vegetation composition was not possible owing to the logistical constraints of collecting ground-truth data on remote islands. The accuracy assessment of remotely sensed land cover classification included visual inspection and comparison with other available mapping data, field reports, and past botanical surveys (Starr and Martz, 1999a; Starr and Martz, 1999b; Starr and others, 2001; Klavitter, 2006; Starr and others, 2006; Starr and others, 2008). Expert opinions from USFWS field biologists were solicited for general classification accuracy of Laysan Island (E. Flint, T. Speetjens, and M. Stelmach).

Land cover classes were designated as habitat for wildlife on the basis of species-specific nesting (or pupping) behavior known from each island. Potential inundation to wildlife habitats was described as the sum of all utilized land cover classes typically used by each species for breeding or nesting habitat without differentiating between vertical habitat structures within land

cover classes. For example, tree/shrub landcover was quantified equally for Great Frigatebird, which nest on top of trees and shrubs, and Red-tailed Tropicbird, which nest on the ground beneath trees and shrubs. Wetlands were not included as suitable nesting habitat for wildlife, but this land cover is important foraging habitat and a source of water for endemic passerines, waterfowl, and migratory shore birds. The distribution of breeding wildlife on the four islands of this study and the habitats typically used were compiled from site visits, literature, and personal communication with USFWS managers (Poole, 2012; John Klavitter, USFWS, oral commun. 2011; also see Reynolds and others, 2012).

By overlaying the predicted inundation patterns with the remotely sensed land cover maps defined here, it was possible to estimate the amount of wildlife habitat likely to be inundated by SLR and wave-driven processes. However, the potential land cover change from SLR could be predicted using two different vegetation response models: (1) a static vegetation response model, in which SLR occurs at a rate that outpaces vegetation regeneration, and (2) a dynamic vegetation response model, in which land cover shifts upslope of SLR inundation via replanting or natural succession. The static vegetation response model used here predicts that land cover does not shift upslope as water levels rise but, rather, the inundated land cover is lost. In contrast, the dynamic vegetation response model assumes vegetation will regenerate toward higher elevations as sea levels rise, "migrating" from one elevation to the next, following the methods described by LaFever and others (2007). Krause and others (2012) suggested that Sand, Eastern, and Laysan Islands require additional adaptive models to improve predictions of dynamic inland vegetation change. Because vegetation response models have not been developed for these ecosystems, only the simpler static vegetation response models were applied in this study of Midway Atoll and Laysan Island.

Uncertainty in Inundation Models

Three sources of uncertainty affect the vertical accuracy of the inundation models presented here: (1) uncertainty in tidal elevations, (2) uncertainty in topographic elevations, and (3) uncertainty in wave-driven set-up and run-up values. For Laysan Island, a robust tidal datum does not exist because there is no tide gauge on the island. Thus, without many alternatives, the National Oceanic and Atmospheric Administration (2011a) predicted tide of –0.065 m relative to mean sea level (MSL) at the moment when the stereo-pair images were captured was used as a reference elevation, and the MSL tidal datum was defined relative to this level. The accuracy of the predicted tides at Laysan Island is unknown because there has never been verification. However, given the small tidal range in the Central Pacific, the relatively flat tidal levels within 6 hours of the time of the photos (<0.10 m range), and the small deviations between predicted and verified tides at Midway Atoll within 12 hours of the photo time (0.07 m), it would be expected that National Oceanic and Atmospheric Administration's predicted tide relative to predicted MSL would be within 0.10 m of the actual tide relative to actual MSL. This uncertainty estimate expresses the relative difference between predicted tidal stage and actual tidal stage (for example, predicted tide relative to predicted MSL versus actual tide relative to actual MSL), not the absolute accuracy of the predicted tide relative to an ellipsoid, geoid, or other fixed surface. For Midway Atoll, less tidal uncertainty exists because Sand Island has both predicted and verified tides (National Oceanic and Atmospheric Administration, 2011a).

The uncertainty in topographic elevation on Laysan was estimated using 27 survey-grade (>cm accuracy) Global Positioning System (GPS) points collected in 2011 (National Oceanic and Atmospheric Administration, 2011b). National Oceanic and Atmospheric Administration surveyors located survey points in flat, open areas to ensure that horizontal uncertainty did not

have a major effect on vertical accuracy. The root-mean squared error (RMSE) between the elevations provided in PhotoSat Information Ltd.'s (2010, unpublished) DEM and the 27 survey points was 0.32 m. Using the same validation procedures for Midway Atoll, the RMSE was computed as 0.39 m.

Lastly, sensitivity analysis of the input parameters to the wave inundation model indicate that modeled wave height and wave period were within less than 2 percent of the mean values for wave height and wave period, while the standard deviation in beach slope was approximately 2 percent. The resulting mean error in run-up was 0.11 m. Since these uncertainties (expressed as standard deviation [SD]) are uncorrelated, they can be combined into an overall uncertainty term (Coastal Services Center, 2010):

$$SD_{Total} = (SD_{Tidal}^{2} + SD_{Topography}^{2} + SD_{Run\text{-}up}^{2})^{0.5}$$

From the uncertainty estimates above, the overall vertical uncertainty or RMSE was computed to be 0.35 m for Laysan. The comparable calculation for Midway yielded a RMSE of 0.41 m. These vertical uncertainties have a variable effect on horizontal inundation extent, depending on topography: areas with gradual slopes will exhibit more horizontal uncertainty than areas with steep slopes. Inundation extents or boundaries can be created from data of any quality and are not sensitive to accuracy, although data accuracy determines the area of confidence around inundation boundaries (Coastal Services Center, 2010). The National Oceanic and Atmospheric Administration uses a value of 80 percent confidence as the threshold between high and low confidence. By definition, the Z-score at the inundation boundary equals zero, with the probability of inundation on this boundary equaling 50 percent. At elevations above the inundation boundary, the probability of inundation decreases according to the normal probability distribution, such that a location +0.84 SDs above the inundation level has a 20 percent probability of inundation (or 80 percent probability of being dry). Similarly, a location -0.84 SDs below the inundation level has an 80 percent probability of inundation (or 20 percent probability of remaining dry). Between these two thresholds lies an area of low confidence (<80 percent), while beyond these thresholds lie areas of high confidence (≥80 percent).

In terms the modeled results, none of the projected inundation boundaries are biased by positional uncertainty, although the true position of the boundary may be higher or lower given the uncertainty in the model. For all SLR scenarios under consideration, if the desire was to maintain 80 percent confidence that the inundation boundary would remain dry, then as a precaution, +0.29 m of elevation on Laysan (0.84 x RMSE) would need to be added to the flood surface and the horizontal boundary allowed to adjust accordingly. For Midway Atoll, the comparable increment of elevation to add would be +0.34 m. Although one could adopt such a precautionary approach, it was decided to analyze inundation extent using only unbiased inundation boundaries. Because multiple scenarios of SLR were modeled and a range of inundation boundaries were presented, the effects of uncertainty on inundation extent are relatively easy to visualize by examining the changes in inundation extent as a result of different increments of SLR.

The run-up elevations determined using the Stockdon and others (2006) methodology is very dependent on the local coastal slope and assumes a relatively uniform beach slope from the upper shoreface to the back-beach dune system. A steep beachface up to a berm crest that is backed by a relatively low-slope back beach can result in a rather long projected inundation zone that progresses inland until the inundation transect intersects a point on the island's topography where elevation exceeds the run-up calculated using the Stockdon and others (2006) methodology. Such cases would tend to over-predict the distance inland, and thus the potential

area inundated, along the given transect. Stating this, however, the Stockdon and others (2006) methodology would correctly predict run-up to exceed the berm crest, and seawater would then spread out inland and alongshore from the location where the elevation of the berm crest was breached. Because the procedures used to project run-up inland do not take this lateral spreading into account (except for the major basins on Laysan), it thus under-predicts the potential inundation into adjacent transects. It is not clear how these two procedural issues with projecting and mapping inundation may offset one another. Friction, which would limit run-up distances, was not accounted for in the longer run-up trajectories; similarly, scour, which would increase the potential run-up distances (see, for example, Fletcher and others, 1995), was not accounted for in the simulations. Furthermore, these modeling efforts also assume constant meteorological and atmospheric forcing that drives the waves and run-up, which, as discussed earlier, may be different in the future owing to global climate change. Because of the low confidence level of existing projections, however, it was not possible to accurately predict the future change to wind, waves, and the resulting wave-driven inundation. Lastly, although Webb and Kench (2010) suggest that atoll island morphology has shown little response to the +0.3 m of SLR over the past 50 years, it is not clear how island morphology may respond to much higher SLR scenarios (for example, +1.00 m, +1.50 m, and +2.00 m modeled here). These issues, together with the lack of understanding of how the islands' hydrogeology may change under future climate change scenarios, result in the presentation of the inundation extents and associated changes in land cover classes and habitats discussed in the following sections not as exact values, but rather as relative values to be compared to one another for the different SLR models and SLR scenarios.

Results

General Deep-water Oceanographic and Meteorological Forcing

The WIS hindcast data for deep-water ocean surface waves and wind show both seasonal and spatial trends for the study area, as shown in figures 8–11 and listed in tables 2–3. Monthly mean wave heights, periods, and directions range from 1.80 m to 4.61 m, 9.5 s to 12.5 s, and 4° to 354°, respectively. Monthly top 5 percent wave heights and their periods and directions range from 2.96 m to 8.99 m, 8.9 s to 15.3 s, and 4° to 359°, respectively. Monthly mean wind speeds and directions range from 5.6 m/s to 9.5 m/s and 16° to 264°, respectively. Monthly top 5 percent wind speeds and their directions range from 10.1 m/s to 17.6 m/s and 36° to 319°, respectively. Not only are the wave heights, wave periods, and wind speeds greatest during the winter months, but they are also then the most variable, with episodic high-energy conditions during winter storms punctuating more frequent, lower energy periods characterized by trade or variable winds. Although the waves are relatively unidirectional from the northwest during the winter (figs. 9-10), the winds are almost evenly distributed around the islands (fig. 11), reflecting the passage of shear lines and weather fronts through the area. During the summer months, both the waves and winds are relatively unidirectional and appear primarily controlled by trade-wind patterns. Of note is the infrequent contribution of waves of low height but long period out of the south during the summer, likely due to storms in the Southern Ocean during the southern hemisphere's winter.

From these data, two wave and wind end-members (top 5 percent) were used as boundary input into the Laysan and Midway models. Winter conditions with very large North Pacific winter swell and storm winds were defined as having significant wave height (H_s) of 8.53 m, a peak wave period (T_p) of 15.0 s, a mean wave direction (θ_{wave}) of 307°, a wind speed (U_w) of 16.9 m/s, and a mean wind direction (θ_{wind}) of 273°. High-end summer conditions characterized by

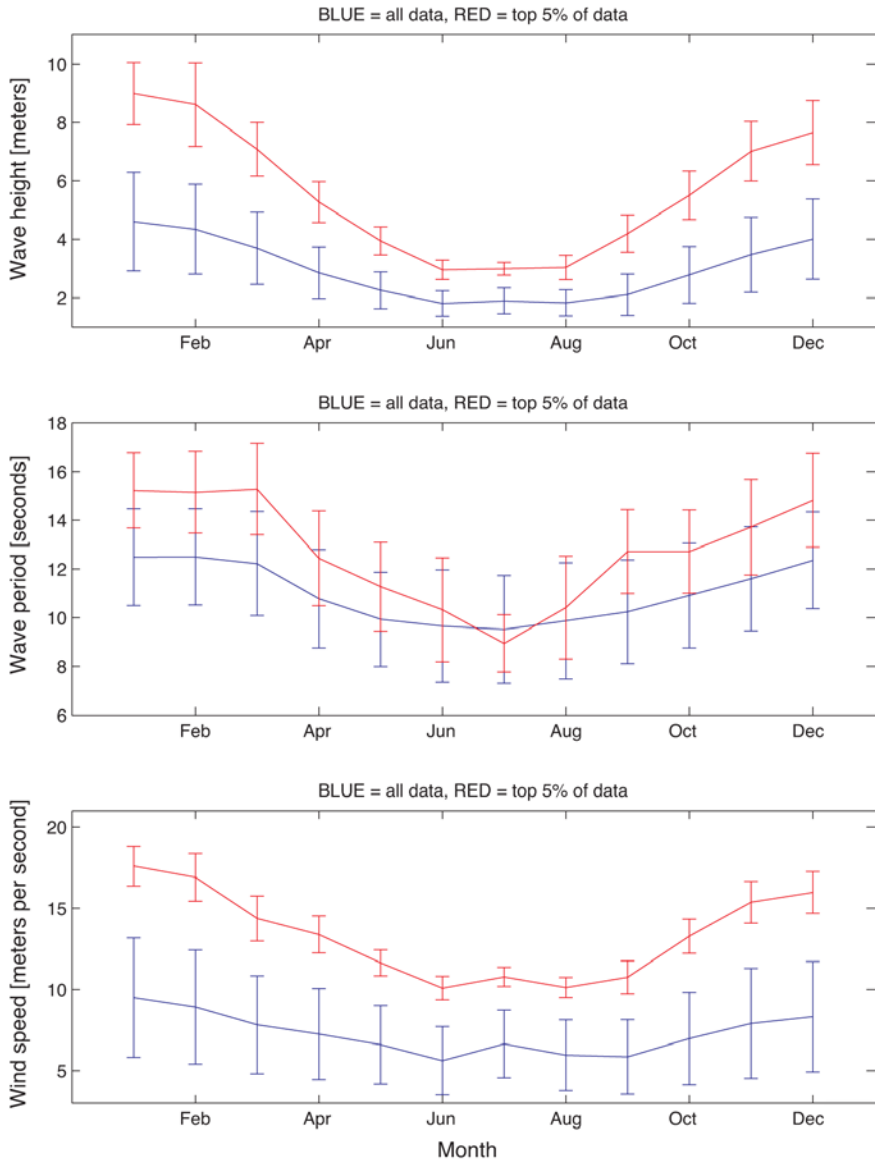

Figure 8. Time series plot showing monthly means and 1-standard deviation error bars of wave heights, in meters, wave periods, in seconds, and wind speeds, in meters per second, based on U.S. Army Corps of Engineers (2011) hindcast data for the years 1981–2004 at 28° 00’ N, 174° 00’ W. Blue represents all of the data; red represents the top 5 percent of the data.

relatively (for trade-wind conditions) large trade-wind waves and winds were defined as having a significant wave height (H_s) of 3.00 m, a peak wave period (T_p) of 9.8 s, a mean wave direction (θ_{wave}) of 71°, a wind speed (U_w) of 10.4 m/s, and a mean wind direction (θ_{wind}) of 77°.

Modeled Waves and Water Levels on the Atolls

Maps showing the spatial variation in modeled significant wave height (H, in meters) output by the Delft3D model for the four atoll islands under both winter and summer conditions are presented in appendix 1. A synthesis of the mean and variability in changes in waves and the resulting water levels from around the four islands are shown in figures 12 and 13 for North

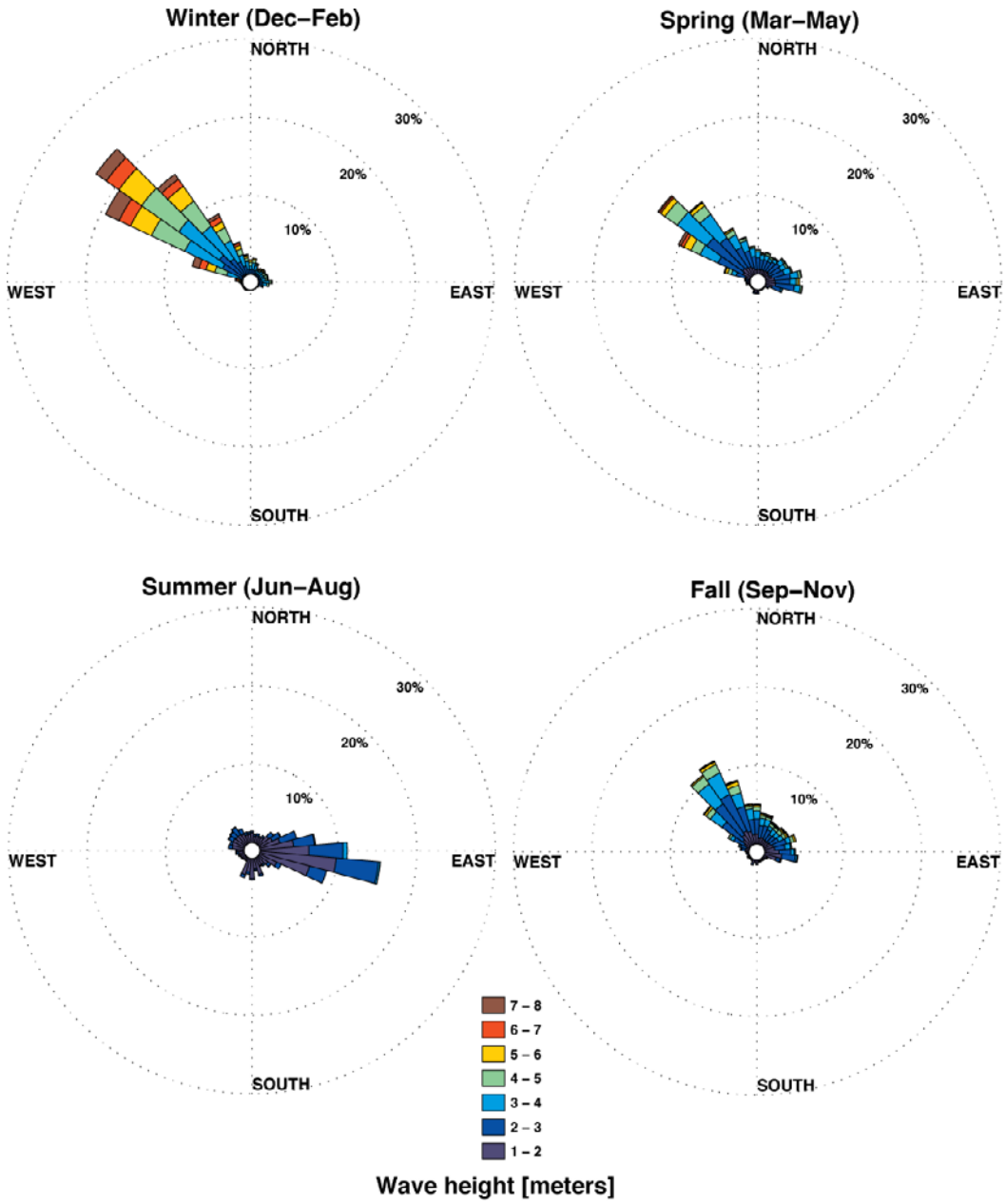

Figure 9. Directional plot of seasonal variations in wave height, in meters, by wave direction, in compass orientation, based on U.S. Army Corps of Engineers (2011) hindcast data for the years 1981–2004 at 28° 00’ N, 174° 00’ W. Radial axis, frequency of occurrence, in percent, increase outward from the center of the plot.

Pacific winter conditions and summer trade-wind conditions, respectively. As discussed earlier, most reef crests and reef flats are depth-limited for waves, in that wave heights are limited to a fraction of the water depth. Thus, as water depth increases with SLR over the atolls’ reef flat, it allows for larger waves to propagate onto or develop on the reef flat. On average, wave heights around the atoll islands’ shorelines for both winter and summer conditions are approximately 0.4 m to 0.5 m higher than at present with +1.0 m of SLR and approximately 0.9 m to 1.0 m higher with +2.0 m of SLR. There are no definite mean trends in wave period around the islands during

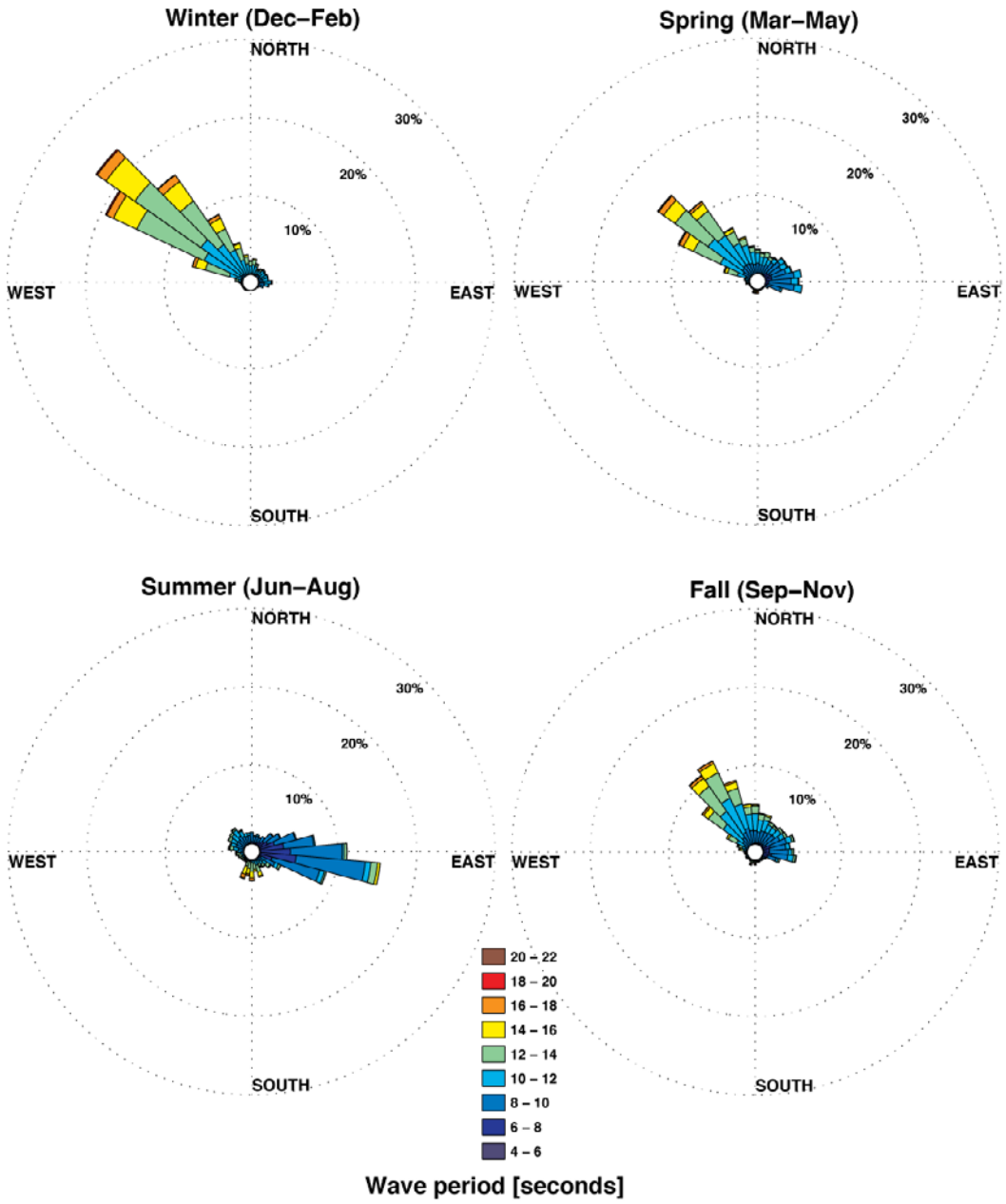

Figure 10. Directional plot of seasonal variations in wave period, in seconds, by wave direction, in compass orientation, based on U.S. Army Corps of Engineers (2011) hindcast data for the years 1981-2004 at 28° 00’ N, 174° 00’ W. Radial axis, frequency of occurrence, in percent, increase outward from the center of the plot.

winter conditions that are characterized by longer period swell from the northwest, but wave periods during summer conditions that are characterized by shorter period waves from the northeast are, on average, 1 s shorter with +2.0 m of SLR. Because wave length in shallow water is primarily a function of the ratio of wave period to water depth, with increasing SLR, mean wave lengths around the atoll islands under winter conditions are approximately 7 m to 10 m longer than at present with +1.0 m of SLR and approximately 15 m to 20 m longer with +2.0 m of SLR. There is less increase during the summer (fig. 13), when the wave periods are slightly

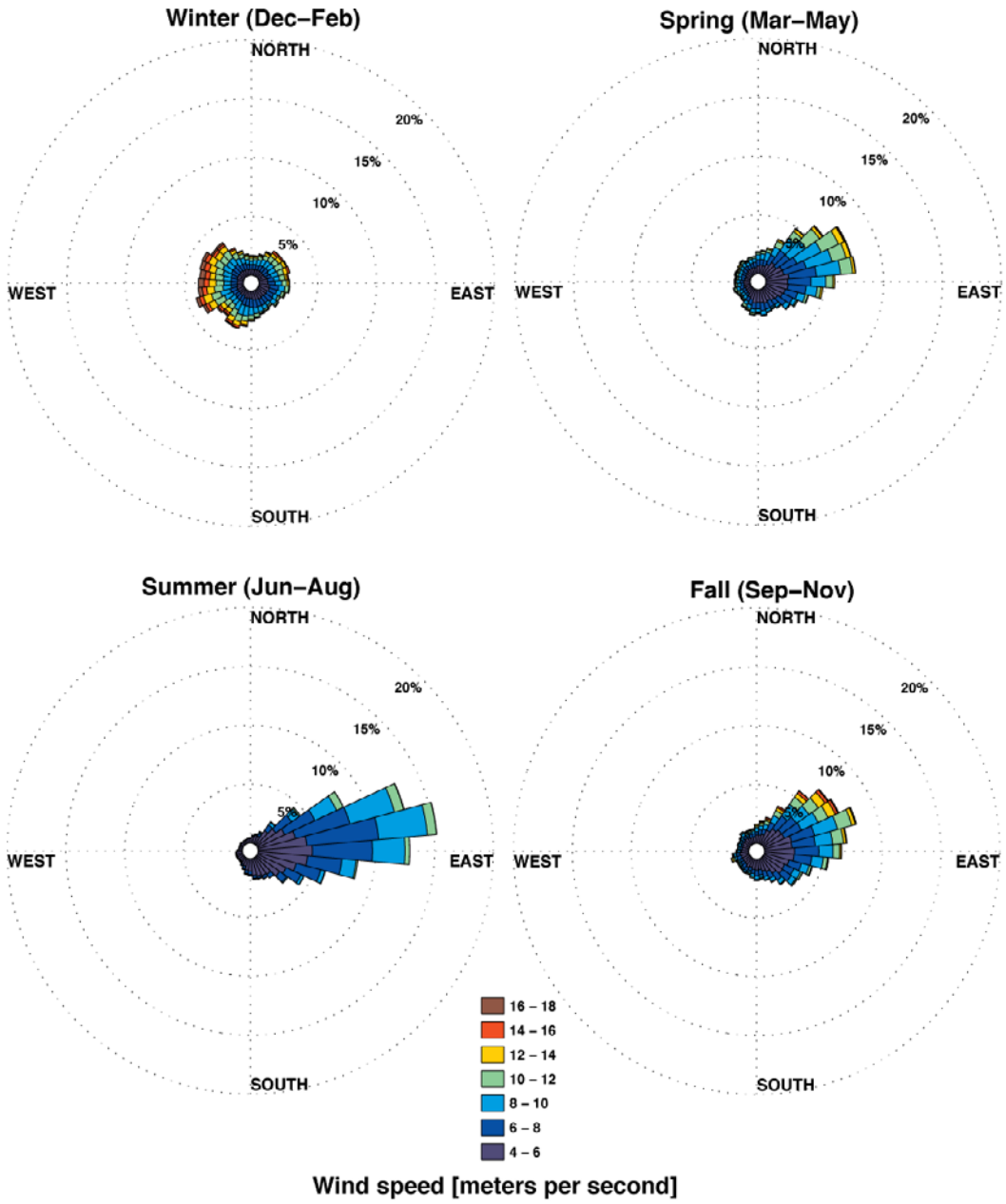

Figure 11. Directional plot of seasonal variations in wind speed, in meters per second, by wind direction, in compass orientation, based on U.S. Army Corps of Engineers (2011) hindcast data for the years 1981–2004 at 28° 00’ N, 174° 00’ W. Radial axis, frequency of occurrence, in percent, increase outward from the center of the plot.

lower with increasing SLR. Mean set-up values around the atoll islands, which are a function of the ratio of wave height to water depth, are approximately 0.05 m to 0.08 m lower than at present with +1.0 m of SLR and approximately 0.07 m to 0.15 m lower with +2.0 m of SLR. The mean top 2 percent run-up values around the atoll islands, which are a function of wave height, wave period, and the cross-shore slope of the beachface, are 0.17 m to 0.20 m higher than at present with +1.0 m of SLR and approximately 0.31 m to 0.41 m higher with +2.0 m of SLR. The trend in combined set-up and run-up around the atoll islands mirrors that of the variations in top 2

percent run-up, being 0.06 m to 0.08 m higher than at present with +1.0 m of SLR and approximately 0.11 m to 0.14 m higher with +2.0 m of SLR. Variations in averaged wave parameters along the entire coastline of the atoll islands are relatively small. However, because run-up is a function of the cross-shore slope of the beachface, there is high spatial variability in run-up and combined set-up and run-up, as shown by the large error bars (showing ±1 SD) in figures 12–13. The highest mean values (±1 SD) in top 2 percent run-up are 0.42 m to 0.51 m higher with +1.0 m of SLR than at present and 0.76 m to 0.99 m higher with +2.0 m of SLR. In order to better understand how the spatially varying nature of wave heights and wavelengths resulting from the spatially heterogeneous morphology of the atolls resulted in spatially varying set-up and run-up around the islands, the combined effects of wave set-up and run-up for both the current (+0.00 m) and the highest (+2.00 m) SLR scenarios are shown in appendix 2. Although the resulting wave-driven water levels (combined set-up and run-up) around the islands are also heterogeneous, there is a general trend of higher levels on the portion of the islands closer to the reef crest or the lagoon, likely related to greater set-up influencing depth-limited wave heights on the reef flat. The highest mean values (±1 SD) for the change in wave-driven water levels are 0.96 m to 0.99 m higher with +1.0 m of SLR than at present and 1.91 m to 2.00 m higher with +2.0 m of SLR (figs. 12–13).

In all cases, modeled wave set-up, run-up, and combined wave-driven water levels for all SLR scenarios were greater for North Pacific winter conditions than for summer conditions. This dominance of maximum wave-driven water levels by winter storm conditions for each SLR scenario, in conjunction with the fact that the statistics for wave conditions were chosen to represent those conditions that would be experienced during an average year, resulted in the inundation, land cover class, and habitat class mapping efforts being focused on only North Pacific winter conditions.

Inundation Mapping

Across all SLR scenarios, the extent of inundation predicted under the passive modeling approach covered less area than the inundation extent forecasted by the modeling approach that includes wave-driven water levels (figs. 14–18, table 4). Under the passive modeling approach, each of the five SLR scenarios yielded a similar general spatial pattern, with inundation progressing inland from the coast in the shape of concentric rings. At the highest SLR scenarios, water levels began to exceed the coastal berm in places on Sand (fig. 14), Eastern (fig. 16), and Laysan Islands (fig. 17) and extend inland over low-lying areas as overwash sheets. The overwash at Laysan at the higher SLR scenarios also resulted, assuming no infiltration and unlimited seawater volumes, in raising the hypersaline lake levels and increasing inundation around the lake's mudflats and surrounding vegetation. The introduction of seawater and marine biota into the lake by overwash would change the lake's salinity and potentially impact the hypersaline-adapted aquatic species on Laysan. For Sand, Eastern, and Laysan Islands, passive inundation at +1.50 m SLR was less than 10 percent of the islands' terrestrial areas and less than 20 percent at +2.00 m SLR. On the lowest-lying island, Spit, however, the area inundated by passive SLR increased dramatically at much lower SLR scenarios: the area inundated doubled from 34 percent at +1.00 m SLR to 72 percent at +1.50 m SLR and exceeded 99 percent at +2.00 m SLR.

When passive SLR was combined with wave set-up and run-up to compute the dynamic total water levels, similar patterns of concentric inundation occurred at SLR scenarios less than +1.00 m. For the base scenarios (SLR = +0.00 m), the dynamic wave-driven inundation modeling predicted inundation extents on the order of twice as great as the passive scenarios,

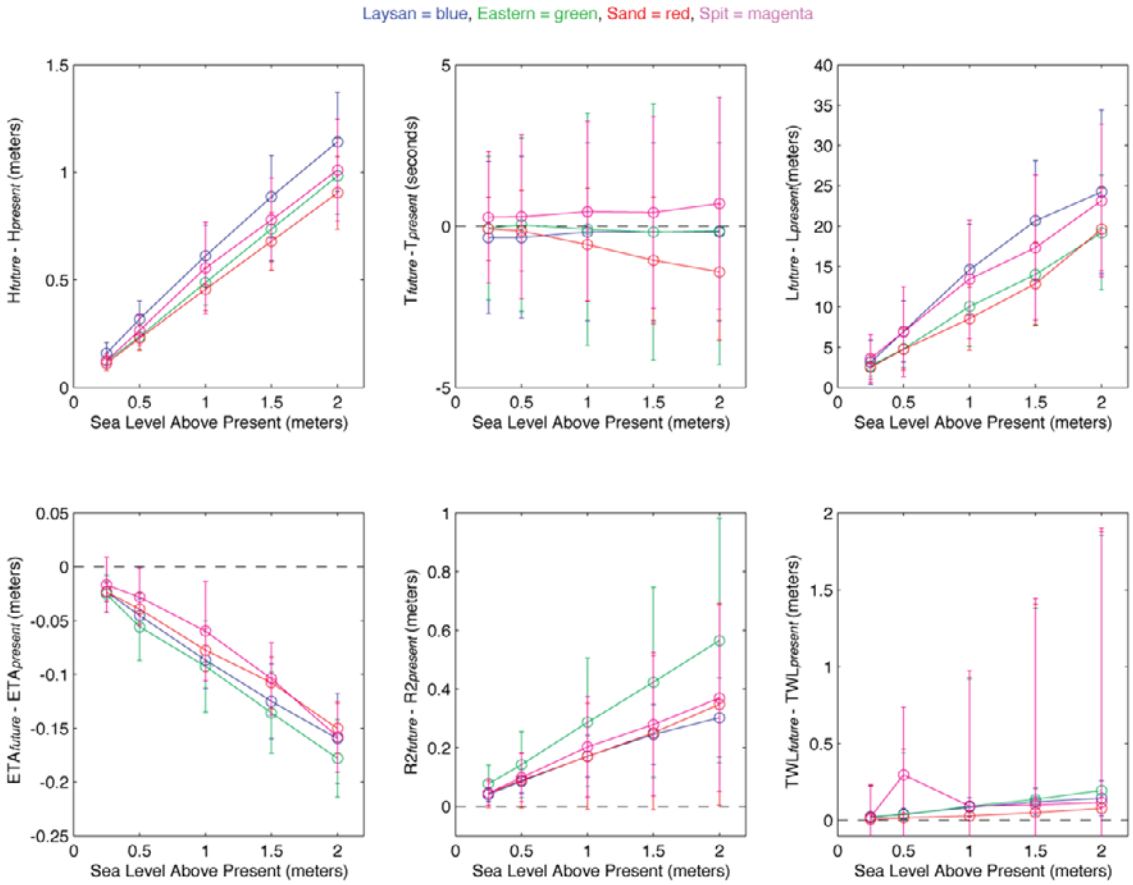

Figure 12. Plots of the mean changes in significant wave height (H, in meters), peak wave period (T, in seconds), and mean wavelength (L, in meters) and the resulting set-up (ETA, in meters), top 2 percent run-up (R2, in meters), and total wave-driven water levels (TWL, in meters) at all model grid locations adjacent to the four islands for the five sea-level rise (SLR) scenarios (+0.00 m, +0.50 m, +1.00 m, +1.50 m, and +2.00 m) relative to present sea level during North Pacific winter conditions. Blue represents data from Laysan Island; green represents data from Eastern Island; red represents data from Sand Island; and magenta represents data from Spit Island.

except at Laysan, where the amount of inundation, although small relative to the area of the island, went up more than an order of magnitude (from 0.1 percent to 1.8 percent). Projected inundation doubled from the +0.00 m to the +0.50 m SLR scenario for all islands except Spit, where wave-driven inundation caused the projected inundation to quadruple to more than 44 percent of the island's area. Between +0.50 m and +1.00 m SLR, the influence of the low topography on inundation results in the projected inundation to increase by 54 percent at Spit, whereas the other islands only show an increase on the order of 5 to 14 percent. Thus, the dynamic model that includes total water levels from wave-driven processes projects Spit Island to have approximately the same area inundated at +1.00 m SLR (98.1 percent) as is projected by the passive modeling at +2.00 m SLR (99.8 percent).

On Sand, Eastern, and Laysan Island, at the higher SLR scenarios of +1.50 and +2.00 m, the dynamic inundation patterns start to diverge considerably from passive inundation patterns, as wave-driven water levels begin to exceed the existing coastal berm and extend considerable distances inland over low-lying areas (figs. 14–17). At +1.50 m SLR, wave-driven water levels

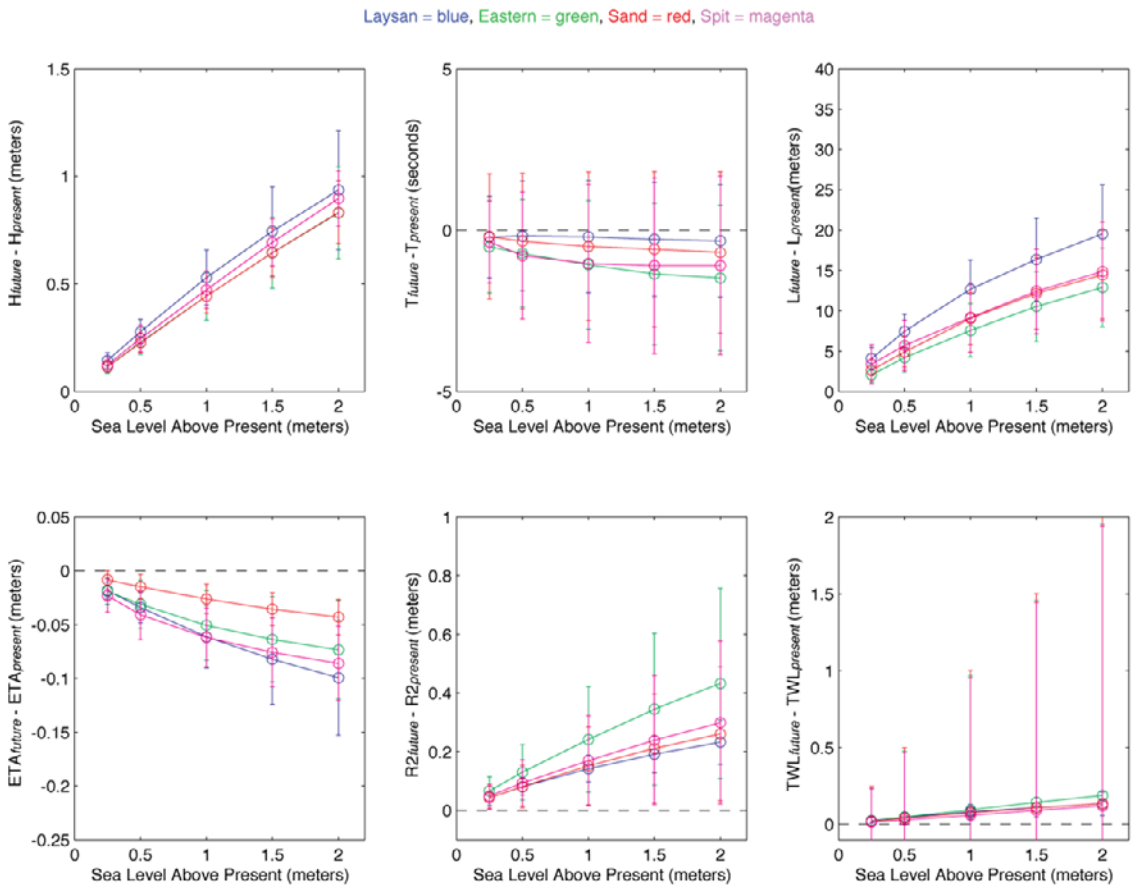

Figure 13. Plots of the mean changes in significant wave height (H, in meters), peak wave period (T, in seconds), and mean wavelength (L, in meters) and the resulting set-up (ETA, in meters), top 2 percent run-up (R2, in meters), and total wave-driven water levels (TWL, in meters) at all model grid locations adjacent to the four islands for five sea-level rise (SLR) scenarios (+0.00 m, +0.50 m, +1.00 m, +1.50 m, and +2.00 m) relative to present sea level during summer trade-wind conditions. Blue represents data from Laysan Island; green represents data from Eastern Island; red represents data from Sand Island; and magenta represents data from Spit Island.

on Laysan breach the dunes in two locations along the east coast, including one location where wave-driven water levels penetrated to the lake zone. The inundated area from these two breaches intersected the two topographic depressions flooded by the storm event of February 2011 (Kristof and others, 2011) and exhibit patterns similar to what was observed during that large storm event. At +2.00 m SLR, Eastern Island shows the greatest difference between the passive and dynamic inundation modeling, the passive model suggesting an inundation extent of 19 percent, but the dynamic model predicting a loss of 91 percent of the island's area.

Land Cover and Habitat Inundation

The relative distribution of land cover classes defined from remote sensing varied by from island to island (tables 5–12; appendix 3). Similarly, the use of various land covers as wildlife habitat also varies by species and by island (tables 13 and 14). Sand Island's land cover includes predominantly human structures, including paved runways (126.5 ha), and grass/herbaceous

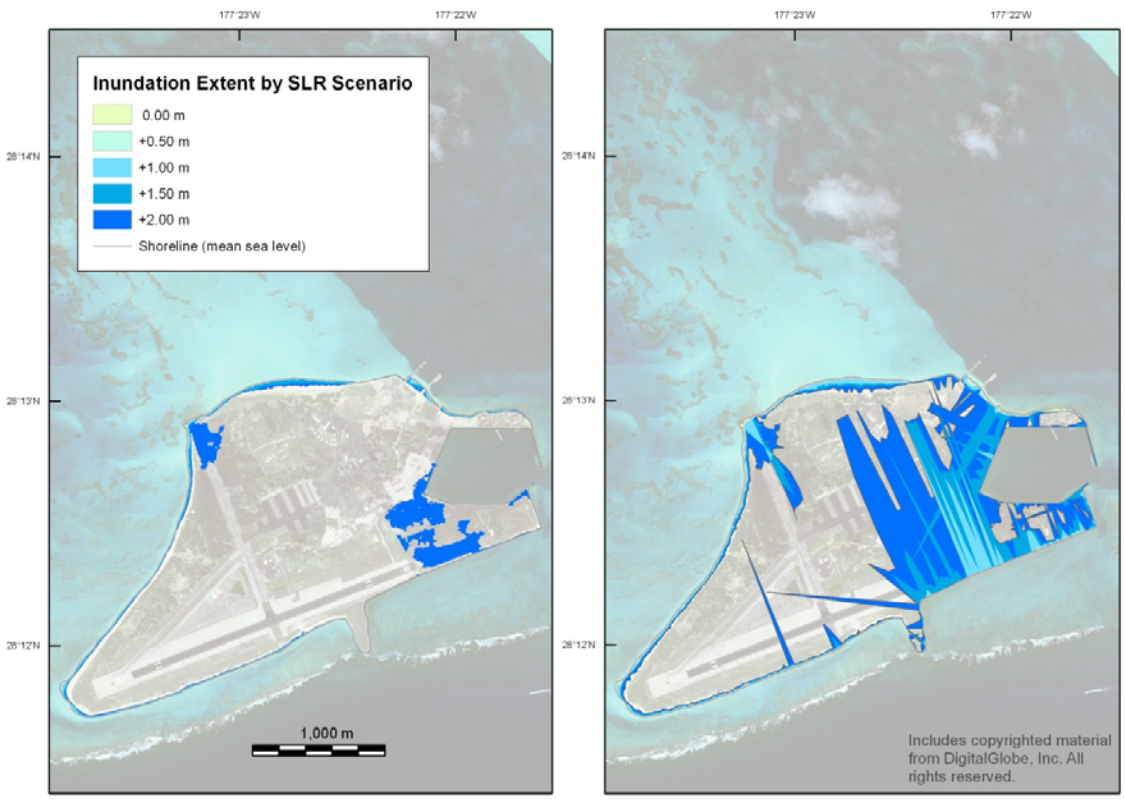

Figure 14. Map of inundation at Sand Island due to both passive (left) and dynamic (right) models for the five sea-level rise (SLR) scenarios (+0.00 m, +0.50 m, +1.00 m, +1.50 m, and +2.00 m) relative to present sea level.

cover. On Eastern Island, grass/herbaceous cover (55.9 ha) and partially vegetated former runway (32.4 ha) encompass the largest land areas. Spit and Laysan Islands, on the other hand, feature primarily bare ground (129.3 ha) and interspersed vegetation, including bunch grass, herbaceous species, vines, and ground cover. The changes in land cover classes follow similar patterns to the changes due to inundation, with all islands losing more of the existing land area at lower values of SLR under the dynamic modeling compared to the passive modeling (tables 5–12). A feature that highlights one of the issues of this modeling is the high percentages of the "beach" class lost in all SLR scenarios. This is a result of the assumption that the land cover classes are static and inundation due to either the passive or dynamic model scenarios will not result in lateral and vertical migration of these features. However, it is clear from the geologic record that SLR results in the recession of the shoreline, in which the beach generally retains its form as it migrates inland and upwards with SLR unless stopped by some fixed feature, such as beachrock or infrastructure. Thus the high rates of beach loss are unlikely because land cover response to inundation is not static; these rates are rather a reflection of the methodology used in the static habitat modeling described above. Depending on the island and modeling scenario, major losses also are seen in bare ground, grass/herbaceous cover, and in the partially vegetated former runways on Sand and Eastern Islands (tables 5–12).

As projected SLR increases, the percentages of areas classified as vegetated (excluding beach, bare ground, partially vegetated runway, and human structures) being inundated on Sand Island increase by an order of magnitude, from 1 and 4 percent for the passive and dynamic models, respectively, at +1.00 m SLR to 11 and 43 percent, respectively, at +2.00 m SLR

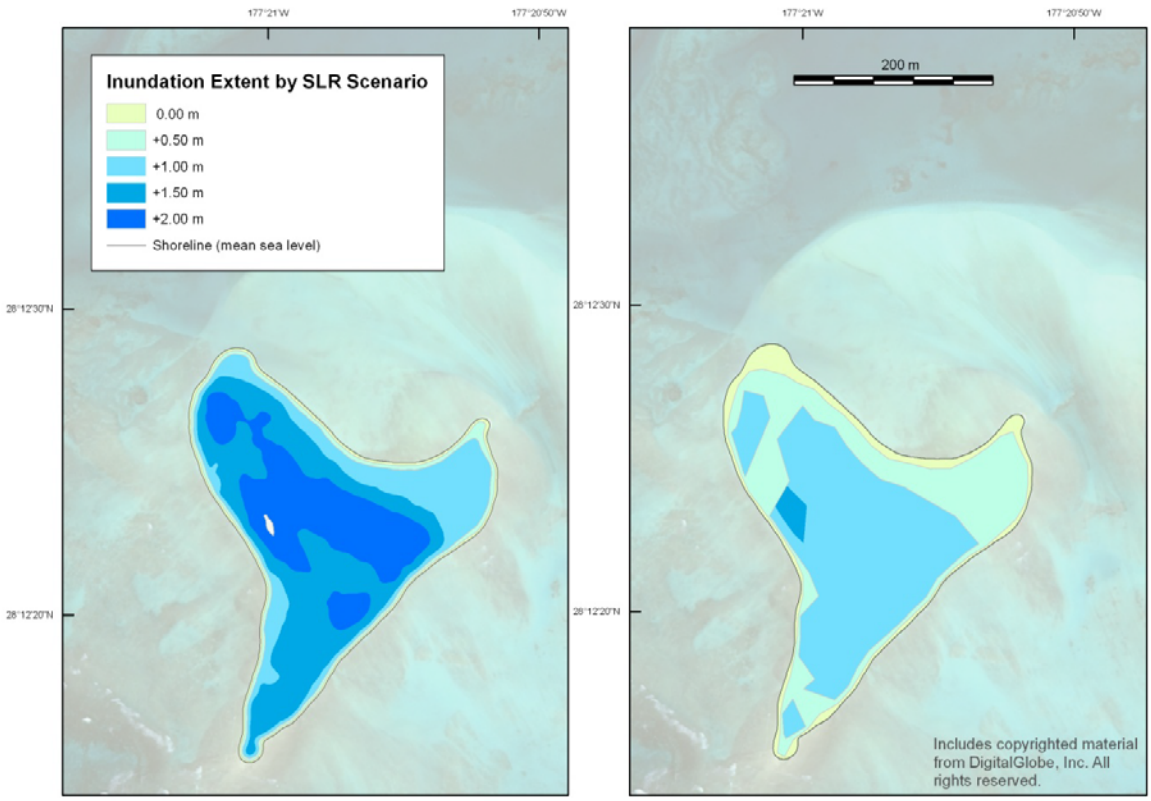

Figure 15. Map of inundation at Spit Island due to both passive (left) and dynamic (right) models for the five sea-level rise (SLR) scenarios (+0.00 m, +0.50 m, +1.00 m, +1.50 m, and +2.00 m) relative to present sea level.

(fig. 19). Similar large increases are also projected for Eastern Island, from 0 and 8 percent inundated at +1.00 m SLR for the passive and dynamic models, respectively, to 12 and 87 percent, respectively, at +2.00 m SLR (fig. 21). Spit Island, because of its low elevations, retains only 25 percent of its vegetated cover classes at +1.50 m SLR for the passive model and loses all of them at +2.00 m SLR; all of its vegetated cover classes are lost at +1.50 m SLR in the dynamic model (fig. 20). By passive modeling, Sand Island is projected to lose less than 1 percent of the area classified as human structures at +1.50 m SLR and only 3 percent at +2.00 m SLR. The dynamic modeling, however, suggests that 3 percent of the area classified as human structures will be inundated at +1.00 m SLR, and almost a third (30 percent) at +2.00 m SLR. Laysan, because of its relatively steep nature, undergoes little change under the passive modeling, losing less than 2 percent of its bare ground even at +2.00 SLR. Just less than 4 percent of bare ground on Laysan is predicted to be inundated at +1.50 m SLR in the dynamic model, but almost 20 percent, or approximately half an order of magnitude more, at +2.00 SLR (fig. 22). Overall, the dynamic modeling predicts, on average, approximately one-half to a full order of magnitude greater inundation of the different land cover classes for a given SLR scenario than is predicted by the passive modeling.

The land cover classes defined for Midway Atoll and Laysan Island are used as wildlife breeding habitat by 25 species, including two endangered endemic passerine species (*Acrocephalus familiaris kingi*, *Telespiza cantans*), an endangered duck (*Anas laysanensis*), 20 other species of Pacific seabirds, the green turtle (*Chelonia mydas*), and the endangered Hawaiian monk seal (*Monachus schauinslandi*). Island-specific species distributions are given in

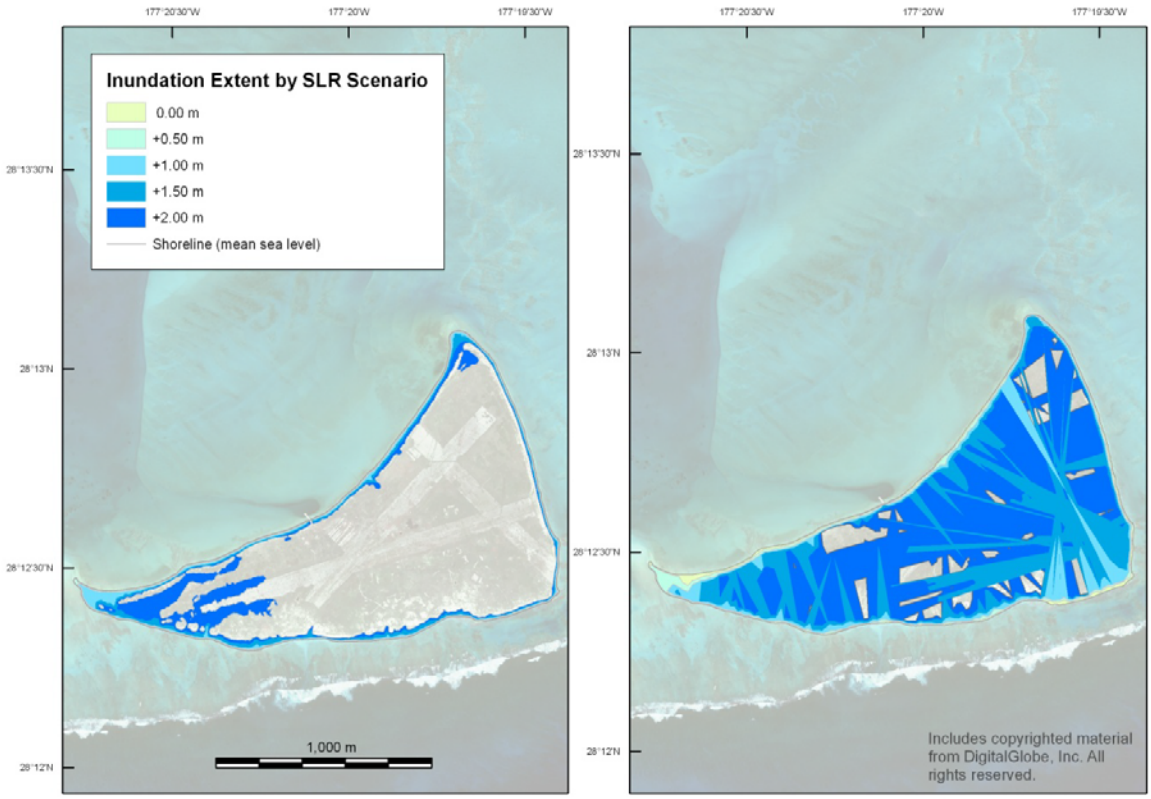

Figure 16. Map of inundation at Eastern Island due to both passive (left) and dynamic (right) models for the five sea-level rise (SLR) scenarios (+0.00 m, +0.50 m, +1.00 m, +1.50 m, and +2.00 m) relative to present sea level.

table 13, and the use of various land-cover classes as habitat is given in table 14.. The distribution of the land cover classes over the four islands is given in table 15. The wildlife habitats included within a land cover class for each island can be used, in conjunction with the data provided in figures 19–22 and tables 5–12, to provide insight into potential habitat loss or inundation impacts to breeding wildlife under both passive and dynamic SLR scenarios. Breeding bird habitat (discussed in detail below) includes all land cover categories except beach, wetland, and human structures.

On Sand Island, the percentage of breeding bird habitat (312. 6 ha) vulnerable to inundation at +1.00 m SLR is 0 and 4.5 percent, respectively, for the passive and dynamic models (tables 5 and 9). At +2.00 m SLR on Sand Island (fig. 19), passive inundation floods 7.6 percent of nesting bird habitat, while dynamic inundation floods 39.9 percent (tables 5 and 9). At Spit Island, bird-breeding habitat (3.9 ha) vulnerable to inundation at +1.00 m SLR is 2.6 and 94.9 percent, respectively, for the passive and dynamic models (tables 6 and 10). At +2.00 m SLR on Spit Island (fig. 19), passive inundation floods 67.2 percent of nesting bird habitat, while dynamic inundation is 100 percent (tables 6 and 10, fig. 20). For Eastern Island, losses in breeding bird habitat (125.4 ha) are also projected, with 0.1 and 6.9 percent inundated at +1.00 m SLR for the passive and dynamic models, respectively (table 7 and 11). At +2.00 m SLR on Eastern Island, passive inundation floods 10.9 percent of nesting bird habitat, while dynamic inundation is 90.1 percent (tables 7 and 11, fig. 21). The breeding bird habitat inundation patterns for Laysan Island with mapped colonies and nest distribution data are reported by Berkowitz and others (2012).

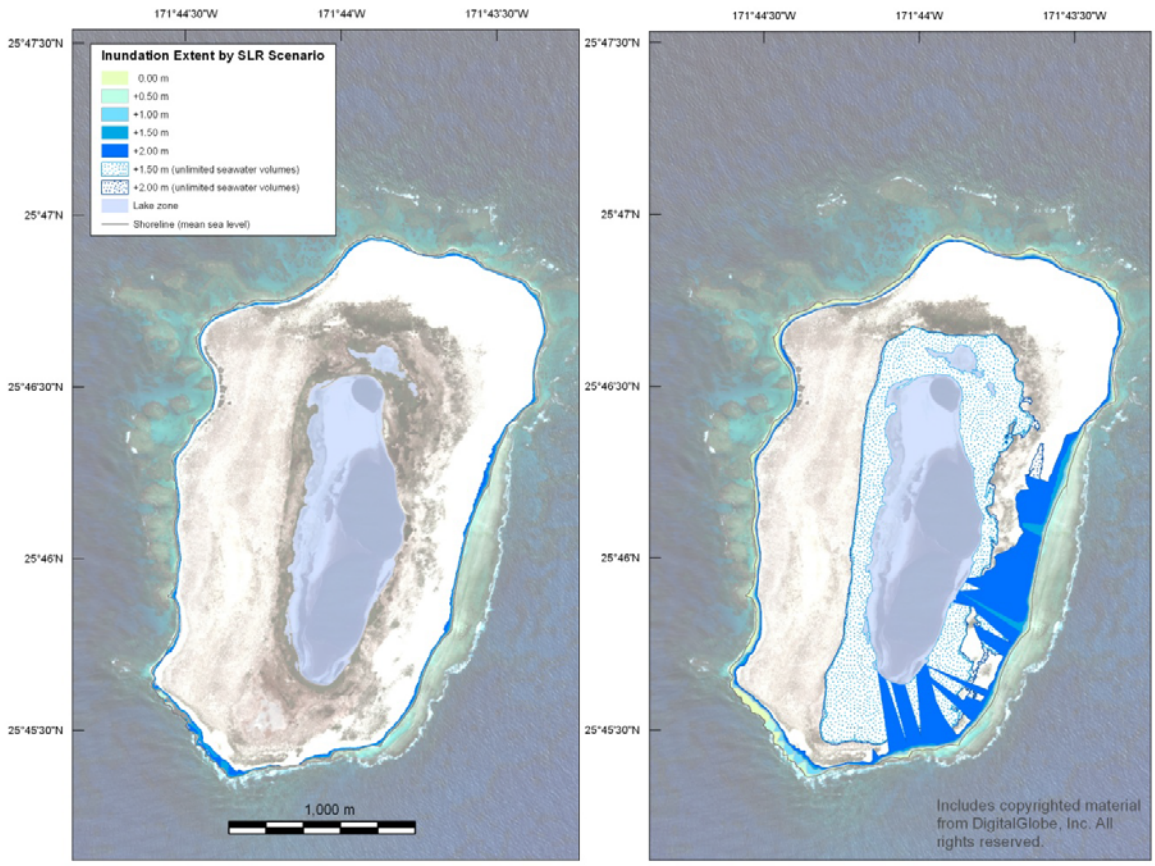

Figure 17. Map of inundation at Laysan Island due to both passive (left) and dynamic (right) models for the five sea-level rise (SLR) scenarios (+0.00 m, +0.50 m, +1.00 m, +1.50 m, and +2.00 m) relative to present sea level.

Discussion

It is apparent that the passive "bathtub" inundation models for sea level rise (SLR) at atolls predict less inundation than the dynamic model that includes wave-driven water levels. This is especially true at higher SLR scenarios, in which SLR reduces wave breaking over the atolls' reef crests, resulting in larger wave heights and longer wave periods at the present-day shoreline, which, in turn, result in greater wave-driven run-up and inundation. These larger run-up values, combined with the background SLR and the relatively low-lying nature of the atoll islands, result in greater inundation for a given SLR scenario than predicted by the passive modeling. These differences between the passive and dynamic models can be viewed two ways. First, more of the atoll islands are projected to be inundated at a given sea level scenario by incorporating wave-driven processes than is predicted by the passive "bathtub" models. In addition, because global sea level is rising, the five scenarios used here basically can be viewed as spanning a spectrum of time in the future, in that a +0.50 m SLR scenario will happen sooner in the future than a +1.00 m SLR scenario. If SLR is therefore somewhat interchangeable with time, then the dynamic model results provided here suggest that a given percentage of the atoll islands and their associated land cover and wildlife habitats will be inundated at lower values of SLR and thus sooner in the future than predicted by the passive "bathtub" models.

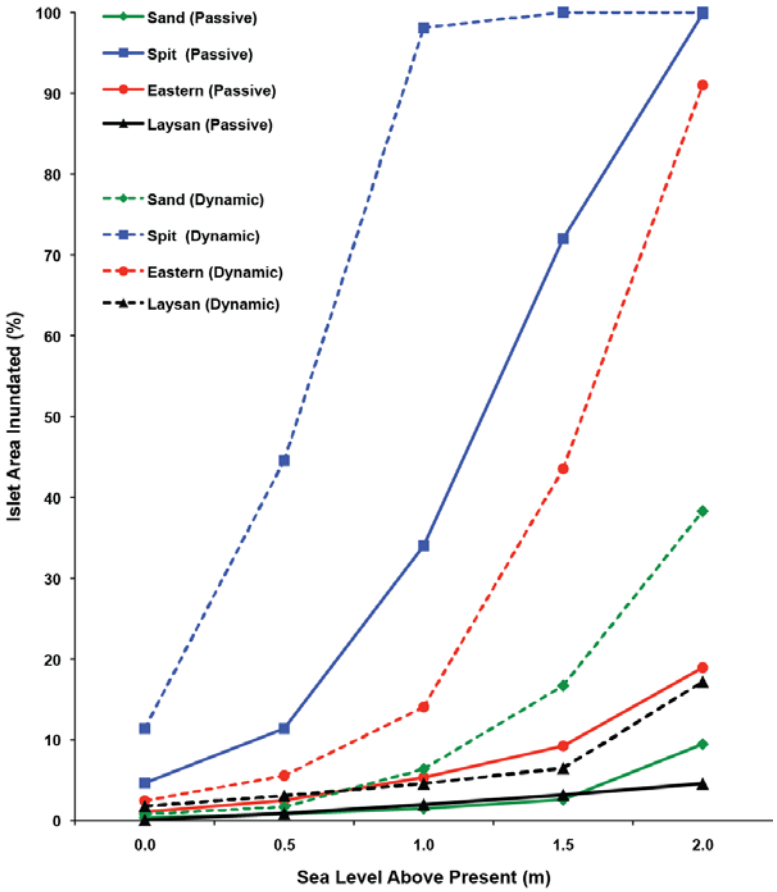

Figure 18. Plot of percentage of land area inundated on the four islands due to both passive (dashed lines) and dynamic (solid lines) models for the five sea-level rise (SLR) scenarios (+0.00 m, +0.50 m, +1.00 m, +1.50 m, and +2.00 m) relative to present sea level.

The results from this modeling study also call attention to the influence of island geomorphology on susceptibility to sea-level rise and wave-induced impacts. Although including wave-driven processes in modeling inundation generally predicted as much as an order of magnitude greater inundation than with the passive "bathtub" methodology, Midway's Sand, Spit, and Eastern Islands were modeled to undergo much greater inundation for a given value of sea-level rise using both types of models than Laysan Island. Midway's islands, on a classic atoll with islands on the shallow atoll rim and a deep central lagoon, are subjected to smaller nearshore wave heights and shorter wavelengths as a result of depth-limited breaking of incident deep-water waves on the shallow reef crests of the atoll's rim. However, because predicted rates of sea-level rise will outstrip new vertical reef flat accretion, the protection of the island's shorelines by depth-limited breaking will be significantly reduced by sea-level rise, resulting in much greater wave heights and wavelengths on the atoll's reef flats than at present. As shown here, larger nearshore wave heights and longer wavelengths would lead to higher wave-driven water levels along the islands' shorelines and thus greater inundation. Laysan, on the other hand, which is characterized by a deep (20–30 m) atoll rim and a central island, allows larger deep-water wave heights to propagate closer to shore than at Midway. Because of this, Laysan is shaped more like a high-energy island with steeper coastal topography and a higher mean elevation than the islands on a classic atoll. This more energetic nearshore wave environment

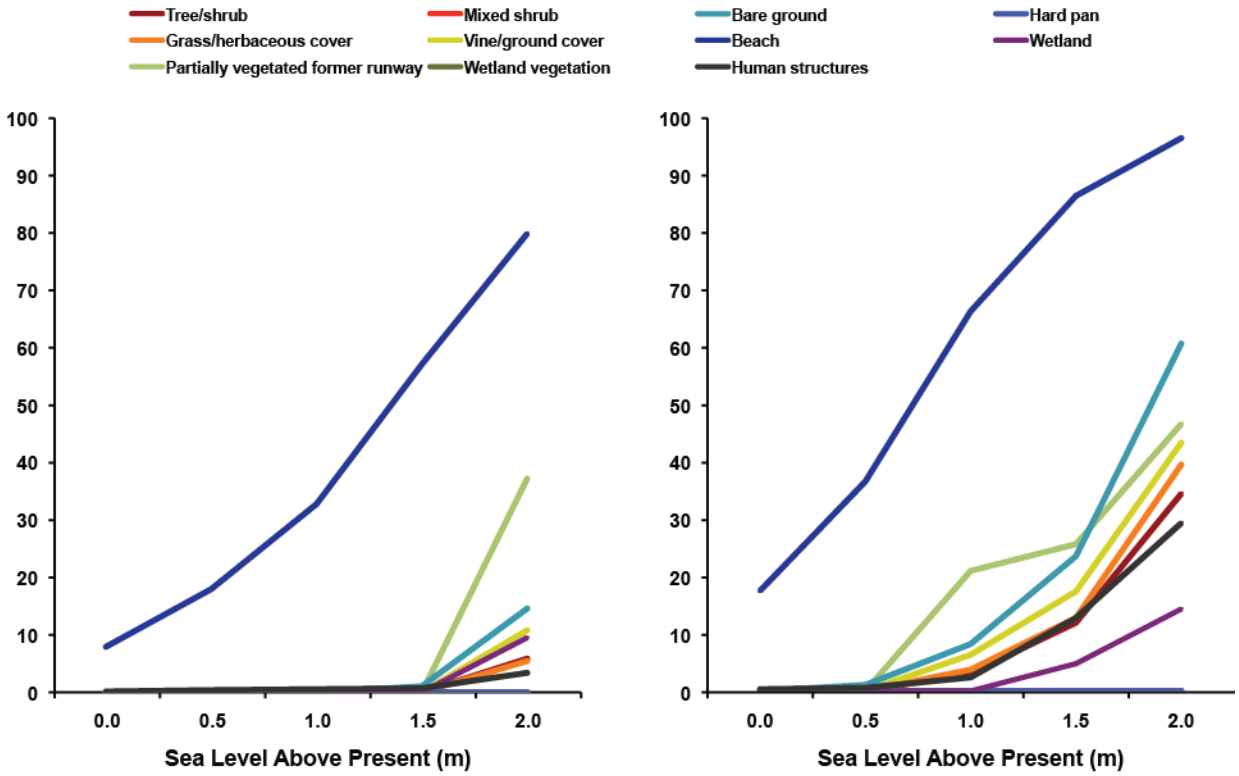

Figure 19. Plot of percentage of land cover classes inundated on Sand Island due to both passive (left) and dynamic (right) models for the five sea-level rise (SLR) scenarios (+0.00 m, +0.50 m, +1.00 m, +1.50 m, and +2.00 m) relative to present sea level.

and resulting steeper and higher coastal topography results in Laysan Island undergoing much less inundation for a given sea-level rise scenario than Midway's Sand, Spit, and Eastern Islands. Together, these modeling results and observations demonstrate that classic atolls with islands on the shallow atoll rim are more susceptible to the combined effects of sea-level rise and wave-driven inundation than islands on atolls characterized by a deep atoll rim.

The wave-driven dynamic inundation models provide insight into the potential inundation that would occur at multiple times during the average year. This is in contrast to a once-in-a-decade inundation event that might allow vegetation and breeding wildlife populations to recover quickly because of its infrequency relative to the rate of vegetation regeneration or wildlife population dynamics (annual breeding cycle). Rather, the use of the top 5 percent of wave conditions predicts events that would occur a few times every year and thus become a part of the natural annual cycle, potentially influencing wildlife distribution or reproductive success of highly philopatric species, which persistently return to the same breeding site and therefore are vulnerable to habitat inundation (Hatfield and others, 2012). As discussed previously, the inundation extents and associated changes in land cover and associated habitats and species provided in this report are not presented as exact values, but rather as values to be compared relative to one another for the different SLR scenarios. For additional details on species vulnerability to sea-level rise and storm events at Laysan Island, see Berkowitz and others (2012).

The effort described here is the first attempt at providing insight into how passive, GIS-based models of SLR impacts on atolls compare to dynamic models that include wave-driven

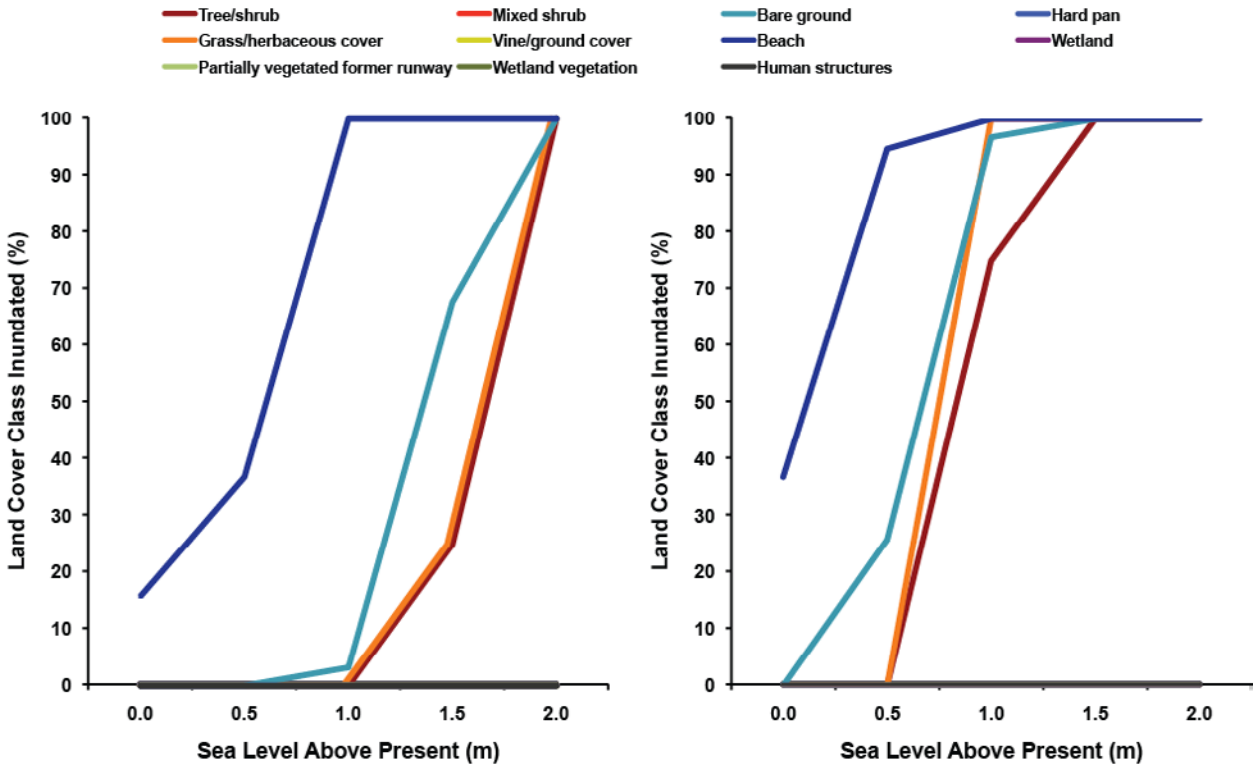

Figure 20. Plot of percentage of land cover classes inundated on Spit Island due to both passive (left) and dynamic (right) models for the five sea-level rise (SLR) scenarios (+0.00 m, +0.50 m, +1.00 m, +1.50 m, and +2.00 m) relative to present sea level.

processes. As discussed earlier, there are a number of issues regarding how these inundation extents were modeled. These issues include the assumptions in the run-up methodology used here, projection of the inundation limits inland, interactions of the run-up with beach morphology and hydrogeology, and potential changes in the future atmospheric and oceanographic forcing. These issues could be addressed in order to model dynamic inundation more accurately. Models that better simulate infragravity wave motions ("surf beat", with periods on the order of 30–300 s), which dominate run-up, and compute run-up water depths and volumes more accurately could be nested in the models developed here to better constrain dynamic inundation and volumes of seawater overwash. Ground-penetrating radar surveys and coring efforts could better constrain the islands' sedimentology and stratigraphy. Such data would be necessary to accurately model the geomorphic evolution of the islands under the SLR scenarios using the models that include a dynamic geomorphic response to changes in waves and water levels. Such information on sedimentology, stratigraphy, and structure would also be necessary, in conjunction with the emplacement of groundwater monitoring wells, to accurately model the influence of SLR and dynamic inundation on the freshwater resources that sustain the islands' vegetation, as well as influence seep and lake water levels (see Tribble, 2008).

Conclusions

Meteorologic and oceanographic forcing were used to model dynamic wave-driven water levels and inundation at Midway Atoll and Laysan Island in the Northwestern Hawaiian Islands for five different sea-level rise (SLR) scenarios and compare the results to passive inundation

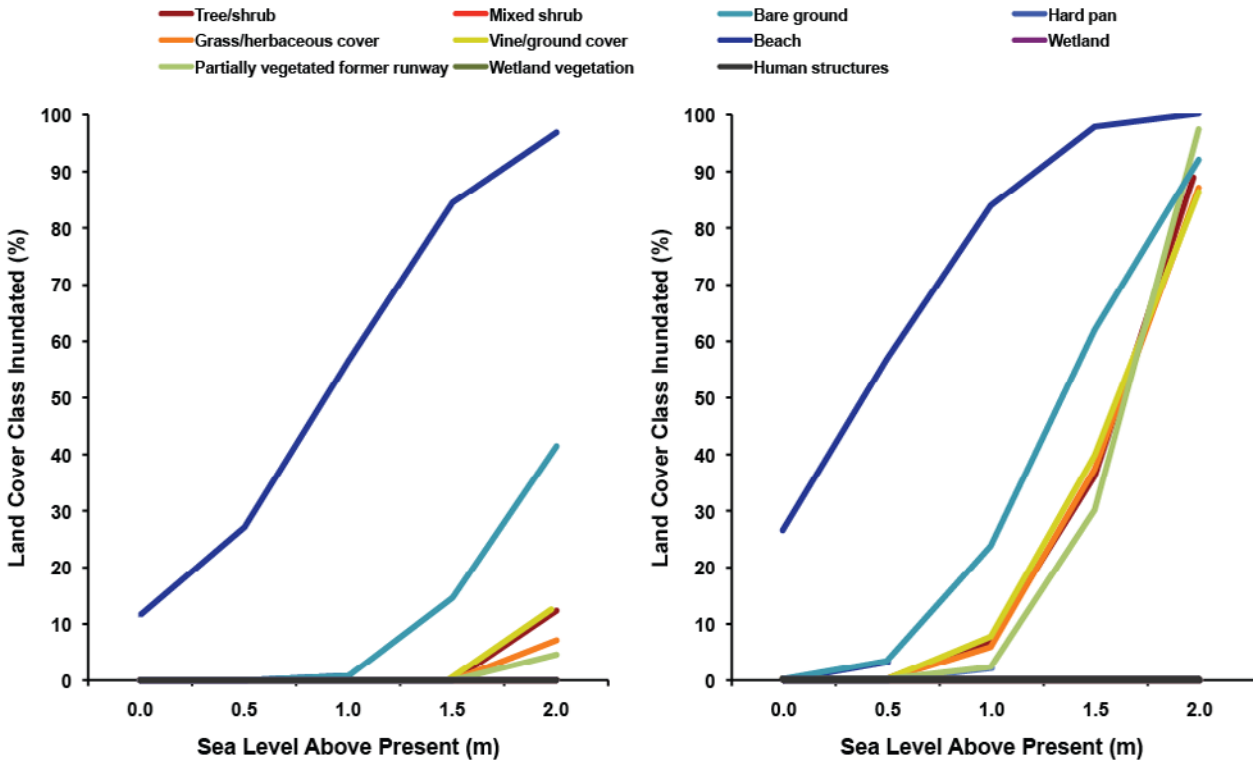

Figure 21. Plot of percentage of land cover classes inundated on Eastern Island due to both passive (left) and dynamic (right) models for the five sea-level rise (SLR) scenarios (+0.00 m, +0.50 m, +1.00 m, +1.50 m, and +2.00 m) relative to present sea level.

modeling of the same islands. Key findings from these modeling efforts and subsequent analyses include:

1. The modeled dynamic wave set-up, run-up, and total wave-driven water levels for all SLR scenarios were greater for North Pacific winter swell conditions than for the summer trade-wind waves. At higher SLR scenarios, less wave breaking on the reef crests resulted in larger waves and longer wavelengths on the islands' shorelines. Although wave-driven set-up decreased at higher SLR scenarios, the increases in wave height and wavelength at higher SLR scenarios resulted in greater wave-driven run-up and thus higher total water levels along the islands' shorelines.

2. Across all SLR scenarios (+0.00, + 0.50, + 1.00, + 1.50, and + 2.00 m), the extent of inundation predicted under the passive modeling approach covered less area than the inundation extent forecasted by the dynamic modeling approach. For the higher SLR scenarios, the dynamic inundation patterns start to diverge considerably from passive inundation patterns, as wave-driven water levels began to exceed existing coastal berms and extend considerable distances inland over low-lying areas.

3. The changes in land cover classes follow similar patterns to the overall patterns of inundation, with all islands losing more of the existing land cover at lower values of future SLR under the dynamic modeling than suggested by the passive modeling. Overall, the dynamic modeling predicts, on average, almost one-half to a full order of magnitude greater inundation of the different land cover classes for a given SLR scenario than is predicted by the passive modeling.

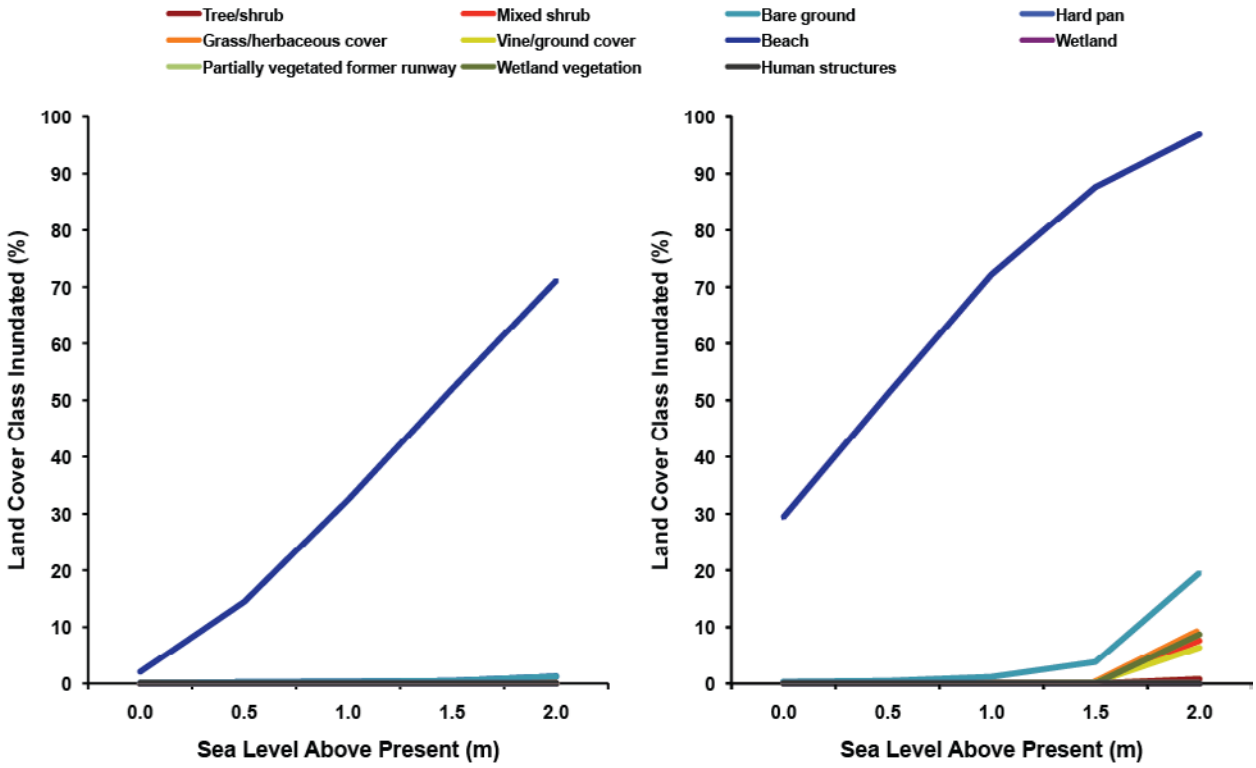

Figure 22. Plot of percentage of land cover classes inundated on Laysan Island due to both passive (left) and dynamic (right) models for the five sea-level rise (SLR) scenarios (+0.00 m, +0.50 m, +1.00 m, +1.50 m, and +2.00 m) relative to relative to present sea level.

4. Assuming that sea level will continue to rise over the next century, the dynamic model results that include wave-driven processes presented here suggest that a given percentage of the atoll islands and their associated habitats will be episodically inundated at lower values of SLR and thus sooner in the future than predicted by the passive "bathtub" models.

5. Observations and the modeling results presented here suggest that classic atolls with islands on the shallow atoll rim are more susceptible to the combined effects of sea-level rise and wave-driven inundation than atolls characterized by a deep atoll rim.

The dynamics of SLR and wave-driven inundation on low-lying atoll islands are complex in nature. The results presented here can provide information to identify the areas of vulnerability specific to each island. These models help display the relative impacts expected to occur, given the current knowledge of these complex systems, and may improve understanding of potential effects on natural resources needed for planning management of the atoll islands in the face of changing climate and sea level.

Acknowledgments

This work was funded by the U.S. Geological Survey's Pacific Coastal and Marine Science Center (USGS-PCMSC), the U.S. Geological Survey's Pacific Islands Ecological Research Center (USGS-PIERC), and the U.S. Fish and Wildlife Service' Inventory and Monitoring Program (USFWS-I&M) under Interagency Agreement F11RG00376 ("Predicting the Impact of Storm Waves and Sea-Level Rise within the Papahānaumokuākea Marine National Monument").

We would like to thank Jean Kenyon (USFWS), the USFWS Hawaiian and Pacific Islands National Wildlife Refuge Complex, and the Papahānaumokuākea Marine National Monument for their overarching support of this project. Edwin Elias (Deltares) provided guidance and help with the Delft3D modeling. Jamie Carter (NOAA) and Karen Courtot (USGS-PIERC) contributed technical assistance. Bruce Richmond and Andrew Stevens (USGS-PCMSC) contributed numerous excellent suggestions and a timely review of our work.

References Cited

Baker, J.D., Littnam, C.L., and Johnston, D.W. 2006, Potential effects of sea-level rise on the terrestrial habitats of endangered and endemic megafauna in the Northestern Hawaiian Islands: Endangered Species Research, v. 4., p. 1–10.

Balazs, G.H., and Chaloupka, M., 2004, Thirty-year recovery trend in the once depleted Hawaiian green sea turtle stock: Biological Conservation, v. 117, p. 491–498.

Battjes, J.A., and Janssen, J.P.F.M., 1978, Energy loss and set- up due to breaking of random waves: Paper presented at 16th International Conference Coastal Engineering, American Society of Civil Engineers, Hamburg, Germany.

Berkowitz, P., Storlazzi, C.D., Courtot, K.N., Krause, C.M., and Reynolds, M.H., 2012, Sea-level rise and wave-driven inundation models for Laysan Island, *in* Reynolds, M.H., Berkowitz, P., Courtot, K.N., and Krause, C.M., eds., 2012, Predicting sea-level rise vulnerability of terrestrial habitat and wildlife of the Northwestern Hawaiian Islands: U.S. Geological Survey Open-File Report 2012–1182, p. 61–124.

Blanchon, P., Eisenhauer, A., Fietzke, J., and Liebetrau, V., 2009, Rapid sea-level rise and reef back-stepping at the close of the last interglacial highstand: Nature, v. 458, p. 881–885.

Booij, N., Ris, R.C., and Holthuijsen, L.H., 1999, A third-generation wave model for coastal regions, Part I. Model description and validation: Journal of Geophysical Research, v. 104, p. 7649–7666.

Boyd, A.J., Stelmach, M.W., Soucie, B.C., and Mainardi, J.A., 2009, Trip report—Laysan Island 24 March 2009 to 19 August 2009: U.S. Fish and Wildlife Service Administrative Report.

Bryan, E.H., 1938, Midway Island, U.S.A.: Paradise of the Pacific, v. 50, no. 6, p. 29–30.

Buddemeier, R.W., and Smith, S.V., 1988, Coral reef growth in an era of rapidly rising sea levels; predictions and suggestions for long-term research: Coral Reefs, v. 7, p. 51–56.

Caires, S., Swail, V.R., and Wang, X.L., 2006, Projections and analysis of extreme wave climate: Journal of Climate, v. 19, p. 5581–5605.

Childs, C., 2004, Interpolating surfaces in ArcGIS Spatial Analyst: ArcUser, July-September, p. 32–35.

Coastal Services Center, 2010, Mapping inundation uncertainty: Charleston, South Carolina, National Oceanic and Atmospheric Administration, Coastal Services Center, 10 p.

Cornett, C., Leopold, D., O'Bryan, J., and Siudzinski, C., 2008, Trip report—Laysan Island 20 March 2008 to 30 September 2008: U.S. Fish and Wildlife Service, Administrative Report.

Deltares, 2012, Delft3D homepage, Wedbsite, accessed at *http://delftsoftware.wldelft.nl/index.php?option=com_content&task=view&id=109*.

Environmental Systems Research Institute, Inc. 2010, ArcGIS 10.0 SP1 software.

Farmer, C., Plentovich, S., Conant, S., Hagerty, R., Kohley, R., Luscomb, P., Wilcox, M., Work, T., Aldeguer, W., Brinck, K., Marshall, A., and Tsukayama, D., 2012, Second Millerbird translocation, 10–25 August 2012. Nihoa and Laysan Islands, Northwest Hawaiian Islands, Papahānaumokuākea Marine National Monument: Honolulu, Hawaii, U.S. Fish and Wildlife Service, Administrative Report.

Field, M.E., Ogston, A.S., and Storlazzi, C.D., 2011, Rising sea level may cause decline of fringing coral reefs: Eos (American Geophysical Union Transactions), v. 92, p. 273–274.

Fletcher, C.H., Richmond, B.M., Barnes, G.M., and Schroeder, T.A., 1995, Marine flooding on the coast of Kaua‘i during Hurricane Iniki; hindcasting inundation components and delineating washover: Journal of Coastal Research, v. 11, no. 1, p. 188–204.

Fredsøe, J., 1984, Turbulent boundary layers in wave-current motion: Journal of Hydraulic Engineering, American Society of Civil Engineering, v. 110, no. 8, p. 1103–1120.

Gesch, D.B., Guiterezz, B.T., and Gill, S.K., 2009, Coastal elevations, *in* Coastal sensitivity to sea level rise; a focus on the Mid-Atlantic region: Washington, D.C., A report by the U.S. Climate Change Science Program and the Subcommittee on Global Change Research, U.S. Environmental Protection Agency, p. 25–42.

Grinsted, A., Moore, J.C., and Jevrejeva, S., 2009, Reconstructing sea level from paleo and projected temperatures 200 to 2100 A.D.: Climate Dynamics, v. 34, no. 4, p. 461–472.

Grothe, P.R., Taylor, L.A., Eakins, B.W., K.S. Carignan, K.S., Lim, E., Warnken, R.R., and Caldwell, R.J., 2010, Digital elevation models of Midway Atoll—procedures, data sources and analysis: Boulder, Colo., National Oceanic and Atmospheric Administration, Technical Memorandum NESDIS NGDC-33, 24 p., accessed at *http://www.ngdc.noaa.gov/dem/squareCellGrid/download/642*.

Hatfield, J., Reynolds, M.H., Seavy, N.E., and Krause, C.M., 2012, Population dynamics of Hawaiian seabird colonies vulnerable to sea-level rise: Conservation Biology, v. 26, no. 4, p. 667–678.

Hoeke, R.K., Storlazzi, C.D., and Ridd, P.V., 2011, Hydrodynamics of a bathymetrically complex fringing coral reef embayment—wave climate, in situ observations and wave prediction: Journal of Geophysical Research–Oceans, v. 166, C04018, doi.*10.1029/2010JC006170*.

Holthuijsen, L.H., Booij, N., and Ris, R.C., 1993, A spectral wave model for the coastal zone: New Orleans, 2nd International Symposium on Ocean Wave Measurement and Analysis, p. 630–641.

Hunt, C.D., and Peterson, F.L., 1980, Groundwater resources of Kwajalein Islands, Marshall Islands: University of Hawaii at Manoa’s Water Resources Research Center Technical Report 126, 101 p.

Intergovernmental Panel on Climate Change, 2007, Climate change 2007—the physical science basis, Solomon, S., Qin, D., Manning, M.,Chen, Z., Marquis, M., Averyt, K.B., Tignor, M., and Miller, H.L., eds., *in* The fourth assessment report (AR4) of the Intergovernmental Panel on Climate Change: Cambridge, United Kingdom, Cambridge University Press, Contribution of Working Group I, 996 p.

Jevrejeva, S., Grinsted, A., and Moore, J.C., 2009, Anthropogenic forcing dominates sea-level rise since 1850: Geophysical Research Letters, v. 36, L20706.

Klavitter, J., 2006, Native plants of Midway Atoll NWR: U.S. Fish and Wildlife Service Report, accessed at *http://www.fws.gov/midway/Midway%20native%20plants.pdf*.

Komen, G., Hasselmann, S., and Hasselmann, K., 1984, On the existence of a fully developed wind-sea spectrum: Journal of Physical Oceanography, v. 14, no. 8, p. 1271–1285.

Krause, C.M., Courtot, K.N., Berkowitz, P., Carter, J., and Reynolds, M.H., 2012, Climate change vulnerability assessment of the low-lying Northwestern Hawaiian Islands, *in* Reynolds, M.H., Berkowitz, P., Courtot, K.N., and Krause, C.M., eds, Predicting sea-level rise vulnerability of terrestrial habitat and wildlife of the Northwestern Hawaiian Islands: U.S. Geological Survey Open-File Report 2012–1182, p. 7–60.

Kristof, A.A., Watson, J.C., Cook, E.L., and Tyhurst, P.C., 2011, Trip report—Laysan Island 8 August 2010 to 30 March 2011: U.S. Fish and Wildlife Service, Administrative Report, 100 p.

LaFever, D.H., Lopez, R.R., Feagin, R.A., and Silvy, N.J., 2007, Predicting the impacts of future sea-level rise on an endangered lagomorph: Environmental Management, v. 40, p. 430,437.

Leuliette, E.W., 2012. Sea level trend map: National Oceanic and Atmospheric Administration Laboratory for Satellite Altimetry sea-level rise products, online data, accessed at *http://ibis.grdl.noaa.gov/SAT/SeaLevelRise/*.

Lowe, R.J., Falter, J.L., Monismith, S.G., and Atkinson, M.J., 2009, A numerical study of circulation in a coastal reef-lagoon system: Journal of Geophysical Research, v. 114, C06022, 18 p.

Madsen, O.S., Poon, Y.-K., and Graber, H.C., 1988, Spectral wave attenuation by bottom friction—theory: American Society of Civil Engineers, 21st International Conference on Coastal Engineering, Torremolinos, Spain.

McDermond, D.K., and Morgan, K.H., 1993, Status and conservation of North Pacific albatrosses, *in* Vermeer, K., Briggs, K.T., Morgan, K.H., and Siegel-Causey, D., eds., The status, ecology and conservation of marine birds of the North Pacific: Canadian Wildlife Service, Special Publication p. 70–81.

Merrifield, M.A., Merrifield, S.T., and Mitchum, G.T., 2009, An anomalous recent acceleration of global SLR: Journal of Climate, v. 22, p. 5772–5781.

Mickler, R., 2009, Sea level rise risk assessment for DoD coastal installations: Department of Defense SERDP Project #08-410 Fact Sheet, accessed at *http://swap-inrmpworkshops.net/files/ClimateChange/Fact_Sheet_Sea_Level_Rise_Risk_Assessment_for_DoD_Coastal_Installations.pdf.*

Milne, G.A., Gehrels, W.R., Hughes, C.W., and Tamisiea, M.E., 2009, Identifying the causes of sea-level change: Nature Geoscience, v. 2, p. 471–478.

Montaggioni, L.F., 2005, History of Indo-Pacific coral reef systems since the last glaciation; development patterns and controlling factors: Earth Science Reviews, v. 71, no.1–2, p. 1–75.

Mori, N., Yasuda, T., Mase, H., Tom, T., and Oku, Y., 2010, Projection of extreme wave climate change under global warming: Hydrological Research Letters, v. 4, p. 15–19

Nicholls, R.J., and Cazenave, A., 2010, Sea-level rise and its impact on coastal zones: Science, v. 328, p. 1517–1520.

National Oceanic and Atmospheric Administration, 2011a, online data, accessed at *http://tidesandcurrents.noaa.gov/*.

National Oceanic and Atmospheric Administration, 2011b. Northwestern Hawaiian Islands lidar validation mission: Honolulu, Hawaii, National Oceanic and Atmospheric Administration, Pacific Services Center, 137 p.

Office of Coast Survey, 2011, National Oceanic and Atmospheric Administration, Online data: Accessed at *http://www.nauticalcharts.noaa.gov/mcd/Raster/*.
Ogston, A.S., and Field, M.E., 2010, Predictions of turbidity due to enhanced sediment resuspension resulting from sea-level rise on a fringing coral reef—evidence from Molokai, HI: Journal of Coastal Research, v. 26, no. 6, p. 1027–1037.
Olson, S.L., 1996, History and ornithological journals of the *Tanager* expedition of 1923 to the Northwestern Hawaiian Islands, Johnston and Wake Islands: Atoll Research Bulletin, v. 433, p. 1–210.
Overpeck, J., Otto-Bliesner, B.L., Miller, G.H., Muhs, D.R., Alley, R.B., and Kiehl, J.T., 2006, Paleoclimatic evidence for future ice-sheet instability and rapid SLR: Science, v. 311, no. 5768, p. 1698–1701.
Pacific Islands Benthic Habitat Mapping Center, 2011, online data: Accessed at *http://www.soest.hawaii.edu/pibhmc/pibhmc_nwhi_lay_bathy.htm*.
Pfeffer, W.T., Harper, J.T., and O'Neel, S., 2008, Kinematic constraints on glacier contributions to 21st-century SLR: Science, v. 321, p. 1340–1343.
Poole, A.F., ed., 2012, The Birds of North America, online report, accessed at *http://bna.birds.cornell.edu/BNA/*.
Rahmstorf, S. 2007, A semi-empirical approach to projecting future SLR: Science, v. 315, no. 5810, p. 368–370.
Reynolds, M.H., Berkowitz, P., Courtot, K.N., and Krause, C.M., eds., 2012, Predicting sea-level rise vulnerability of terrestrial habitat and wildlife of the Northwestern Hawaiian Islands: U.S. Geological Survey Open-File Report 2012–1182, 138 p.
Ris, R.C., Booij, N., and Holthuijsen, L.H., 1999. A third-generation wave model for coastal regions, part II—verification: Journal of Geophysical Research, v. 104, no. 4, p. 7649–7666.
Speulda-Drews, L.A., 2010, Midway Atoll National Wildlife Refuge Historic Preservation Plan 2010: Honolulu, Hawaii, U.S. Fish and Wildlife Service, Midway Atoll National Wildlife Refuge, p. 102 p.
Starr, F., and Martz, K., 1999, S.S. Midway Expedition—trip report: U.S. Fish and Wildlife Service, 35 p.
Starr, F., Martz, K., and Loope, L., 2001, Botanical inventory of Kure Atoll: Prepared for Department of Land and Natural Resources, Division of Forestry and Wildlife, Honolulu, Hawaii.
Starr, F., Starr, K., and Loope, L., 2006, Annotated checklist of the vascular plants on Midway Atoll, Hawaii: An addendum to the 1999 botanical survey of Midway Atoll.
Starr, F., Starr, K., and Loope, L., 2008, Botanical Survey of Midway Atoll: Prepared for the United States Fish and Wildlife Service, 242 p.
Stockdon, H.F., Holman, R.A., Howd, P.A., and Sallenger, A.H., 2006, Empirical parameterization of setup, swash, and runup: Coastal Engineering, v. 53, p. 573–588.
Storlazzi, C.D., and Wingfield, D.K., 2005, The spatial and temporal variability in oceanographic and meteorologic forcing along central California, 1980–2002: U.S. Geological Survey Scientific Investigations Report 2005-5085, 39 p.
Storlazzi, C.D., and Reid, J.A., 2010, The influence of El Niño-Southern Oscillation (ENSO) cycles on wave-driven sea-floor sediment mobility along central California continental margin: Continental Shelf Research, v. 30, p. 1582–1599.

Storlazzi, C.D., Elias, E., Field, M.E., and Presto, M.K., 2011, Numerical modeling of the impact of SLR on fringing coral reef hydrodynamics and sediment transport: Coral Reefs, v. 30, no. 1, p. 83–96.

Tribble, G., 2008, Ground water on tropical Pacific islands—understanding a vital resource: U.S. Geological Survey Circular 1312, 35 p.

U.S. Army Corps of Engineers 2011, Wave model hindcast data: Wave Information Studies, accessed at *http://frf.usace.army.mil/wis2010/wis.shtml*.

Vermeer, M., and Rahmstorf, S., 2009, Global sea level linked to global temperature: Proceedings of the National Academy of Sciences, v.106, no. 51, p. 21527–21532.

Vetter, J., 2012, Nihoa Millerbird monitoring, Laysan Island trip report, March–August 2012, Laysan Island, Northwestern Hawaiian Islands, Papahānaumokuākea Marine National Monument: Honolulu, Hawaii, U.S. Fish and Wildlife Service, Administrative report.

Wagner, W.L., Herbst, D.R., and Lorence, D.H., 2012, Flora of the Hawaiian Islands: Website, accessed March 2012 at: *http://botany.si.edu/pacificislandbiodiversity/hawaiianflora/index.htm*), v. 2012, no. March.

Webb, A.P., and Kench, P.S., 2011, The dynamic response of reef islands to sea-level rise; evidence from multi-decadal analysis of island change in the central Pacific: Global and Planetary Change, v. 72, no. 3, p. 234–246.

Xie, Y., Sha, Z., and Yu, M., 2008, Remote sensing imagery in vegetation mapping; a review: Journal of Plant Ecology, v. 1, p. 9–23.

Additional Digital Information

For more information on the U.S. Geological Survey's Pacific Coastal and Marine Science Center, please see: *http://walrus.wr.usgs.gov/*

For more information on the U.S. Geological Survey's Pacific Island Ecosystem Research Center, please see: *http://www.usgs.gov/ecosystems/pierc/*

Regarding this report, please contact:

Curt D. Storlazzi (USGS Pacific Coral Reef Project chief): *cstorlazzi@usgs.gov*

Tables

Table 1. Descriptions of the land cover classes in the study area**.**

Land cover class	General description	Dominant species included
Tree/shrub	Contiguous tree or shrub cover, multiple native and non-native species of 2–20 meters tall	*Casuarina equisetifolia, Chenopodium oahuense, Coccoloba uvifera, Cocos nucifera, Hibiscus tiliaceus, Pluchea carolinensis, Scaevola taccada, Tournefortia argentea,*
Mixed shrub	Low-density shrub cover with surrounding bare ground or low vegetation, multiple native or non-native species typically less than 2 m tall	*Pluchea indica, Chenopodium oahuense, Coccoloba uvifera, Hibiscus tiliaceus, Pluchea carolinensis, Scaevola taccada, Tournefortia argentea*
Grass/herbaceous cover	High-density grass, bunch grass, and herbaceous cover; multiple native and non-native species	Bidens alba, *Cynodon dactylon*, *Eleusine indica*, *Eragrostis variabilis*, *Euphorbia heterophylla*, *Eustachys petraea*, *Fimbristylis cymosa*, *Lepidium virginicum*, *Lepturus repens*, *Lobularia maritima*, *Pseudognaphalium sandwicensium*, *Psilotum nudum*, *Solanum nelsonii*, *Verbesina encelioides*
Vine/ground cover	Low-lying vines and low herbaceous groundcover, multiple native and non-native species generally less than 0.25 m tall	Vine: *Boerhavia repens*, *Ipomoea indica*, *Ipomoea pes-caprae*; Ground cover: *Portulaca lutea*, *Tribulus cistoides*
Partially vegetated former runway	Dilapidated runway with some vegetation	Fimbristylis cymosa, *Tribulus cistoides*, *Verbesina encelioides*
Wetland vegetation	Wetland plant species surviving in saturated conditions	Cyperus laevigatus, *Cyperus pennatiformis* var. *bryanii*, *Heliotropium currasavicum*, *Sesuvium portulacastrum*
Bare ground	Bare ground inland of beach (without wave swash) used by nesting birds	Unvegetated
Hard pan*	Former guano mining site with no vegetation or minimal low vegetation	Fimbristylis cymosa, *Portulaca spp., Sporobolus pyramidatus*
Beach	Coastal band subject to tidal inundation and wave swash under typical conditions; generally sand, coral or rock not suitable for bird nesting	Unvegetated
Wetland	Standing water, and seasonally inundated unvegetated mudflats	Unvegetated
Human structures	Runways, buildings, roads, seawalls, etc.	Unvegetated

*Classified based on field maps (U.S. Fish and Wildlife Service data).

Table 2. Monthly mean wave heights, wave periods, wave directions, wind speeds, and wind directions for the study area.

[Statistics based on U.S. Army Corps of Engineers (2011) hindcast data for the years 1981–2004 at 28° 00’ N, 174° 00’ W; Std Dev, standard deviation; m, meters; s, seconds]

Time Period	Mean Wave Height (m)	Std.Dev. Wave Height (m)	Mean Wave Period (s)	Std.Dev. Wave Period (s)	Wave Direction (°)	Mean Wind Speed (m/s)	Std.Dev. Wind Speed (m/s)	Wind Direction (°)
January	4.61	1.69	12.5	2.0	317	9.5	3.7	264
February	4.35	1.54	12.5	2.0	316	8.9	3.5	253
March	3.69	1.23	12.2	2.1	324	7.8	3.0	75
April	2.85	0.88	10.8	2.0	354	7.3	2.8	85
May	2.26	0.63	9.9	1.9	4	6.6	2.4	79
June	1.80	0.44	9.7	2.3	59	5.6	2.1	95
July	1.89	0.44	9.5	2.2	107	6.6	2.1	87
August	1.82	0.44	9.9	2.4	115	6.0	2.2	94
September	2.11	0.70	10.2	2.1	6	5.9	2.3	96
October	2.78	0.97	10.9	2.1	354	7.0	2.8	79
November	3.47	1.29	11.6	2.1	349	7.9	3.4	66
December	4.01	1.37	12.4	2.0	327	8.3	3.4	16
Winter (Dec-Feb)	4.32	1.56	12.4	2.0	320	8.9	3.6	262
Spring (Mar-May)	2.94	1.11	11.0	2.2	342	7.2	2.8	81
Summer (Jun-Aug)	1.84	0.44	9.7	2.3	102	6.1	2.2	92
Fall (Sep-Nov)	2.79	1.16	10.9	2.2	354	6.9	3.0	83

Table 3. Monthly top 5 percent wave heights, wave periods, wave directions, wind speeds, and wind directions for the study area.

[Statistics based on U.S. Army Corps of Engineers (2011) hindcast data for the years 1981–2004 at 28° 00’ N, 174° 00’ W; Std Dev, standard deviation; m, meters; s, seconds]

Time Period	Mean Wave Height (m)	Std.Dev. Wave Height (m)	Mean Wave Period (s)	Std.Dev. Wave Period (s)	Wave Direction (°)	Mean Wind Speed (m/s)	Std.Dev. Wind Speed (m/s)	Wind Direction (°)
January	8.99	1.07	15.2	1.5	305	17.6	1.2	271
February	8.61	1.43	15.1	1.7	305	16.9	1.5	269
March	7.08	0.91	15.3	1.9	309	14.4	1.4	319
April	5.28	0.70	12.4	2.0	359	13.4	1.1	53
May	3.94	0.48	11.3	1.8	346	11.6	0.8	56
June	2.96	0.33	10.3	2.1	357	10.1	0.7	65
July	2.99	0.22	8.9	1.2	84	10.8	0.6	76
August	3.03	0.42	10.4	2.1	111	10.1	0.6	83
September	4.20	0.64	12.7	1.7	341	10.8	1.0	94
October	5.51	0.83	12.7	1.7	4	13.3	1.1	50
November	7.01	1.02	13.7	2.0	7	15.4	1.3	36
December	7.65	1.10	14.8	1.9	318	16.0	1.3	297
Winter (Dec-Feb)	8.53	1.23	15.0	1.7	307	16.9	1.4	273
Spring (Mar-May)	6.06	0.97	14.2	2.0	316	13.4	1.3	38
Summer (Jun-Aug)	3.00	0.33	9.8	1.9	71	10.4	0.7	77
Fall (Sep-Nov)	6.06	1.00	13.3	2.0	4	14.0	1.4	43

Table 4. Areal extent and change in area for all islands due to both passive and dynamic scenarios of sea-level rise.

[m, meters; ha, hectares]

Island	Area (ha)	Sea level: +0.00 m		Sea level: +0.50 m		Sea level: +1.00 m		Sea level: +1.50 m		Sea level: +2.00 m	
		Area inundated (ha)	Change (%)	Area inundated (ha)	Change (%)	Area inundated (ha)	Change (%)	Area inundated (ha)	Change (%)	Area inundated (ha)	Change (%)
Passive											
Sand	460.0	1.7	-0.4	3.9	-0.8	6.9	-1.5	12.0	-2.6	43.5	-9.5
Spit	5.8	0.3	-4.7	0.7	-11.4	2.0	-34.0	4.2	-72.0	5.8	-99.8
Eastern	138.4	1.5	-1.1	3.5	-2.5	7.4	-5.4	12.8	-9.2	26.2	-18.9
Laysan	412.0	0.4	-0.1	3.1	-0.9	6.7	-2.0	10.8	-3.2	15.5	-4.6
Dynamic											
Sand	460.0	3.7	-0.8	7.9	-1.7	29.4	-6.4	76.8	-16.7	180.2	-39.2
Spit	5.8	0.7	-11.4	2.6	-44.6	5.7	-98.1	5.8	-100.0	5.8	-100.0
Eastern	138.4	3.4	-2.5	7.7	-5.6	19.5	-14.1	60.3	-43.5	126.0	-91.0
Laysan	412.0	6.1	-1.8	10.5	-3.1	15.5	-4.6	22.1	-6.5	58.0	-17.2

Table 5. Areal extent and change in land cover classes on Sand Island due to passive sea-level rise scenarios.

[m, meters; ha, hectares]

Land cover class	Area (ha)	Sea level: +0.00 m		Sea level: +0.50 m		Sea level: +1.00 m		Sea level: +1.50 m		Sea level: +2.00 m	
		Area inundated (ha)	Change (%)	Area inundated (ha)	Change (%)	Area inundated (ha)	Change (%)	Area inundated (ha)	Change (%)	Area inundated (ha)	Change (%)
Tree/shrub	126.0	0	0	0	0	0	0	0	0	7.4	-5.9
Mixed shrub*	0	0	0	0	0	0	0	0	0	0	0
Grass/herbaceous cover	109.8	0	0	0	0	0	0	0	0	6.0	-5.5
Vine/ground cover	44.4	0	0	0	0	0	0	0	0	4.8	-10.8
Partially vegetated former runway	4.3	0	0	0	0	0	0	0	0	1.6	-37.2
Wetland vegetation	0	0	0	0	0	0	0	0	0	0	0
Bare ground	28.1	0	0	0	0	0	0	0.3	-1.1	4.1	-14.6
Hard pan*	0	0	0	0	0	0	0	0	0	0	0
Beach	18.9	1.5	-7.9	3.4	-18.0	6.2	-32.8	10.8	-57.1	15.1	-79.9
Wetland	2.1	0	0	0	0	0	0	0	0	0.2	-9.5
Human structures	126.5	0.2	-0.2	0.5	-0.4	0.7	-0.6	0.9	-0.7	4.3	-3.4
Total area	460.1	1.7	-0.4	3.9	-0.8	6.9	-1.5	12.0	-2.6	43.5	-9.5

*Landcover classes absent from this island.

Table 6. Areal extent and change in land cover classes on Spit Island due to passive sea-level rise scenarios.

[m, meters; ha, hectares]

Land cover class	Area (ha)	Sea level: +0.00 m		Sea level: +0.50 m		Sea level: +1.00 m		Sea level: +1.50 m		Sea level: +2.00 m	
		Area inundated (ha)	Change (%)	Area inundated (ha)	Change (%)	Area inundated (ha)	Change (%)	Area inundated (ha)	Change (%)	Area inundated (ha)	Change (%)
Tree/shrub	0.4	0	0	0	0	0	0	0.1	-25.0	0.4	-100.0
Mixed shrub*	0	0	0	0	0	0	0	0	0	0	0
Grass/herbaceous cover	0.4	0	0	0	0	0	0	0.1	-25.0	0.4	-100.0
Vine/ground cover	0	0	0	0	0	0	0	0	0	0	0
Partially vegetated former runway*	0	0	0	0	0	0	0	0	0	0	0
Wetland vegetation	0	0	0	0	0	0	0	0	0	0	0
Bare ground	3.1	0	0	0	0	0.1	-3.2	2.1	-67.7	3.1	-100.0
Hard pan*	0	0	0	0	0	0	0	0	0	0	0
Beach	1.9	0.3	-15.8	0.7	-36.8	1.9	-100.0	1.9	-100.0	1.9	-100.0
Wetland	0	0	0	0	0	0	0	0	0	0	0
Human structures*	0	0	0	0	0	0	0	0	0	0	0
Total area	5.8	0.3	-5.2	0.7	-12.1	2.0	-34.5	4.2	-72.4	5.8	-100.0

*Landcover classes absent from this island.

Table 7. Areal extent and change in land cover classes on Eastern Island due to passive sea-level rise scenarios.

[m, meters; ha, hectares]

Land cover class	Area (ha)	Sea level: +0.00 m		Sea level: +0.50 m		Sea level: +1.00 m		Sea level: +1.50 m		Sea level: +2.00 m	
		Area inundated (ha)	Change (%)	Area inundated (ha)	Change (%)	Area inundated (ha)	Change (%)	Area inundated (ha)	Change (%)	Area inundated (ha)	Change (%)
Tree/shrub	8.9	0	0	0	0	0	0	0	0	1.1	-12.4
Mixed shrub*	0	0	0	0	0	0	0	0	0	0	0
Grass/herbaceous cover	55.9	0	0	0	0	0	0	0	0	4	-7.2
Vine/ground cover	15.9	0	0	0	0	0	0	0	0	2	-12.6
Partially vegetated former runway	32.4	0	0	0	0	0	0	0	0	1.5	-4.6
Wetland vegetation	0	0	0	0	0	0	0	0	0	0	0
Bare ground	12.3	0	0	0	0	0.1	-0.8	1.8	-14.6	5.1	-41.5
Hard pan*	0	0	0	0	0	0	0	0	0	0	0
Beach	12.9	1.5	-11.6	3.5	-27.1	7.3	-56.6	10.9	-84.5	12.5	-96.9
Wetland	0	0	0	0	0	0	0	0	0	0	0
Human structures	0	0	0	0	0	0	0	0	0	0	0
Total area	138.3	1.5	-1.1	3.5	-2.5	7.4	-5.4	12.7	-9.2	26.2	-18.9

*Landcover classes absent from this island.

Table 8. Areal extent and change in land cover classes on Laysan Island due to passive sea-level rise scenarios.

[m, meters; ha, hectares]

Land cover class	Area (ha)	Sea level: +0.00 m		Sea level: +0.50 m		Sea level: +1.00 m		Sea level: +1.50 m		Sea level: +2.00 m	
		Area inundated (ha)	Change (%)	Area inundated (ha)	Change (%)	Area inundated (ha)	Change (%)	Area inundated (ha)	Change (%)	Area inundated (ha)	Change (%)
Tree/shrub	13.0	0	0	0	0	0	0	0	0	0	0
Mixed shrub	26.3	0	0	0	0	0	0	0	0	0	0
Grass/herbaceous cover	74.8	0	0	0	0	0	0	0	0	0	0
Vine/ground cover	58.0	0	0	0	0	0	0	0	0	0	0
Partially vegetated former runway*	0	0	0	0	0	0	0	0	0	0	0
Wetland vegetation	13.8	0	0	0	0	0	0	0	0	0	0
Bare ground	129.3	0.1	0	0.3	-0.2	0.4	-0.3	0.6	-0.5	1.6	-1.3
Hard pan	3.1	0	0	0	0	0	0	0	0	0	0
Beach	19.4	0.4	-1.9	2.8	-14.5	6.3	-32.3	10.1	-52.3	13.8	-71.3
Wetland*†	74.2	0	0	0	0	0	0	0	0	0	0
Human structure	0	0	0	0	0	0	0	0	0	0	0
Total area	412.0	0.4	-0.1	3.1	-0.8	6.7	-1.6	10.8	-2.6	15.5	-3.8

*Landcover classes absent from this island.

†Includes unvegetated mudflats that were exposed at the time of classification.

Table 9. Areal extent and change in land cover classes on Sand Island due to dynamic sea-level rise scenarios.

[m, meters; ha, hectares]

Land cover class	Area (ha)	Sea level: +0.00 m		Sea level: +0.50 m		Sea level: +1.00 m		Sea level: +1.50 m		Sea level: +2.00 m	
		Area inundated (ha)	Change (%)	Area inundated (ha)	Change (%)	Area inundated (ha)	Change (%)	Area inundated (ha)	Change (%)	Area inundated (ha)	Change (%)
Tree/shrub	126.0	0	0	0	0	3.9	-3.1	15.0	-11.9	43.3	-34.4
Mixed shrub*	0	0	0	0	0	0	0	0	0	0	0
Grass/herbaceous cover	109.8	0	0	0	0	4.1	-3.7	14.0	-12.8	43.3	-39.4
Vine/ground cover	44.4	0	0	0	0	2.8	-6.3	7.7	-17.3	19.2	-43.2
Partially vegetated former runway	4.3	0	0	0	0	0.9	-20.9	1.1	-25.6	2.0	-46.5
Wetland vegetation	0	0	0	0	0	0	0	0	0	0	0
Bare ground	28.1	0	0	0.3	-1.1	2.3	-8.2	6.6	-23.5	17.0	-60.5
Hard pan*	0	0	0	0	0	0	0	0	0	0	0
Beach	18.9	3.3	-17.5	6.9	-36.5	12.5	-66.1	16.3	-86.2	18.2	-96.3
Wetland	2.1	0	0	0	0	0	0	0.1	-4.8	0.3	-14.3
Human structures	126.5	0.4	-0.3	0.7	-0.6	3.0	-2.4	16.1	-12.7	37	-29.2
Total area	460.1	3.7	-0.8	7.9	-1.7	29.5	-6.4	76.9	-16.7	180.3	-39.2

*Landcover classes absent from this island.

Table 10. Areal extent and change in land cover classes on Spit Island due to dynamic sea-level rise scenarios.

[m, meters; ha, hectares]

Land cover class	Area (ha)	Sea level: +0.00 m		Sea level: +0.50 m		Sea level: +1.00 m		Sea level: +1.50 m		Sea level: +2.00 m	
		Area inundated (ha)	Change (%)	Area inundated (ha)	Change (%)	Area inundated (ha)	Change (%)	Area inundated (ha)	Change (%)	Area inundated (ha)	Change (%)
Tree/shrub	0.4	0	0	0	0	0.3	-75.0	0.4	-100.0	0.4	-100.0
Mixed shrub*	0	0	0	0	0	0	0	0	0	0	0
Grass/herbaceous cover	0.4	0	0	0	0	0.4	-100.0	0.4	-100.0	0.4	-100.0
Vine/ground cover	0	0	0	0	0	0	0	0	0	0	0
Partially vegetated former runway*	0	0	0	0	0	0	0	0	0	0	0
Wetland vegetation	0	0	0	0	0	0	0	0	0	0	0
Bare ground	3.1	0	0	0.8	-25.8	3	-96.8	3.1	-100.0	3.1	-100.0
Hard pan*	0	0	0	0	0	0	0	0	0	0	0
Beach	1.9	0.7	-36.8	1.8	-94.7	1.9	-100.0	1.9	-100.0	1.9	-100.0
Wetland	0	0	0	0	0	0	0	0	0	0	0
Human structures*	0	0	0	0	0	0	0	0	0	0	0
Total area	5.8	0.7	-12.1	2.6	-44.8	5.6	-96.6	5.8	-100.0	5.8	-100.0

*Landcover classes absent from this island.

Table 11. Areal extent and change in land cover classes on Eastern Island due to dynamic sea-level rise scenarios.

[m, meters; ha, hectares]

Land cover class	Area (ha)	Sea level: +0.00 m		Sea level: +0.50 m		Sea level: +1.00 m		Sea level: +1.50 m		Sea level: +2.00 m	
		Area inundated (ha)	Change (%)	Area inundated (ha)	Change (%)	Area inundated (ha)	Change (%)	Area inundated (ha)	Change (%)	Area inundated (ha)	Change (%)
Tree/shrub	8.9	0	0	0	0	0.6	-6.7	3.2	-36.0	7.9	-88.8
Mixed shrub*	0	0	0	0	0	0	0	0	0	0	0
Grass/herbaceous cover	55.9	0	0	0	0	3.2	-5.7	20.8	-37.2	48.6	-86.9
Vine/ground cover	15.9	0	0	0	0	1.2	-7.5	6.3	-39.6	13.7	-86.2
Partially vegetated former runway	32.4	0	0	0	0	0.7	-2.2	9.7	-29.9	31.5	-97.2
Wetland vegetation	0	0	0	0	0	0	0	0	0	0	0
Bare ground	12.3	0	0	0.4	-3.3	2.9	-23.6	7.6	-61.8	11.3	-91.9
Hard pan*	0	0	0	0	0	0	0	0	0	0	0
Beach	12.9	3.4	-26.4	7.3	-56.6	10.8	-83.7	12.6	-97.7	12.9	-100.0
Wetland	0	0	0	0	0	0	0	0	0	0	0
Human structures	0	0	0	0	0	0	0	0	0	0	0
Total area	138.3	3.4	-2.5	7.7	-5.6	19.4	-14	60.2	-43.5	125.9	-91.0

*Landcover classes absent from this island.

Table 12. Areal extent and change in land cover classes on Laysan Island due to dynamic sea-level rise scenarios.

[m, meters; ha, hectares]

Land cover class	Area (ha)	Sea level: +0.00 m		Sea level: +0.50 m		Sea level: +1.00 m		Sea level: +1.50 m		Sea level: +2.00 m	
		Area inundated (ha)	Change (%)	Area inundated (ha)	Change (%)	Area inundated (ha)	Change (%)	Area inundated (ha)	Change (%)	Area inundated (ha)	Change (%)
Tree/shrub	13.0	0	0	0	0	0	0	0	0	0.1	-0.8
Mixed shrub	26.3	0	0	0	0	0	0	0	0	2.0	-7.6
Grass/herbaceous cover	74.8	0	0	0	0	0	0	0.1	-0.1	6.9	-9.3
Vine/ground cover	58.0	0	0	0	0	0	0	0.1	-0.1	3.7	-6.3
Partially vegetated former runway*	0	0	0	0	0	0	0	0	0	0	0
Wetland vegetation	13.8	0	0	0	0	0	0	0	0	1.2	-8.4
Bare ground	129.3	0.4	-0.3	0.6	-0.5	1.5	-1.1	4.9	-3.8	25.2	-19.5
Hard pan	3.1	0	0	0	0	0	0	0	0	0	0
Beach	19.4	5.7	-29.4	9.9	-51.0	14.0	-72.2	17.0	-87.8	18.8	-96.6
Wetland*†	74.2	0	0	0	0	0	0	0	0	0	0
Human structures	0	0	0	0	0	0	0	0	0	0	0
Total area	412.0	6.1	-1.5	10.5	-2.5	15.5	-3.8	22.1	-5.4	57.9	-14.1

*Landcover classes absent from this island.

†Includes unvegetated mudflats that were exposed at the time of classification.

Table 13. Distribution of species by island.

Species	Scientific name	Sand	Spit	Eastern	Laysan
Black-footed Albatross	*Phoebastria nigripes*	X	X	X	X
Laysan Albatross	*Phoebastria immutabilis*	X	X	X	X
Short-tailed Albatross	*Phoebastria albatrus*			X	
Bonin Petrel	*Pterodroma hypoleuca*	X	X	X	X
Bulwer's Petrel	*Bulweria bulwerii*				X
Wedge-tailed Shearwater	*Puffinus pacificus*	X		X	X
Christmas Shearwater	*Puffinus nativitatis*			X	X
Tristram's Storm-petrel	*Oceanodroma tristrami*				X
Red-tailed Tropicbird	*Phaethon rubricauda rubricauda*	X	X	X	X
White-tailed Tropicbird	*Phaethon lepturus dorotheae*	X			
Masked Booby	*Sula dactylatra personata*			X	X
Brown Booby	*Sula leucogaster plotus*			X	X
Red-footed Booby	*Sula sula rubripes*		X	X	X
Great Frigatebird	*Fregata minor palmerstoni*		X	X	X
Little Tern	*Sternula albifrons*	X			
Least Tern	*Sternula antillarum*	X			
Gray-backed Tern	*Onychoprion lunatus*		X	X	X
Sooty Tern	*Onychoprion fuscata oahuensis*			X	X
Brown Noddy	*Anous stolidus pileatus*	X	X	X	X
Black Noddy	*Anous minutus marcusi*	X		X	X
White Tern	*Gygis alba candida*	X	X	X	X
Laysan Teal	*Anas laysanensis*	X		X	X
Laysan Finch	*Telespiza cantans*				X
Nihoa Millerbird*	*Acrocephalus familiaris kingi*				X
Hawaiian monk seal	*Monachus schauinslandi*	X	X	X	X
Hawaiian green turtle†	*Chelonia mydas*	X	X	X	X

*Individuals translocated to Laysan Island in September 2011 and 2012 with successful breeding in 2012 (Farmer and others, 2012; Vetter, 2012).

†Hawaiian green turtle population comprises a unique genetic stock (Balazs and Chaloupka, 2004).

Table 14. Species use by land cover classes.

Species	Tree/ shrub	Mixed shrub	Grass/ herbaceous cover	Vine/ ground cover	Partially vegetated former runway	Wetland vegetation	Bare ground	Hard pan	Beach	Wetland	Human structures
Black-footed Albatross	X	X	X	X	X	X	X				
Laysan Albatross	X	X	X	X	X	X	X	X			
Short-tailed Albatross			X	X							
Bonin Petrel	X	X	X	X							
Bulwer's Petrel							X				
Wedge-tailed Shearwater	X	X	X	X			X				
Christmas Shearwater	X	X	X	X	X						
Tristram's Storm-petrel	X	X	X	X			X				
Red-tailed Tropicbird	X	X	X								
White-tailed Tropicbird	X										
Masked Booby			X	X			X	X			
Brown Booby			X	X			X				
Red-footed Booby	X	X									
Great Frigatebird	X	X									
Little Tern			X	X			X				
Least Tern			X	X			X				
Gray-backed Tern				X	X		X	X			
Sooty Tern			X	X	X		X				
Brown Noddy	X	X	X	X	X		X				
Black Noddy	X	X									X
White Tern	X	X									
Laysan Teal	X	X	X	X							
Laysan Finch	X	X	X	X							
Nihoa Millerbird*	X	X	X	X							
Hawaiian monk seal							X		X		
Hawaiian green turtle							X		X		

*Expected and confirmed habitat use from newly translocated populations to Laysan Island.

Table 15. Land cover classes by island.

[Some land cover classes may exist on islands but are not included in tables 5-12 when the class covers an area less than 0.1 hectare]

Land Cover	Sand	Spit	Eastern	Laysan
Tree/shrub	X	X	X	X
Mixed shrub*				X
Grass/herbaceous cover	X	X	X	X
Vine/ground cover	X		X	X
Partially vegetated former runway	X		X	
Wetland vegetation				X
Bare ground	X	X	X	X
Hard pan				X
Beach	X	X	X	X
Wetland	X			X
Human structures	X			

*Mixed shrub not classified at Midway Atoll due to limitations in image resolution and field-mapping data.

Appendix 1. Maps of Significant Wave Height Around the Atoll Islands.

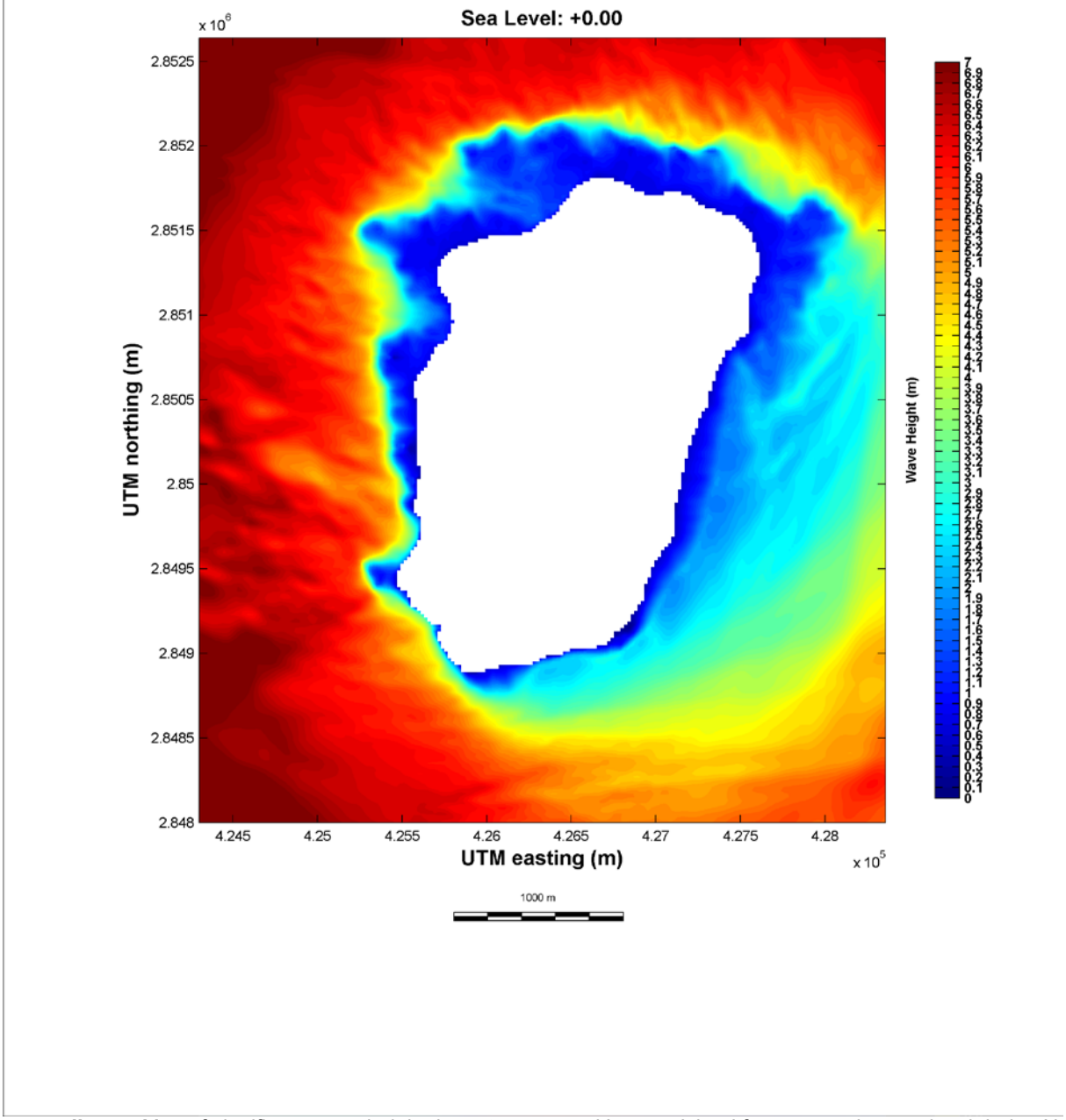

Appendix 1.1. Map of significant wave height, in meters, around Laysan Island for present-day sea level during North Pacific winter conditions.

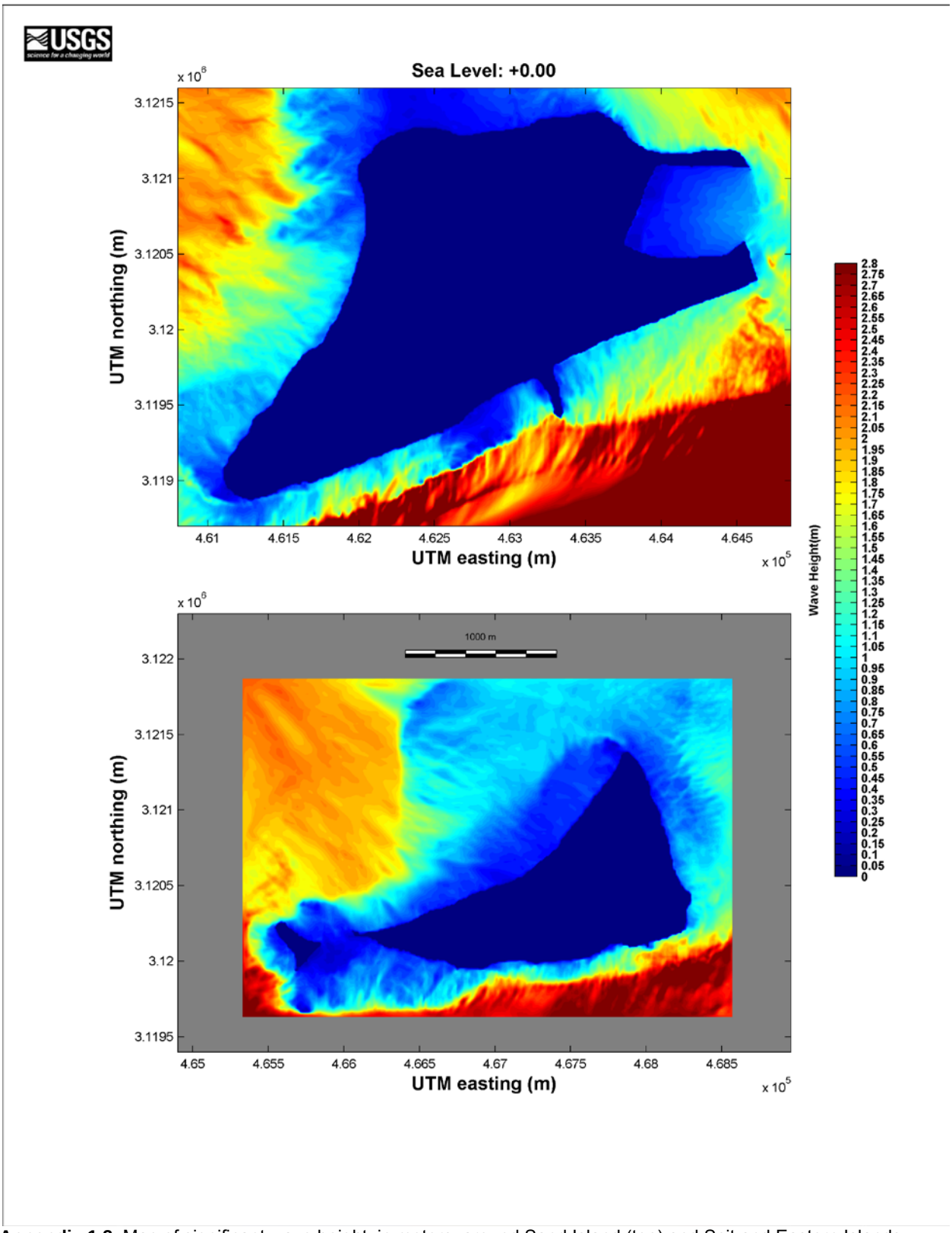

Appendix 1.2. Map of significant wave height, in meters, around Sand Island (top) and Spit and Eastern Islands (bottom) for present-day sea level during North Pacific winter conditions.

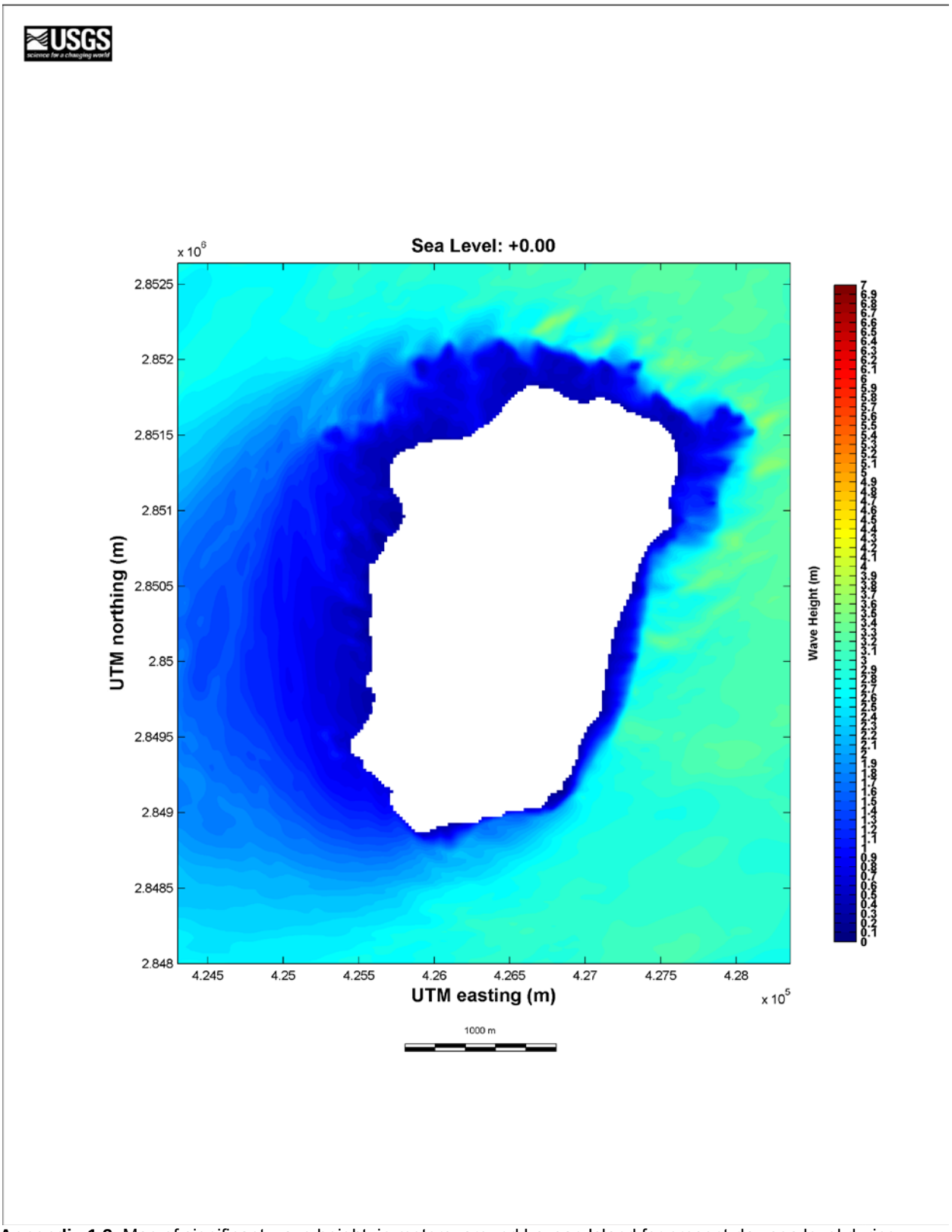

Appendix 1.3. Map of significant wave height, in meters, around Laysan Island for present-day sea level during summer trade-wind conditions.

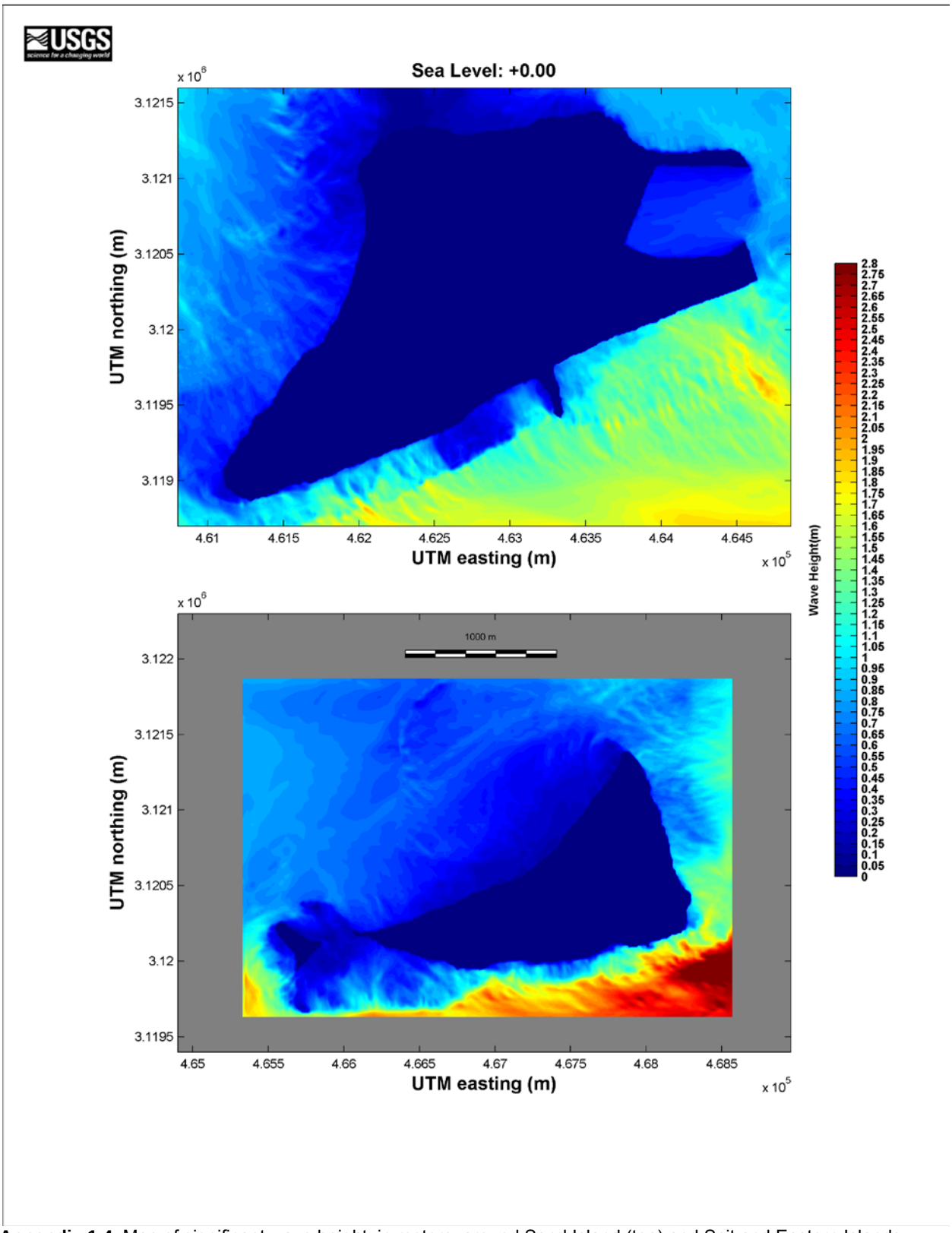

Appendix 1.4. Map of significant wave height, in meters, around Sand Island (top) and Spit and Eastern Islands (bottom) for present-day sea level during summer trade-wind conditions.

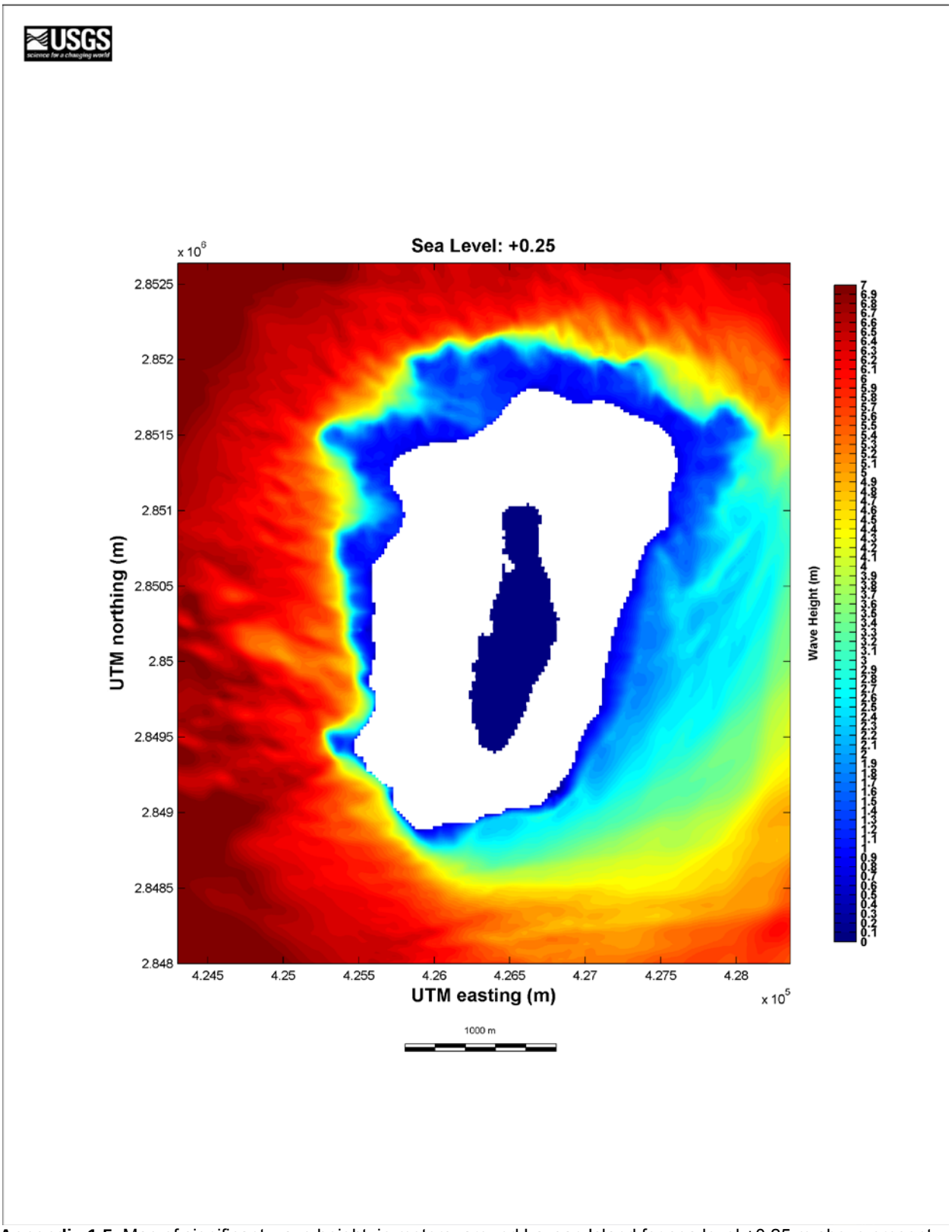

Appendix 1.5. Map of significant wave height, in meters, around Laysan Island for sea level +0.25 m above present during North Pacific winter conditions.

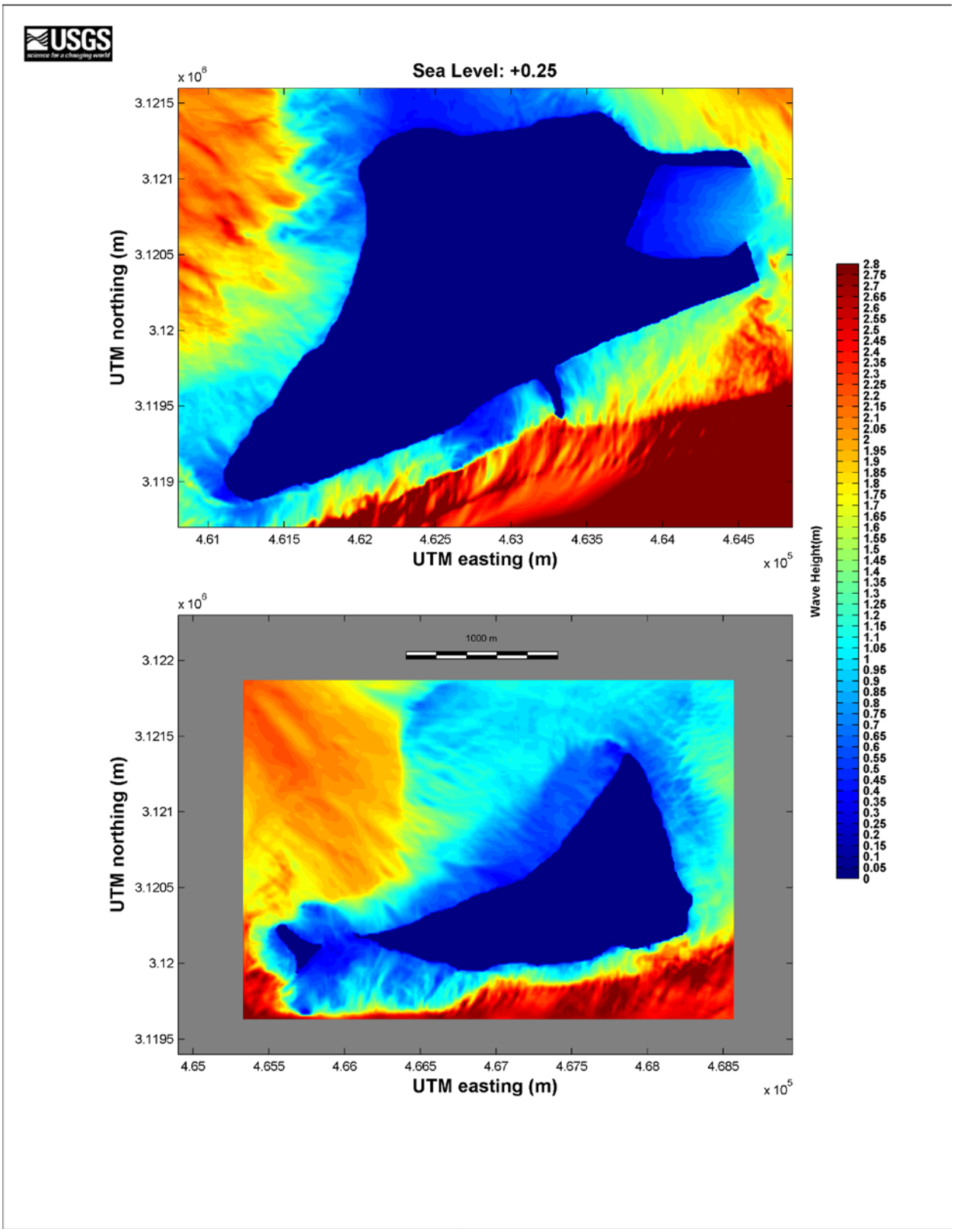

Appendix 1.6. Map of significant wave height, in meters, around Sand Island (top) and Spit and Eastern Islands (bottom) for sea level +0.25 m above present during North Pacific winter conditions.

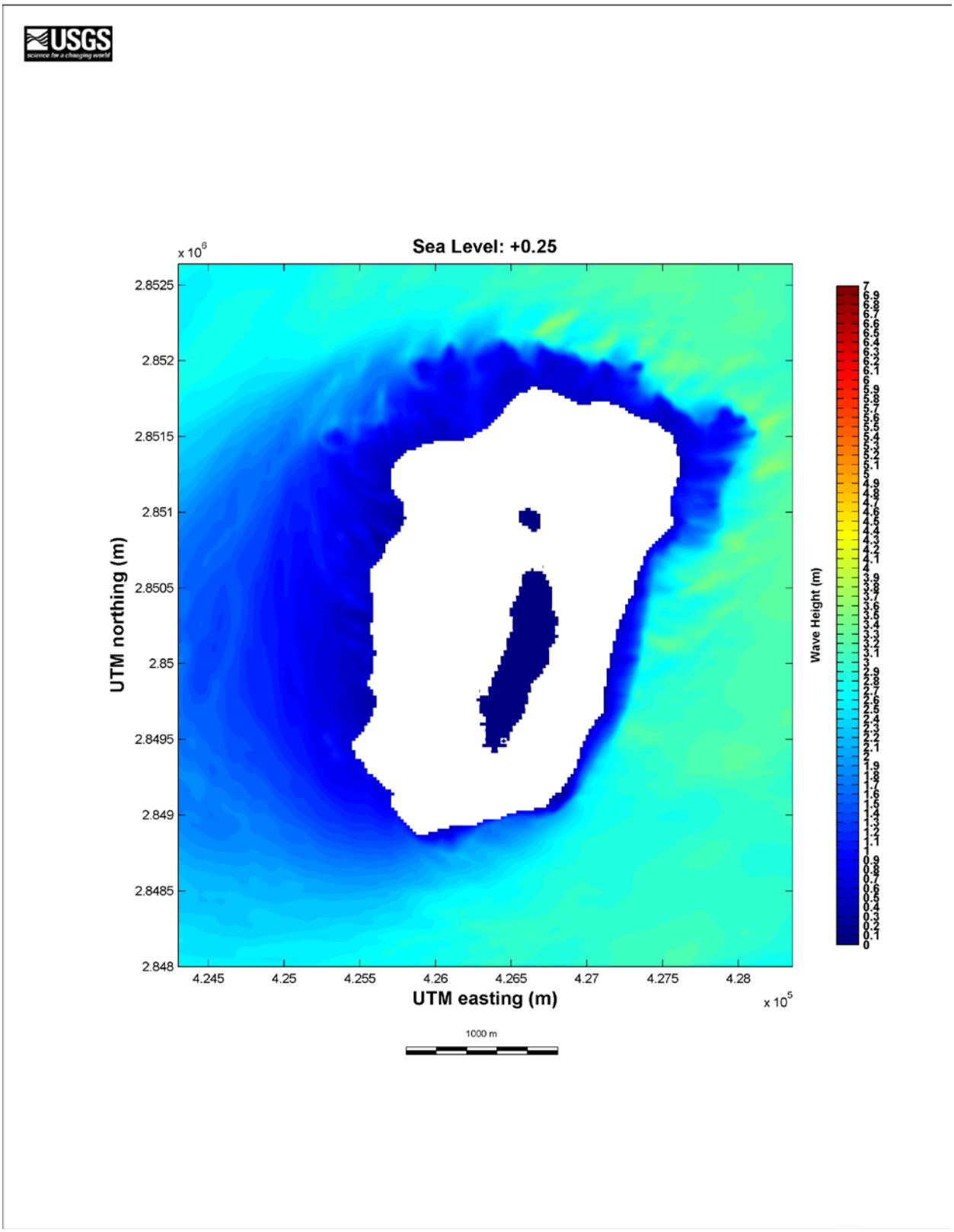

Appendix 1.7. Map of significant wave height, in meters, around Laysan Island sea level +0.25 m above present during summer trade-wind conditions.

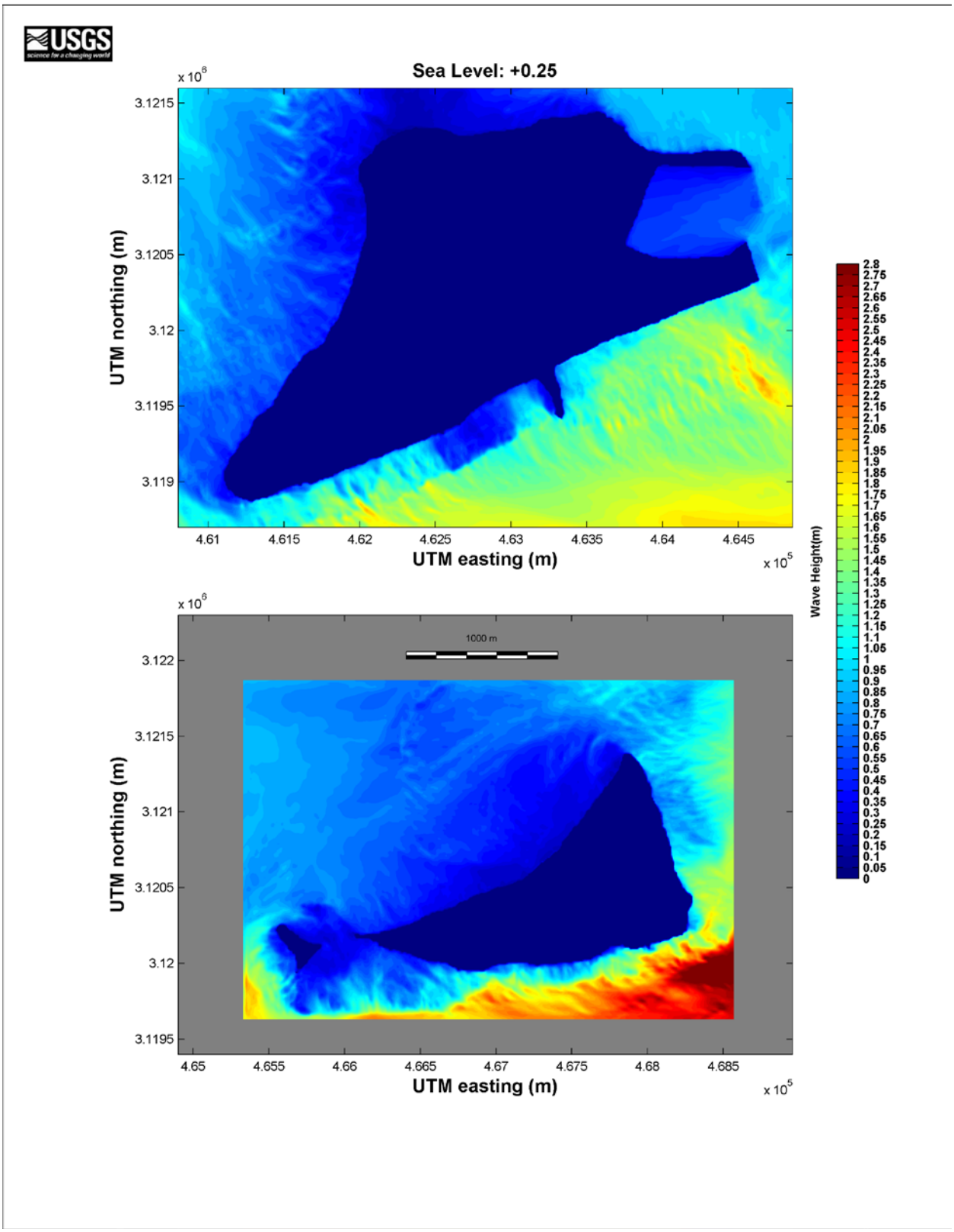

Appendix 1.8. Map of significant wave height, in meters, around Sand Island (top) and Spit and Eastern Islands (bottom) for sea level +0.25 m above present during summer trade-wind conditions.

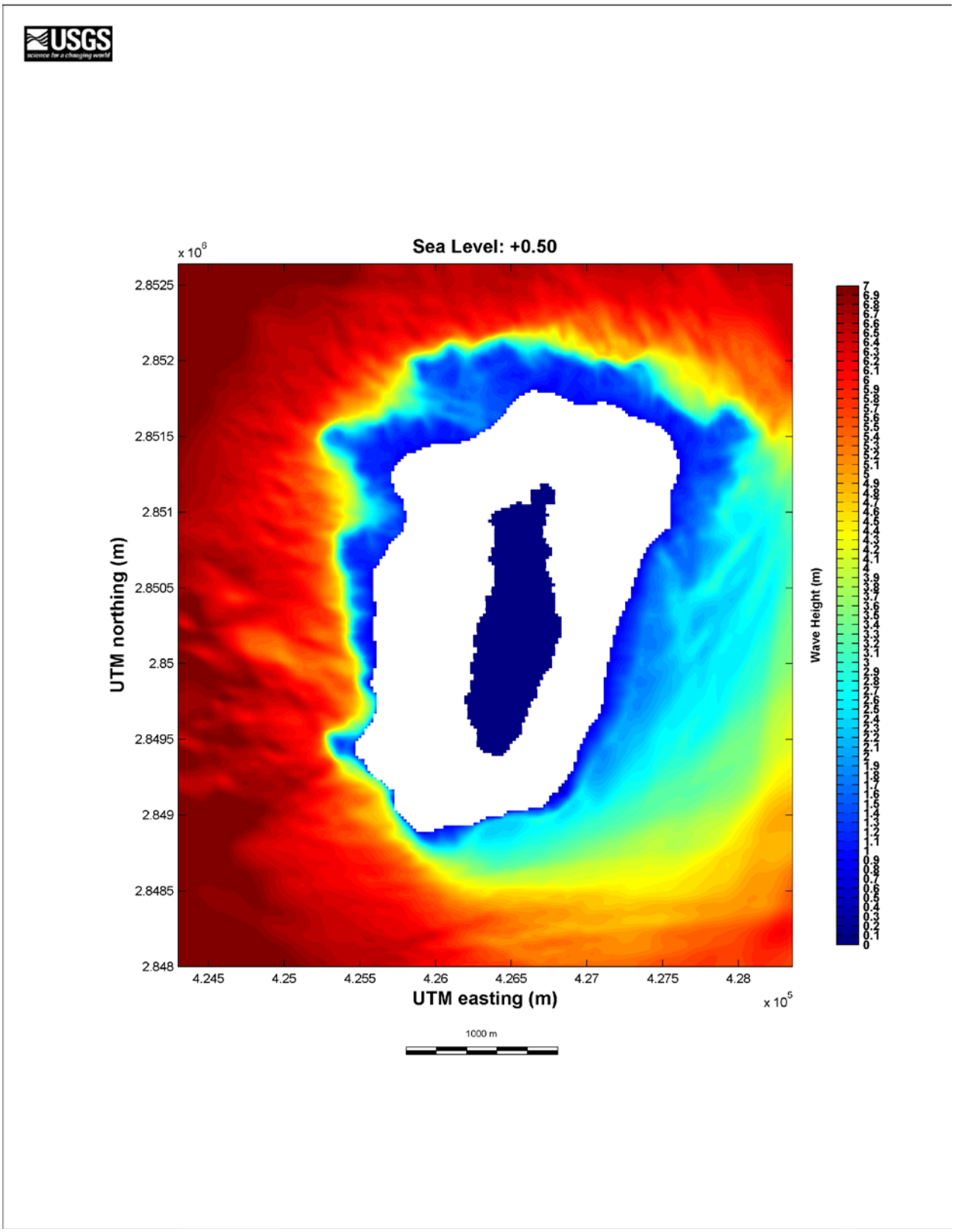

Appendix 1.9. Map of significant wave height, in meters, around Laysan Island for sea level +0.50 m above present during North Pacific winter conditions.

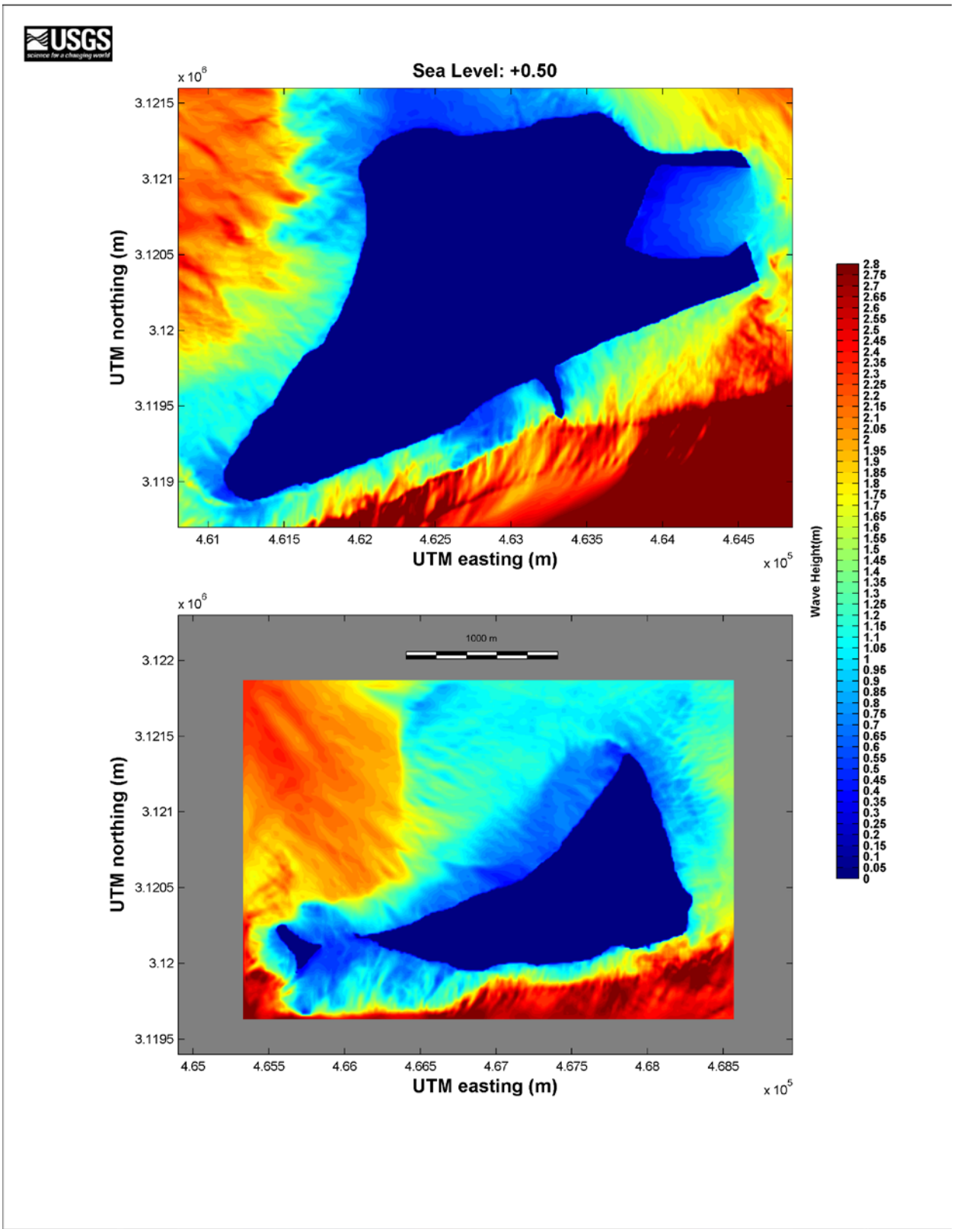

Appendix 1.10. Map of significant wave height, in meters, around Sand Island (top) and Spit and Eastern Islands (bottom) for sea level +0.50 m above present during North Pacific winter conditions.

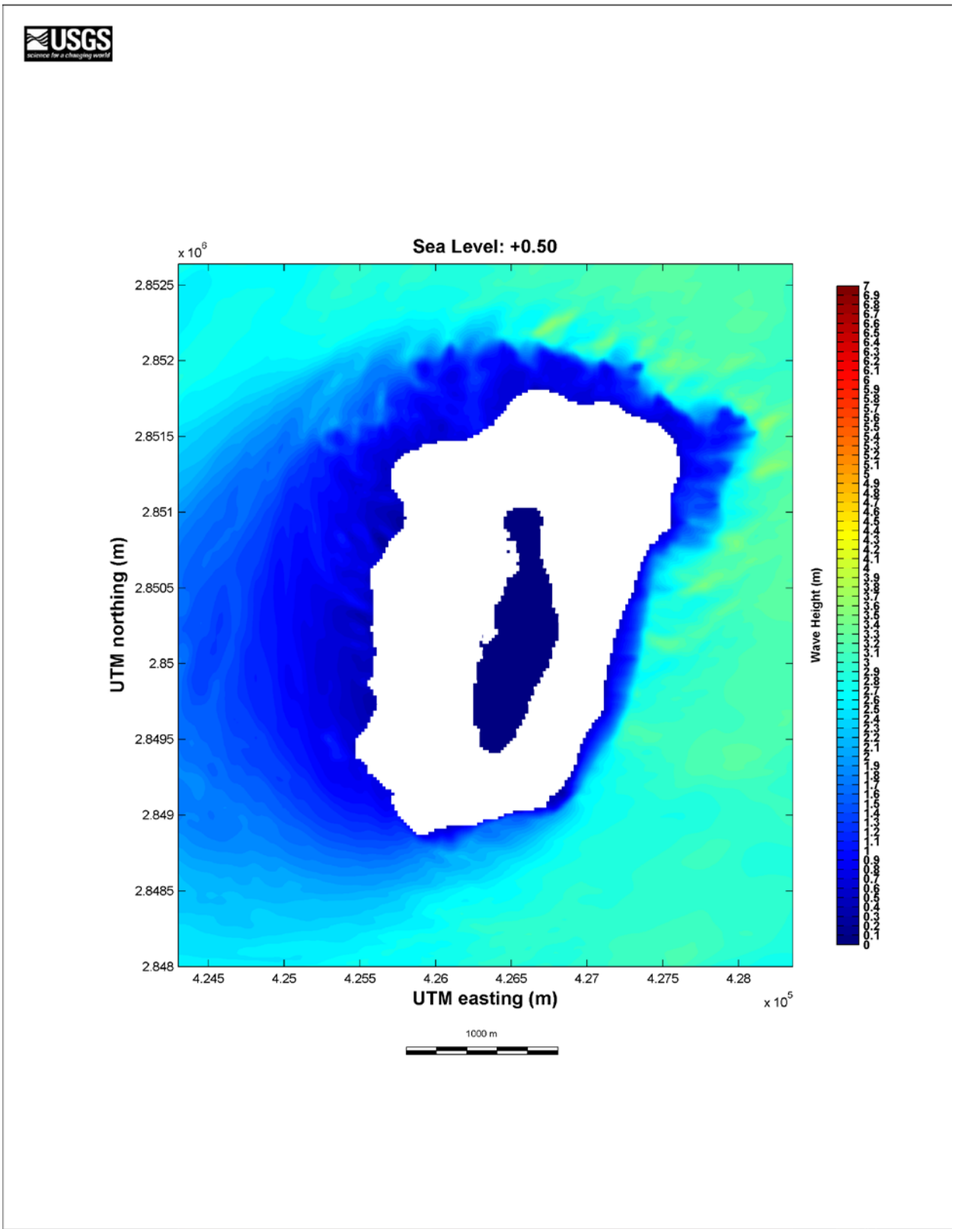

Appendix 1.11. Map of significant wave height, in meters, around Laysan Island sea level +0.50 m above present during summer trade-wind conditions.

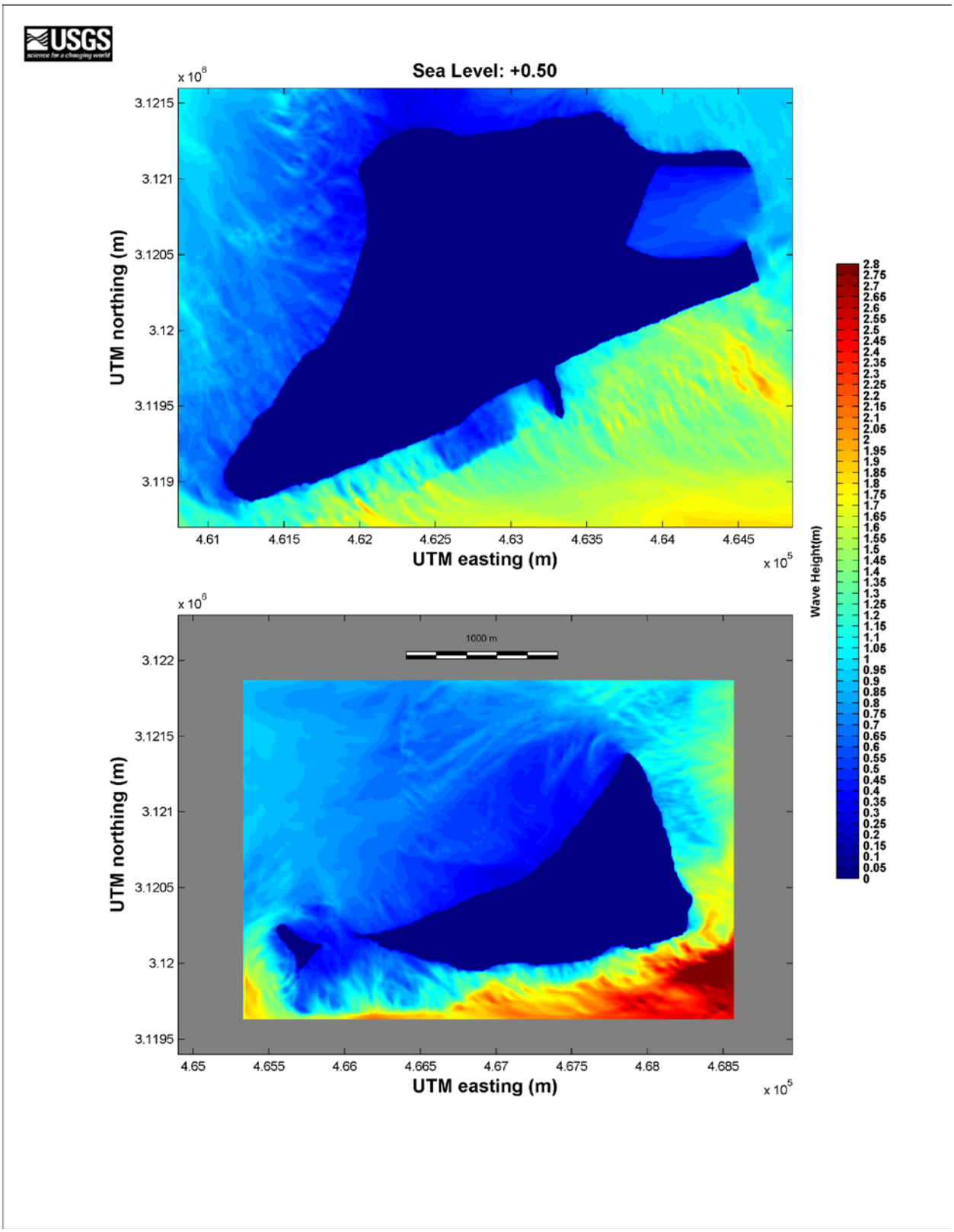

Appendix 1.12. Map of significant wave height, in meters, around Sand Island (top) and Spit and Eastern Islands (bottom) for sea level +0.50 m above present during summer trade-wind conditions.

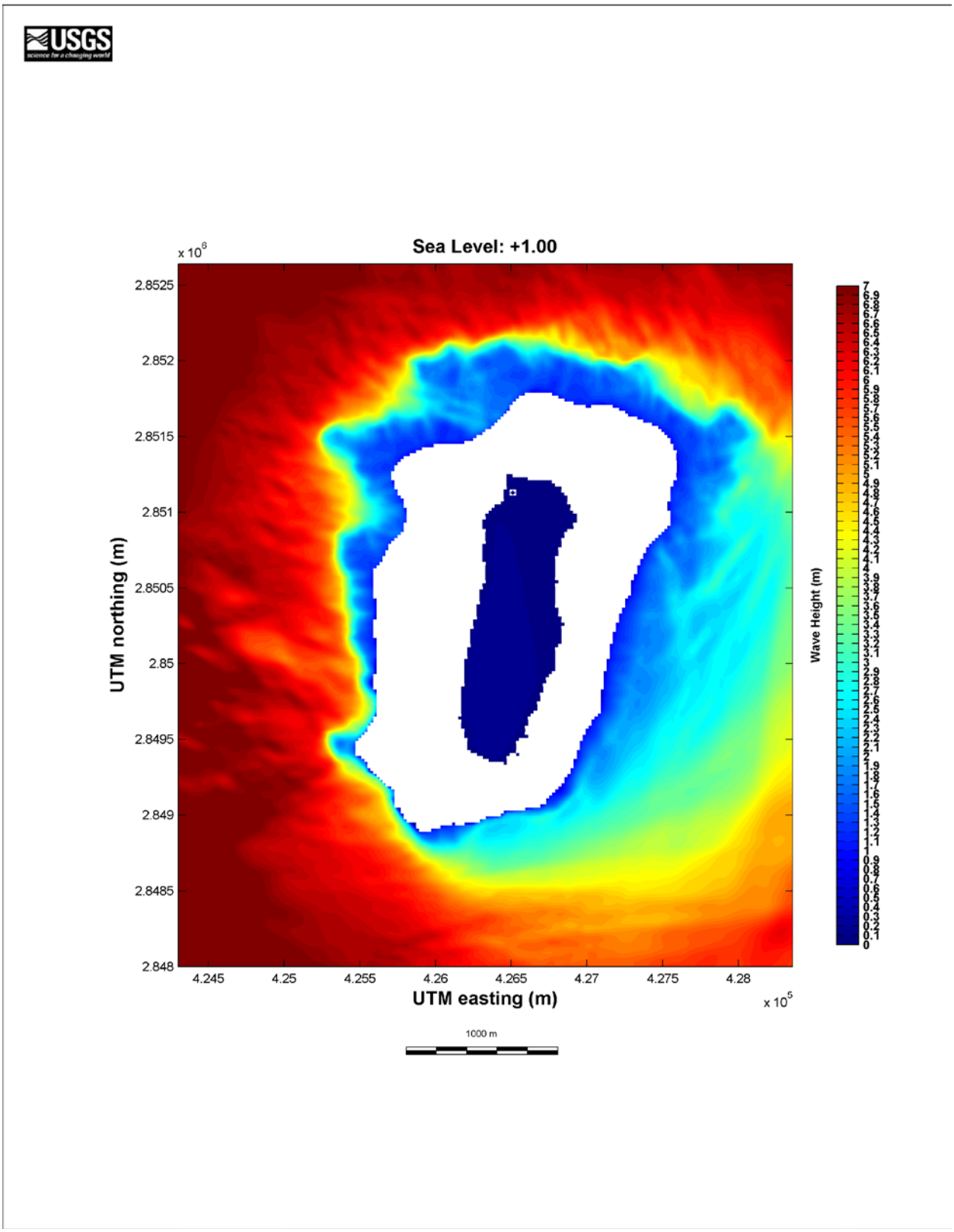

Appendix 1.13. Map of significant wave height, in meters, around Laysan Island for sea level +1.00 m above present during North Pacific winter conditions.

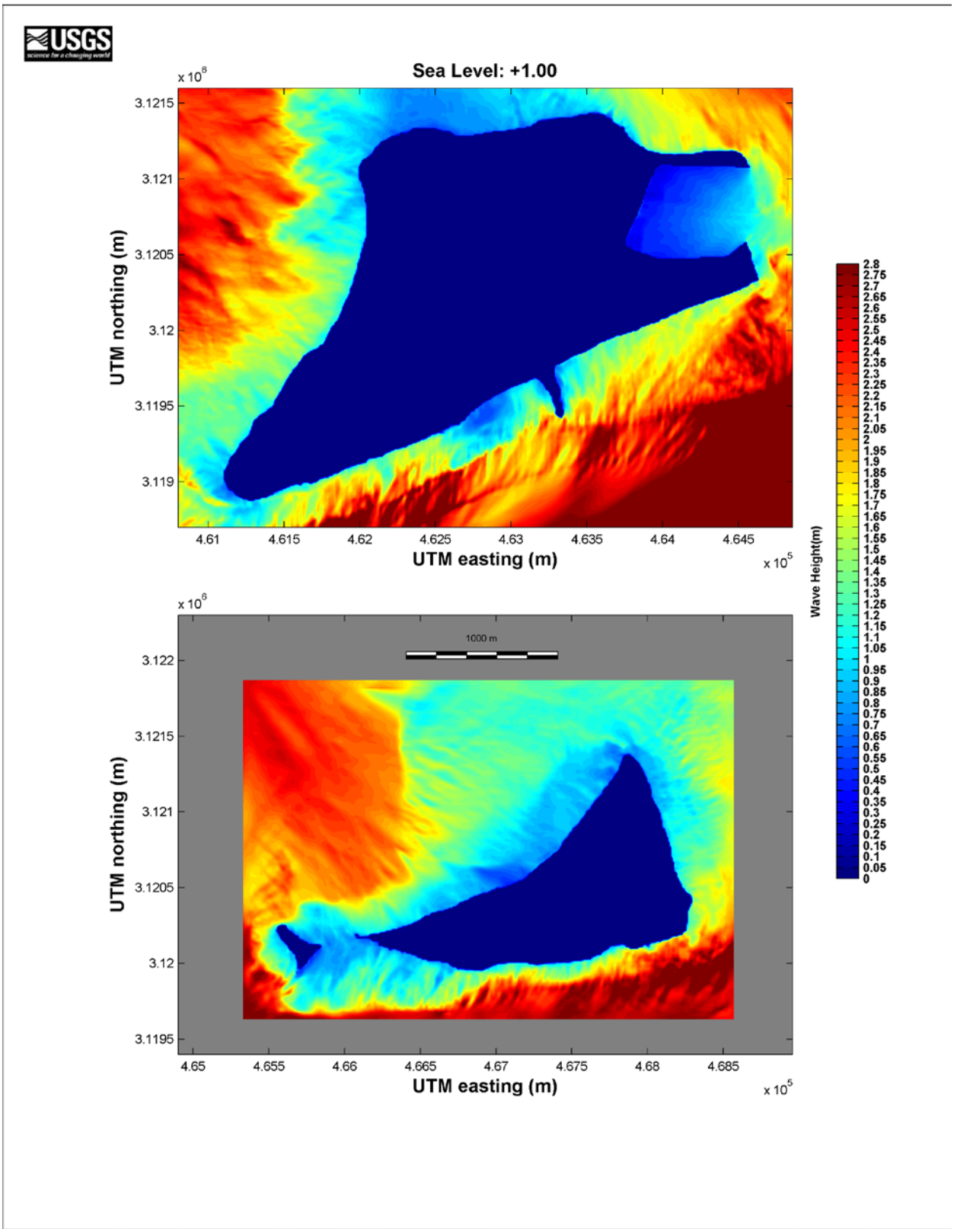

Appendix 1.14. Map of significant wave height, in meters, around Sand Island (top) and Spit and Eastern Islands (bottom) for sea level +1.00 m above present during North Pacific winter conditions.

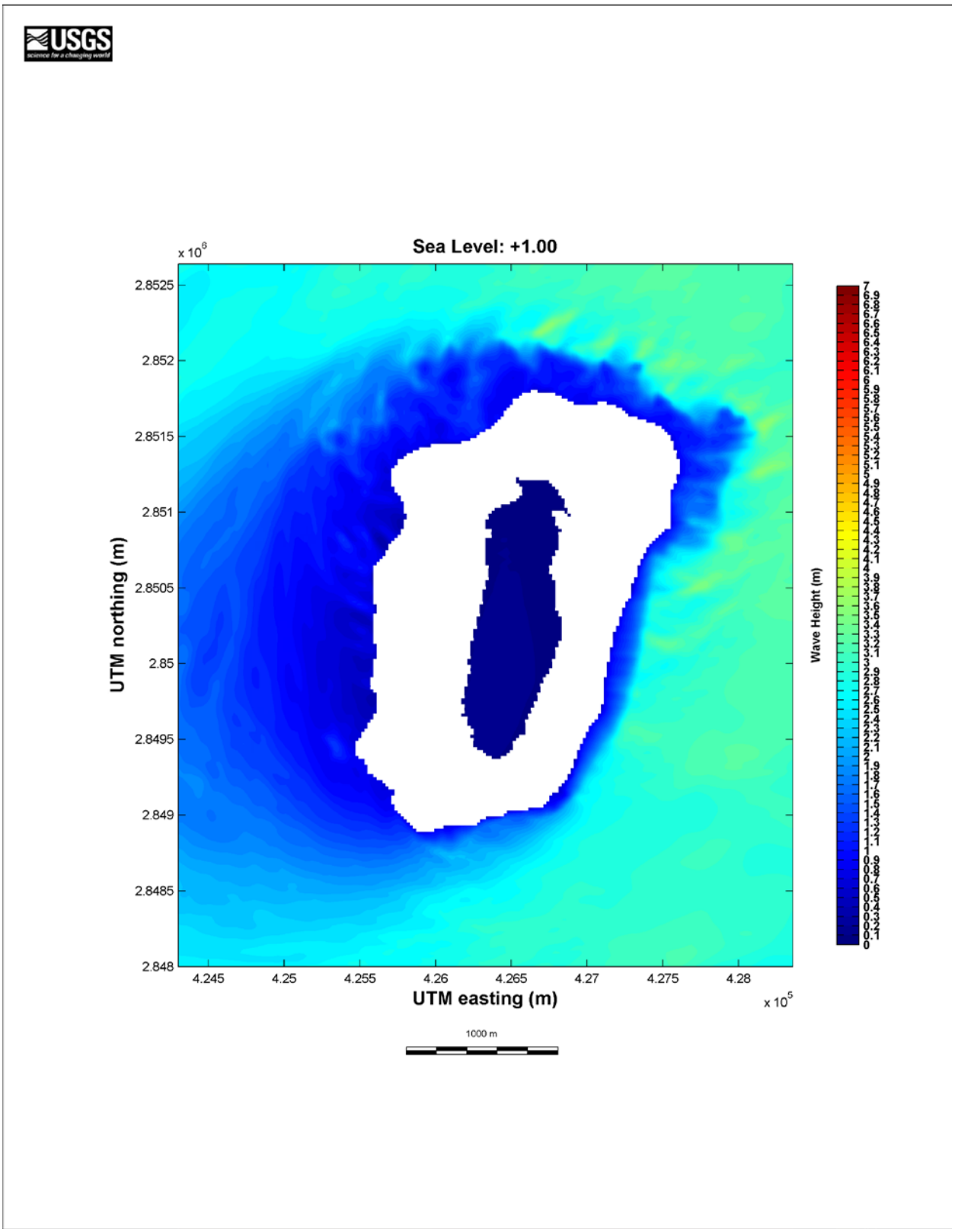

Appendix 1.15. Map of significant wave height, in meters, around Laysan Island sea level +1.00 m above present during summer trade-wind conditions.

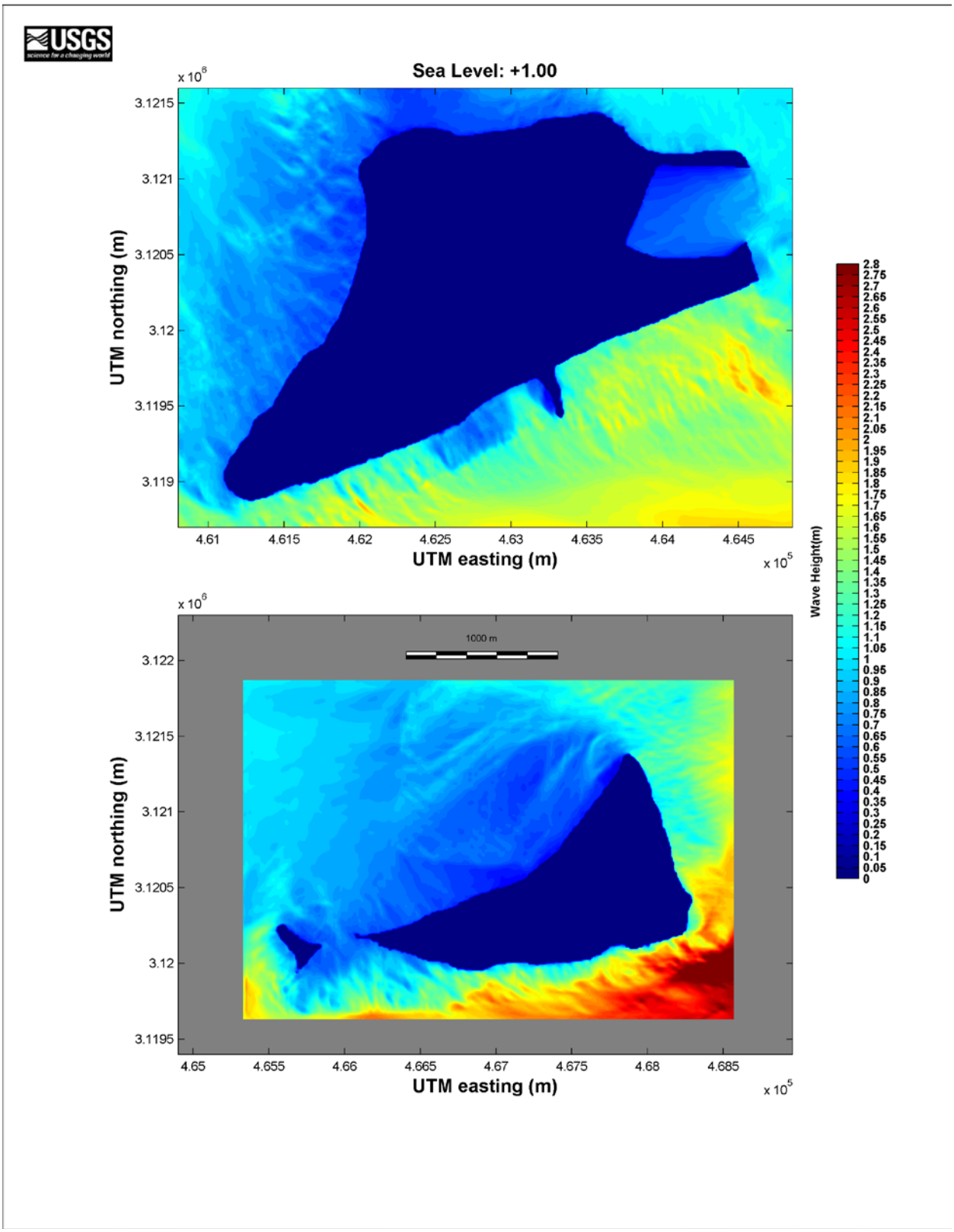

Appendix 1.16. Map of significant wave height, in meters, around Sand Island (top) and Spit and Eastern Islands (bottom) for sea level +1.00 m above present during summer trade-wind conditions.

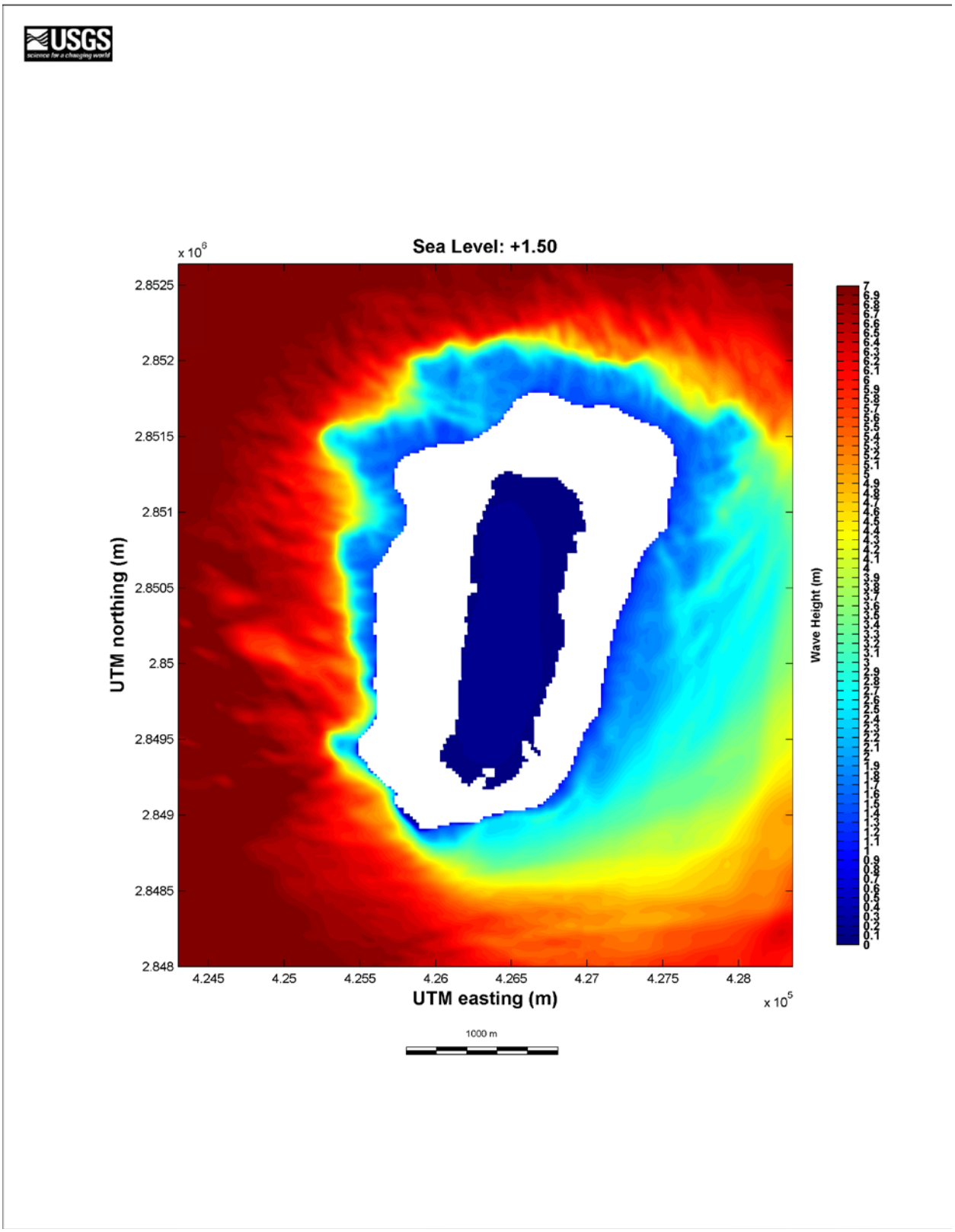

Appendix 1.17. Map of significant wave height, in meters, around Laysan Island for sea level +1.50 m above present during North Pacific winter conditions.

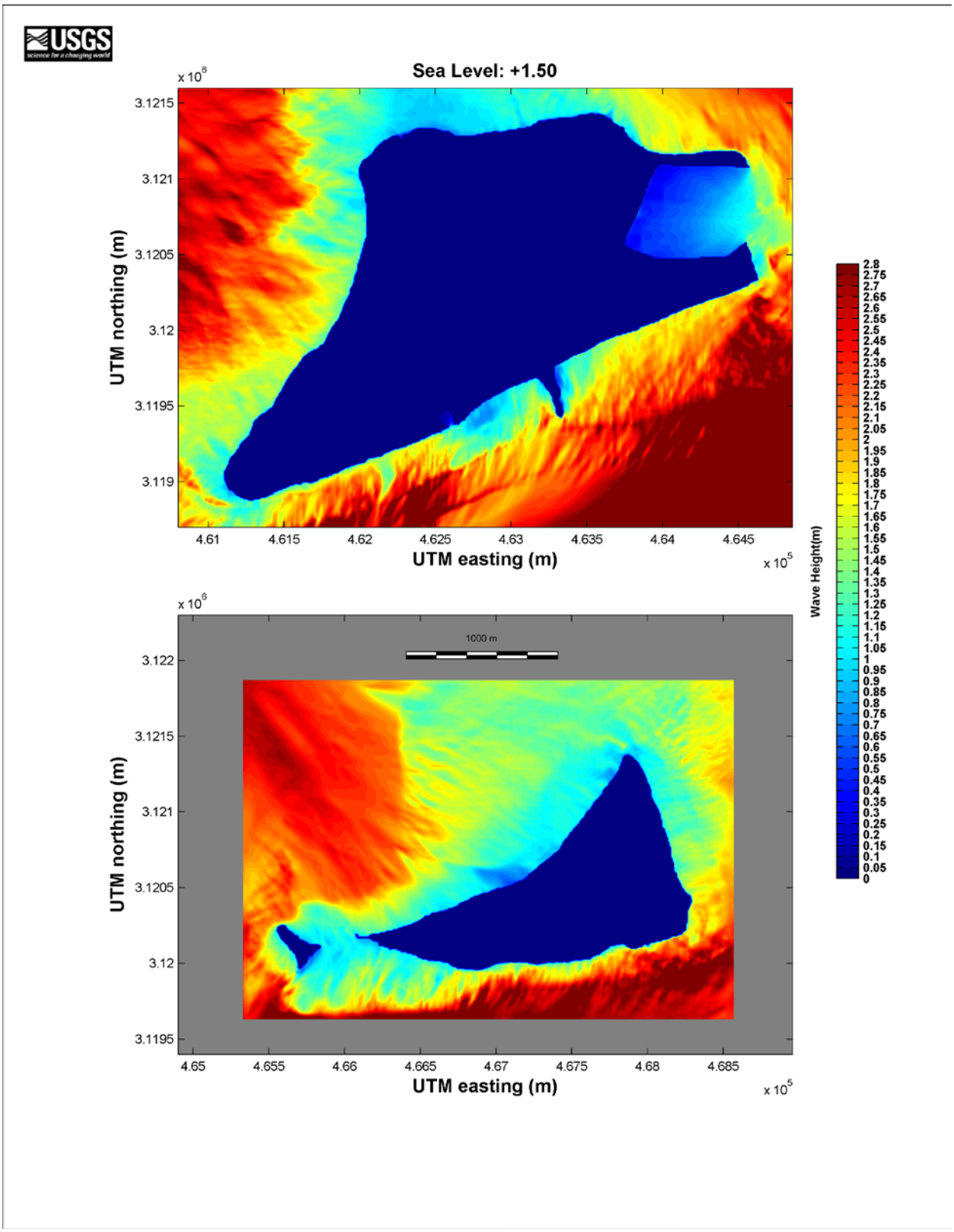

Appendix 1.18. Map of significant wave height, in meters, around Sand Island (top) and Spit and Eastern Islands (bottom) for sea level +1.50 m above present during North Pacific winter conditions.

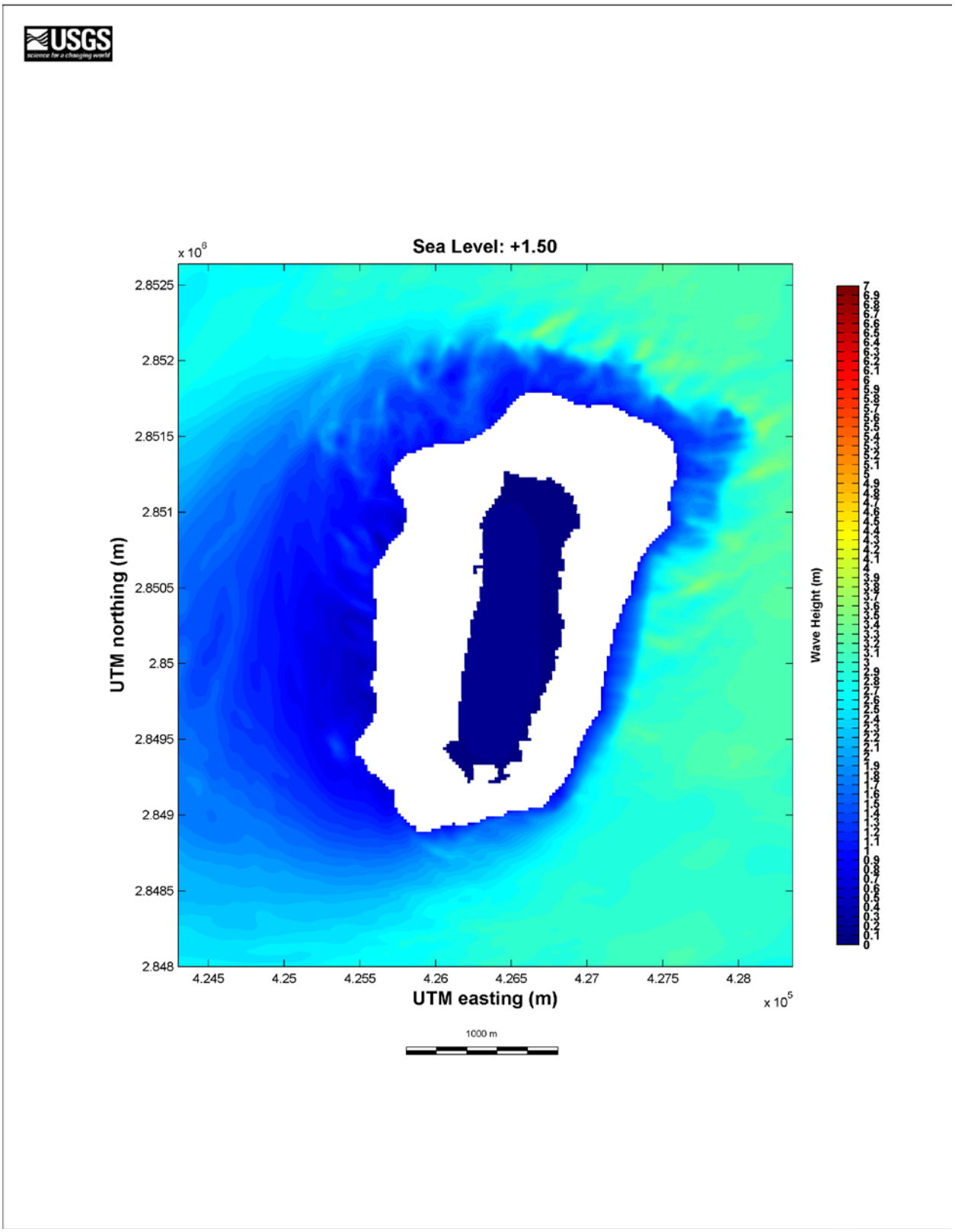

Appendix 1.19. Map of significant wave height, in meters, around Laysan Island sea level +1.50 m above present during summer trade-wind conditions.

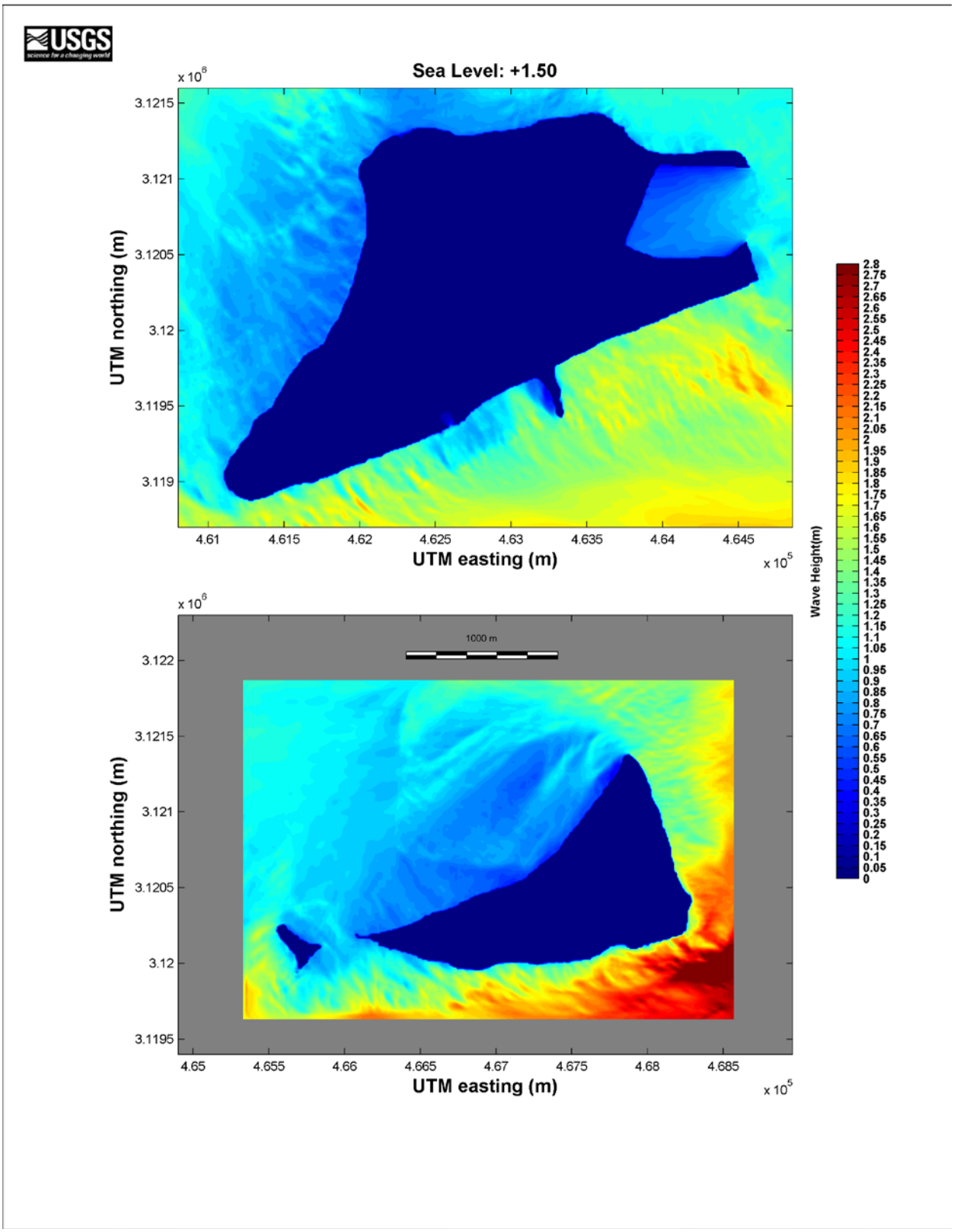

Appendix 1.20. Map of significant wave height, in meters, around Sand Island (top) and Spit and Eastern Islands (bottom) for sea level +1.50 m above present during summer trade-wind conditions.

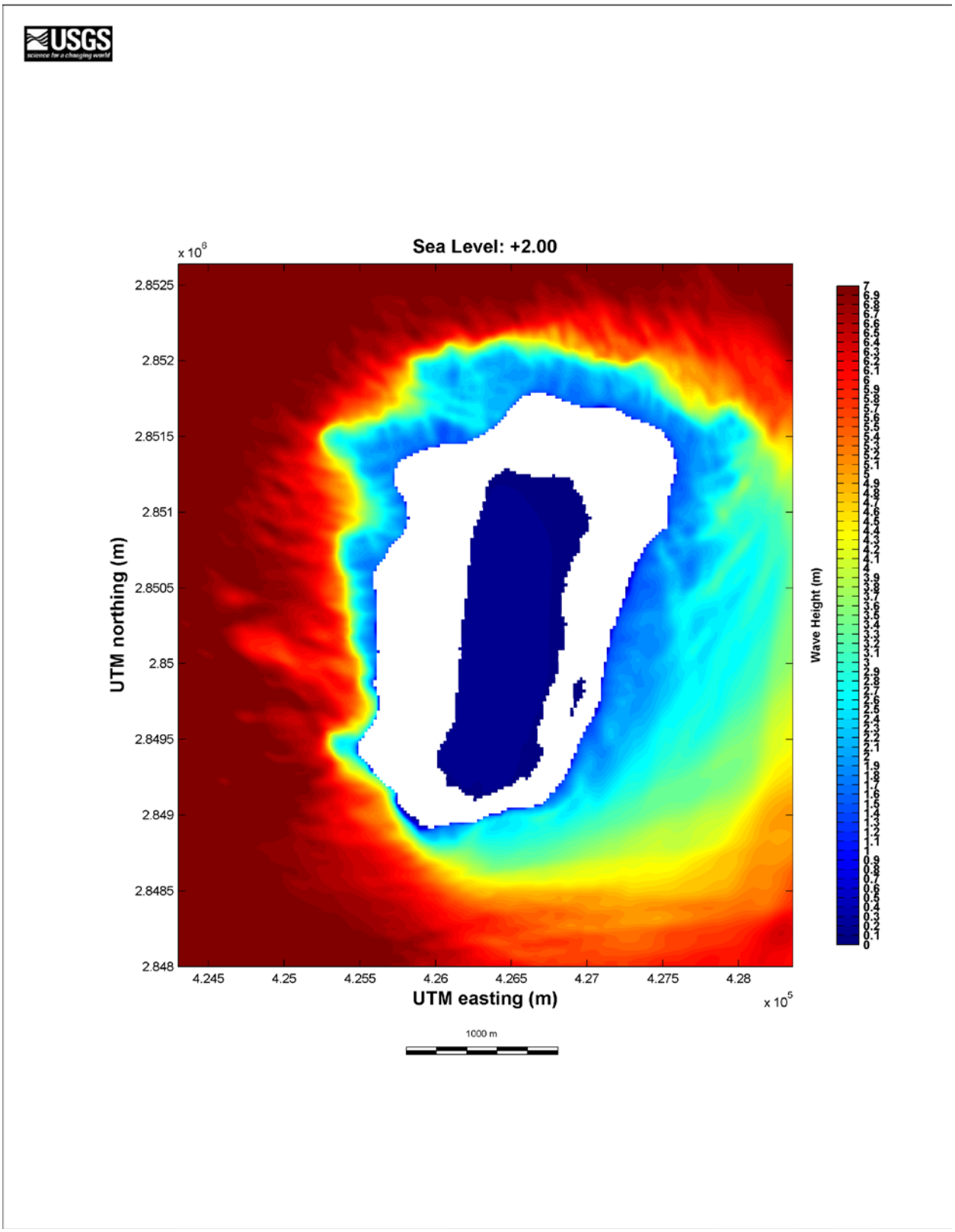

Appendix 1.21. Map of significant wave height, in meters, around Laysan Island for sea level +2.00 m above present during North Pacific winter conditions.

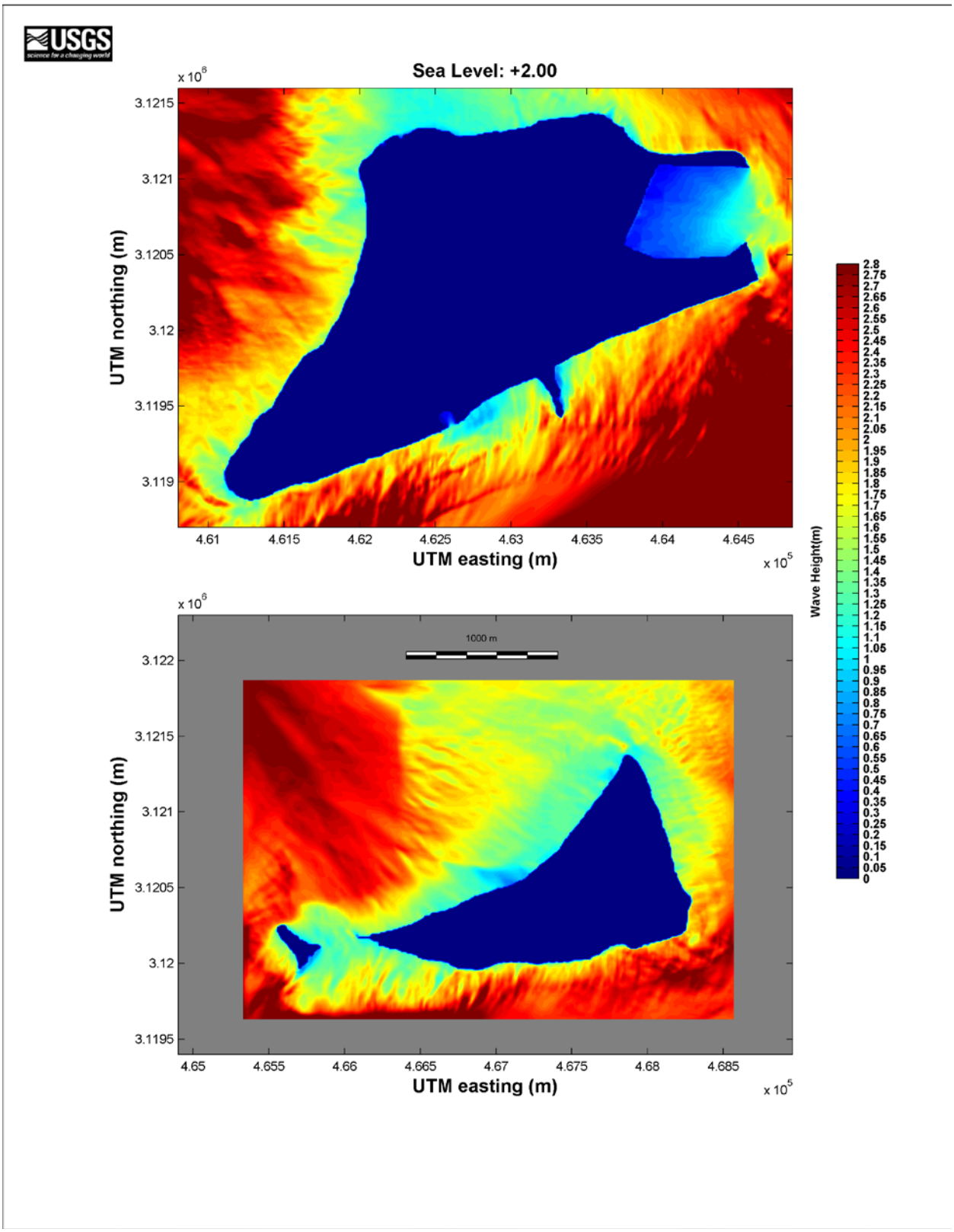

Appendix 1.22. Map of significant wave height, in meters, around Sand Island (top) and Spit and Eastern Islands (bottom) for sea level +2.00 m above present during North Pacific winter conditions.

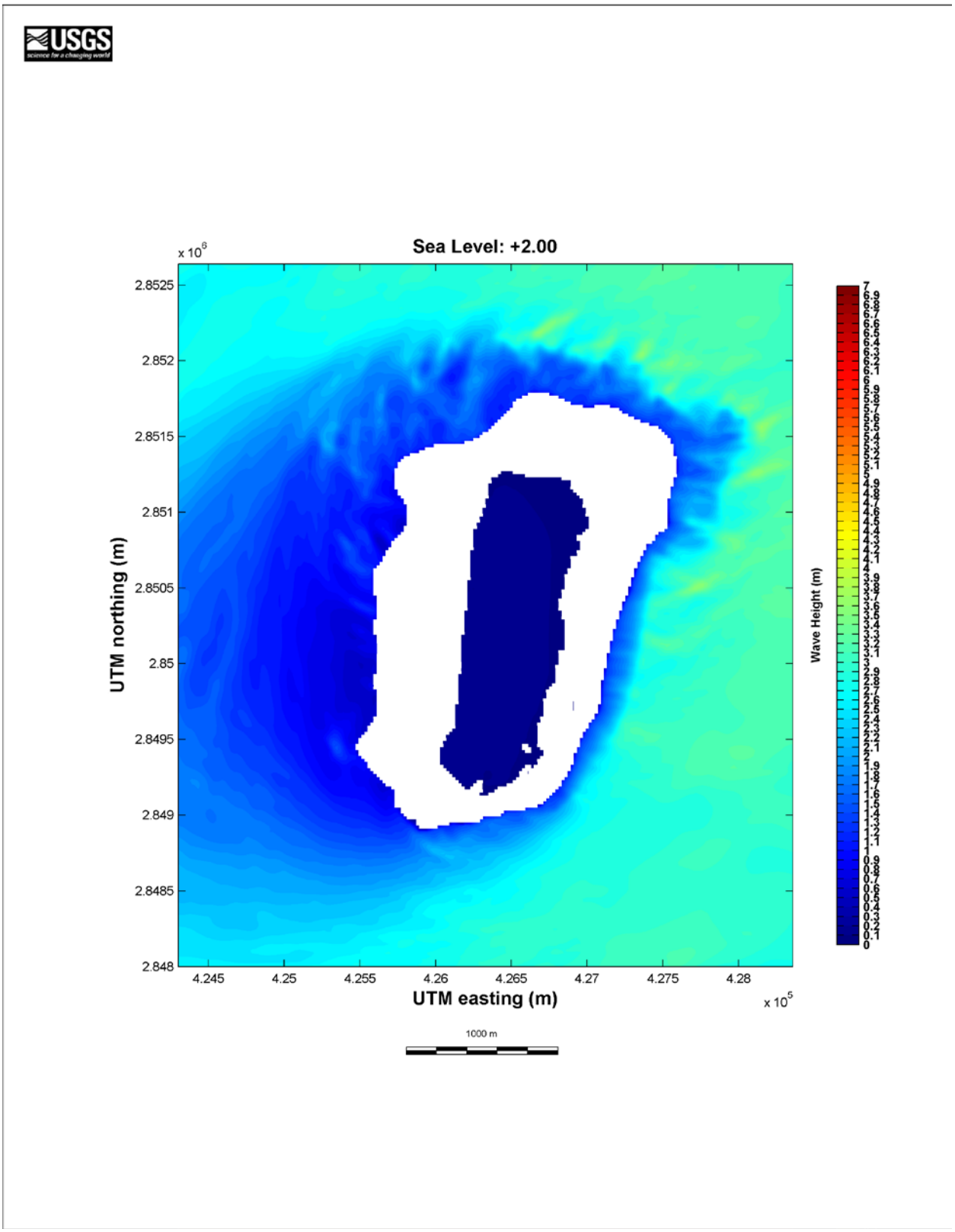

Appendix 1.23. Map of significant wave height, in meters, around Laysan Island sea level +2.00 m above present during summer trade-wind conditions.

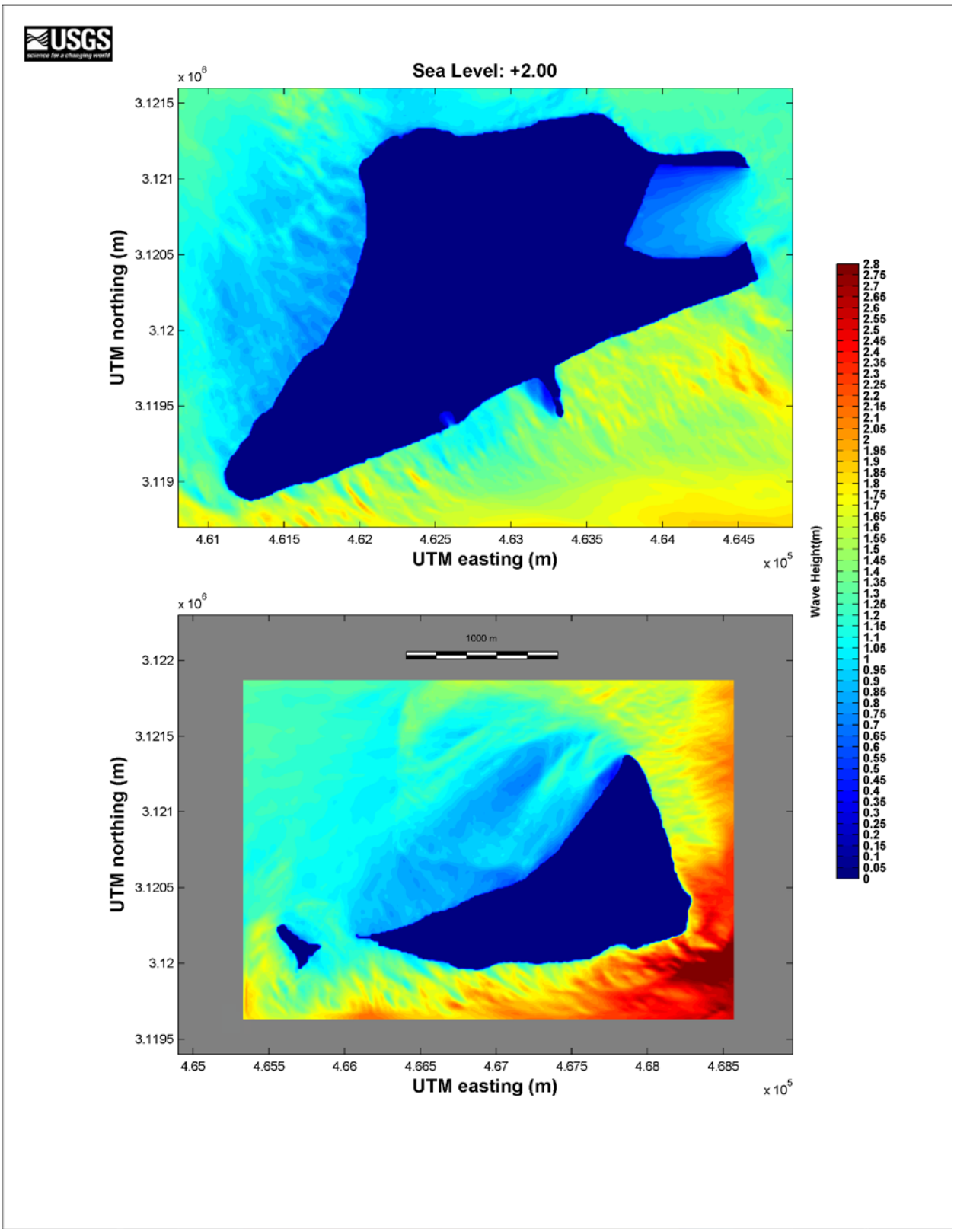

Appendix 1.24. Map of significant wave height, in meters, around Sand Island (top) and Spit and Eastern Islands (bottom) for sea level +2.00 m above present during summer trade-wind conditions.

Appendix 2. Maps of Combined Effects of Wave-Driven Set-up and Run-up around the Atoll Islands.

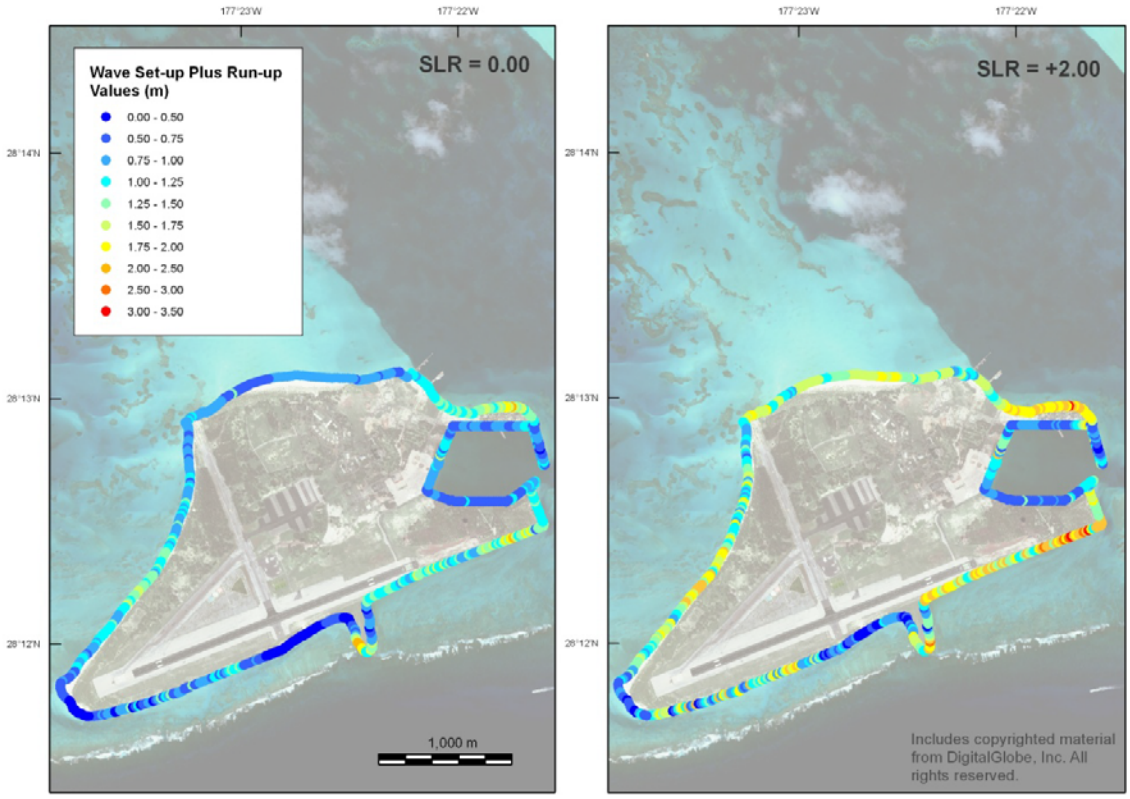

Appendix 2.1. Map of combined effects of wave-driven set-up and run-up around Sand Island at current sea level (+0.00 m) and sea level +2.00 m above present.

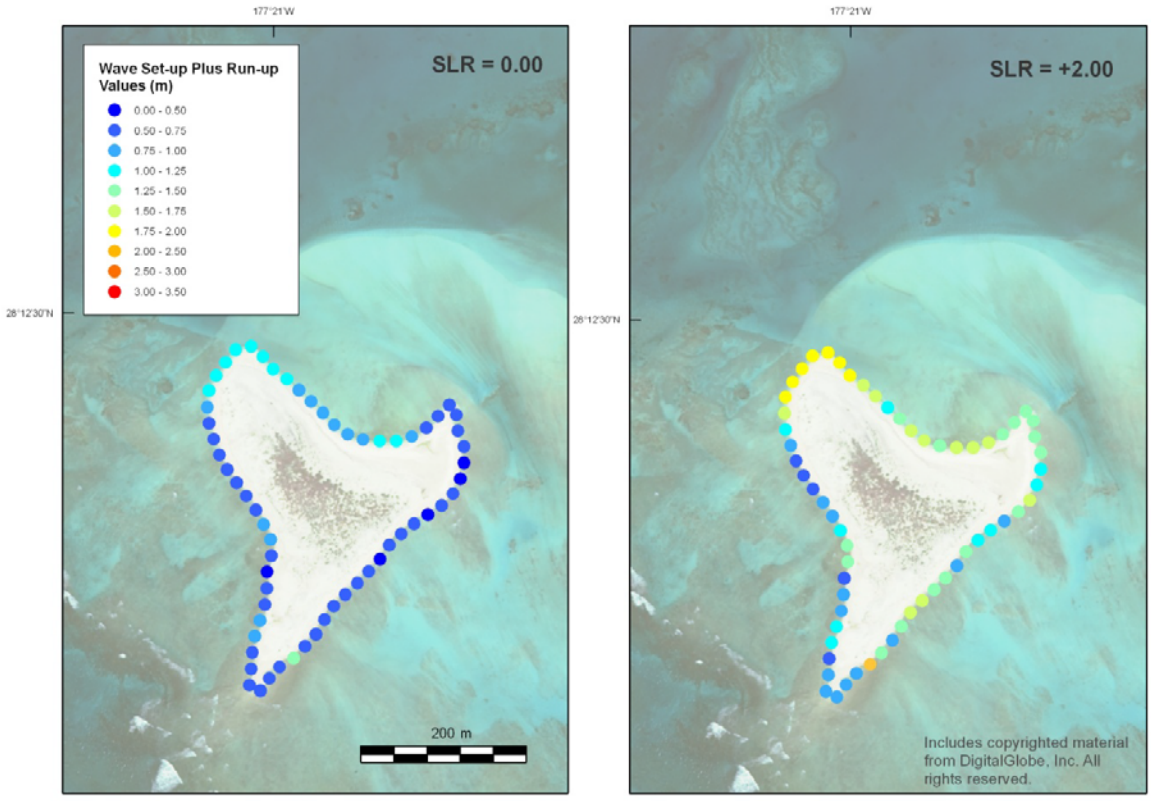

Appendix 2.2. Map of combined effects of wave-driven set-up and run-up around Spit Island at current sea level (+0.00 m) and sea level +2.00 m above present.

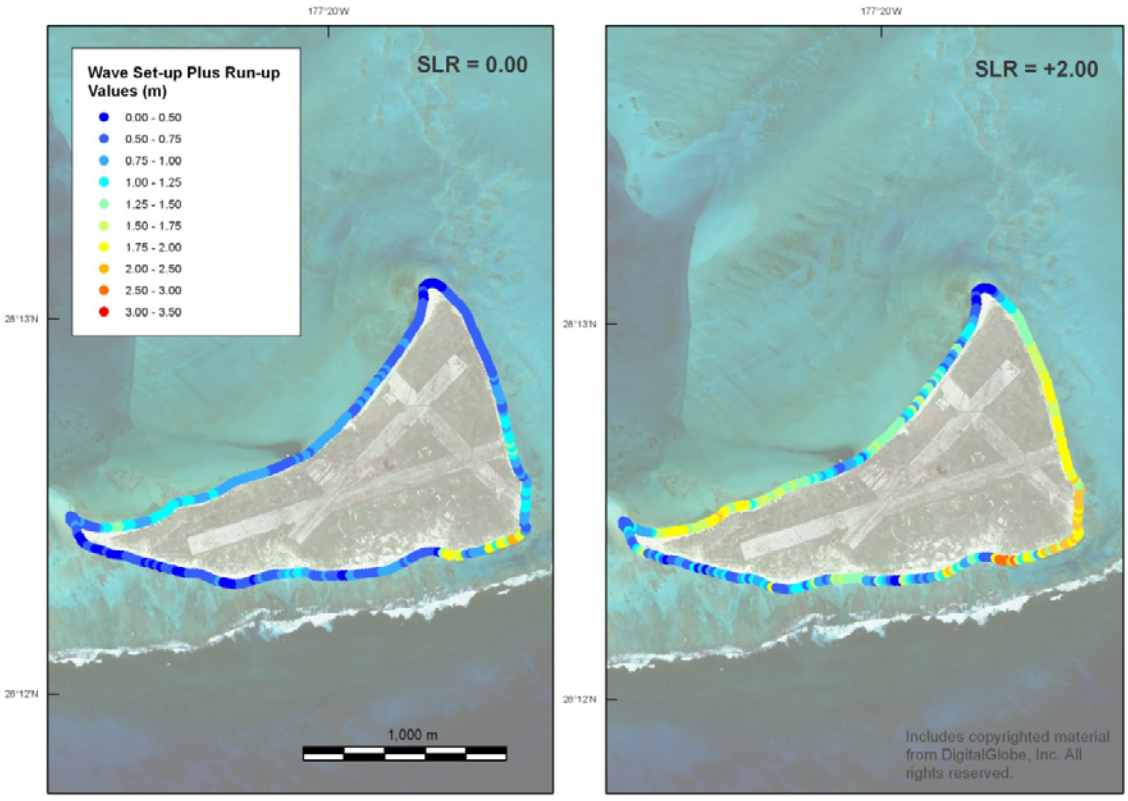

Appendix 2.3. Map of combined effects of wave-driven set-up and run-up around Eastern Island at current sea level (+0.00 m) and sea level +2.00 m above present.

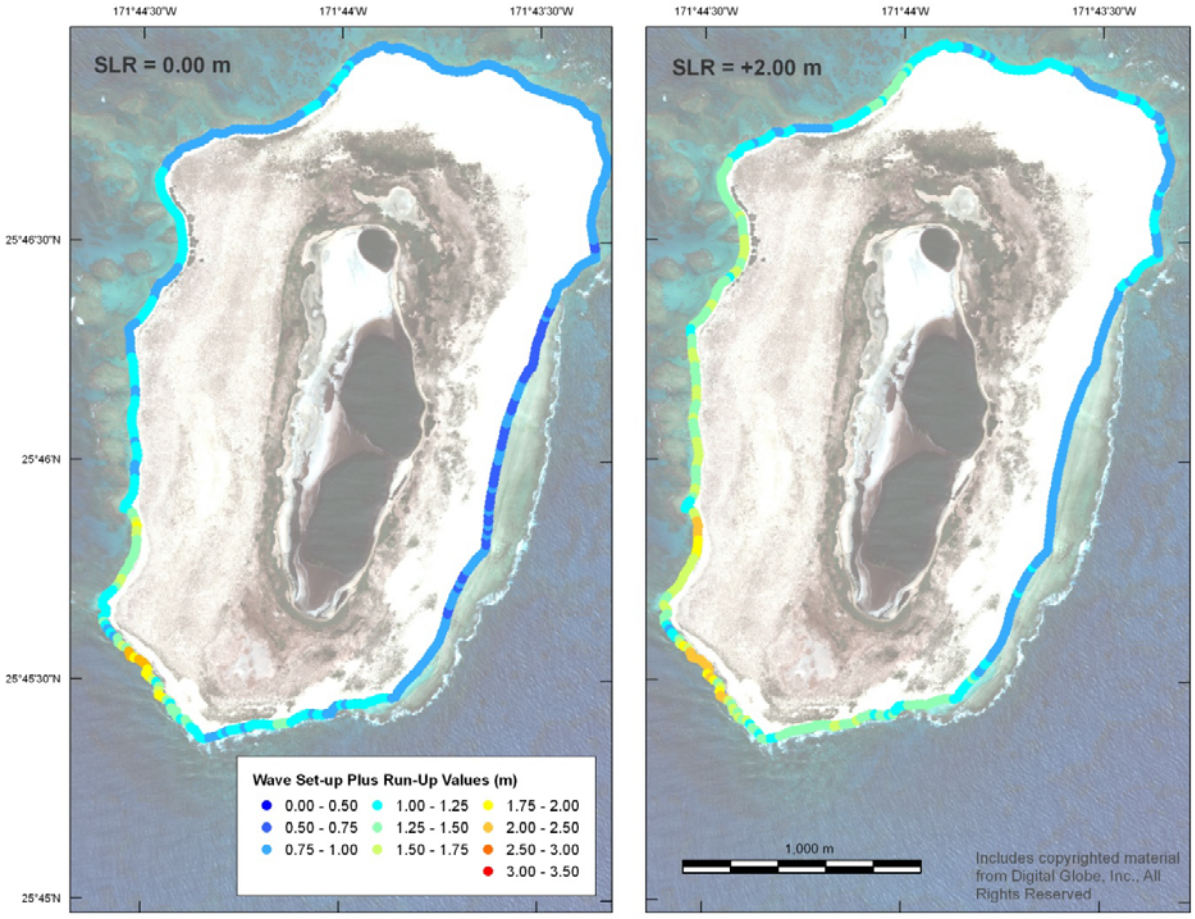

Appendix 2.4. Map of combined effects of wave-driven set-up and run-up around Laysan Island at current sea level (+0.00 m) and sea level +2.00 m above present.

Appendix 3. Maps of Land Cover Classes on the Atoll Islands.

Appendix 3.1. Map of land cover classes on Sand Island. Land cover classes (table 1) can exist on islands but not be visible in the land cover maps when the class covers an area less than 0.1 hectare.

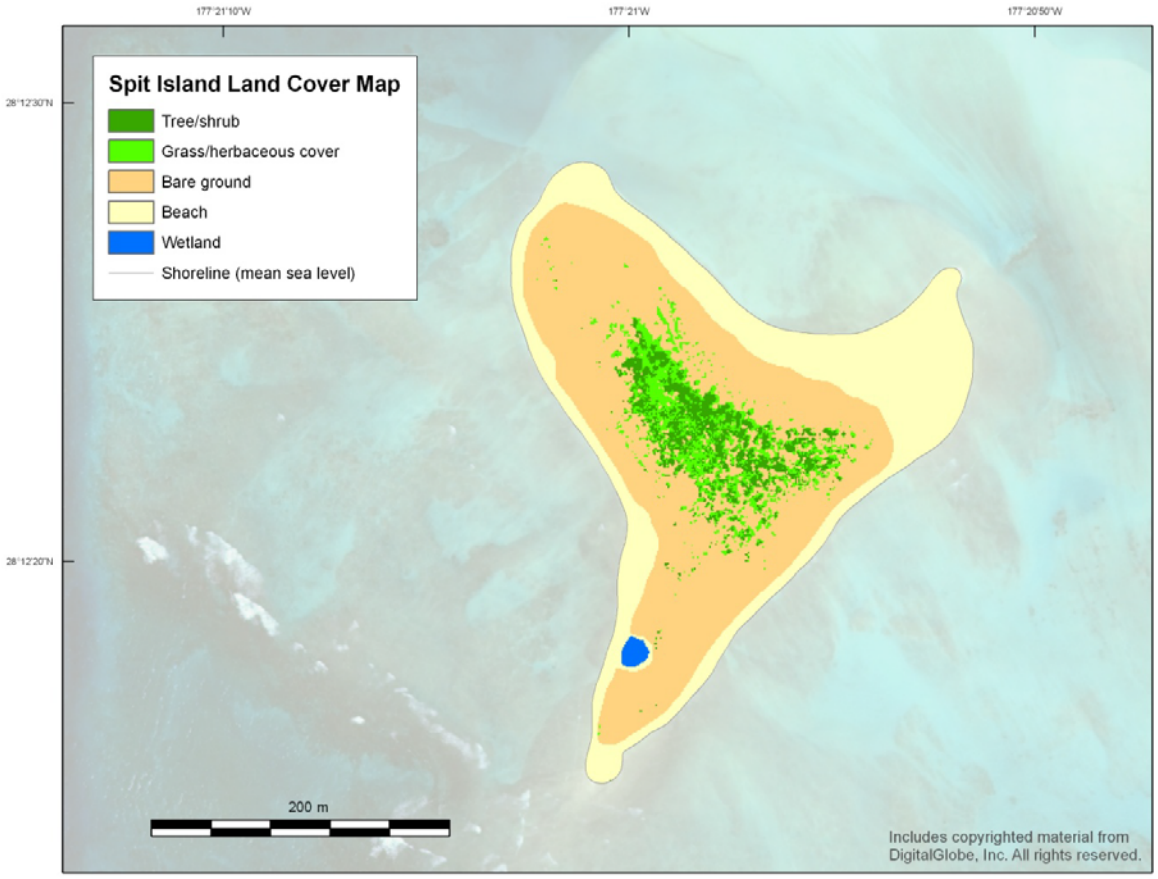

Appendix 3.2. Map of land cover classes on Spit Island. Land cover classes (table 1) can exist on islands but not be visible in the land cover maps when the class covers an area less than 0.1 hectare.

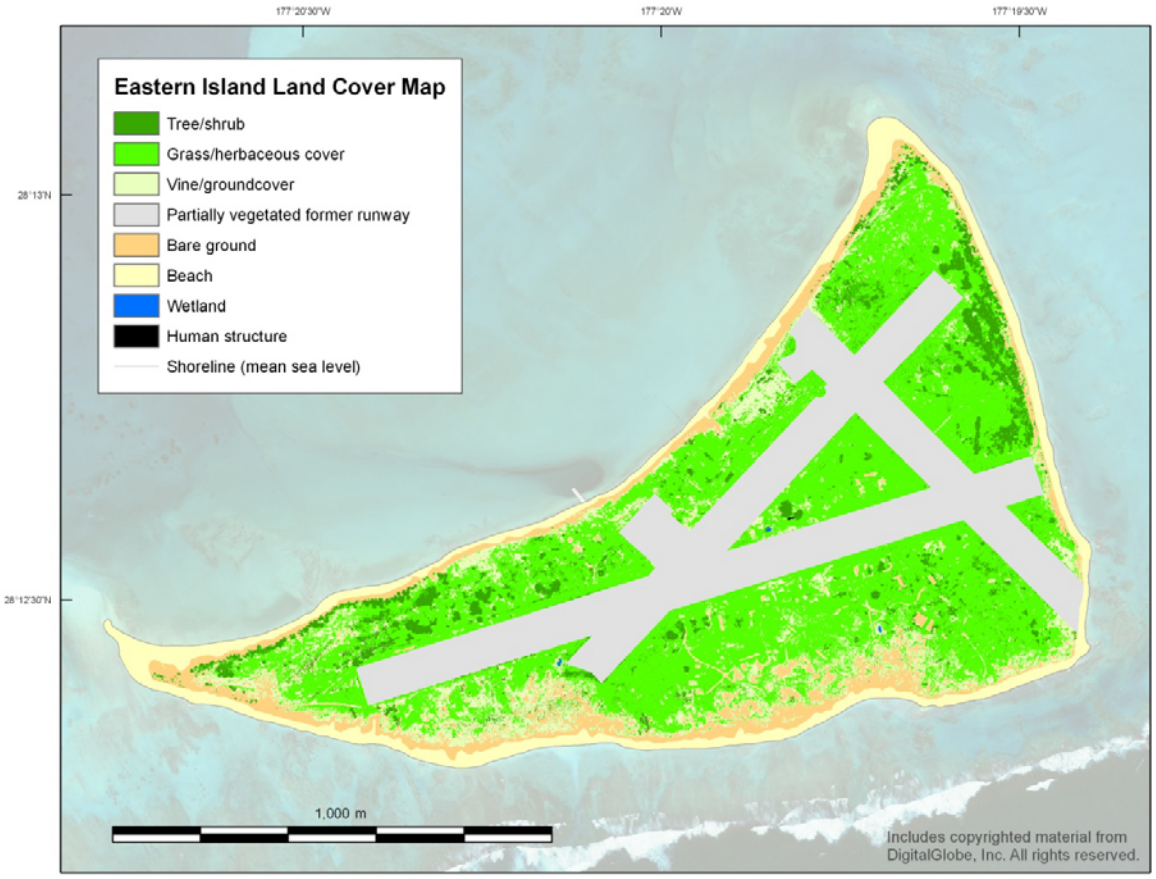

Appendix 3.3. Map of land cover classes on Eastern Island. Land cover classes (table 1) can exist on islands but not be visible in the land cover maps when the class covers an area less than 0.1 hectare.

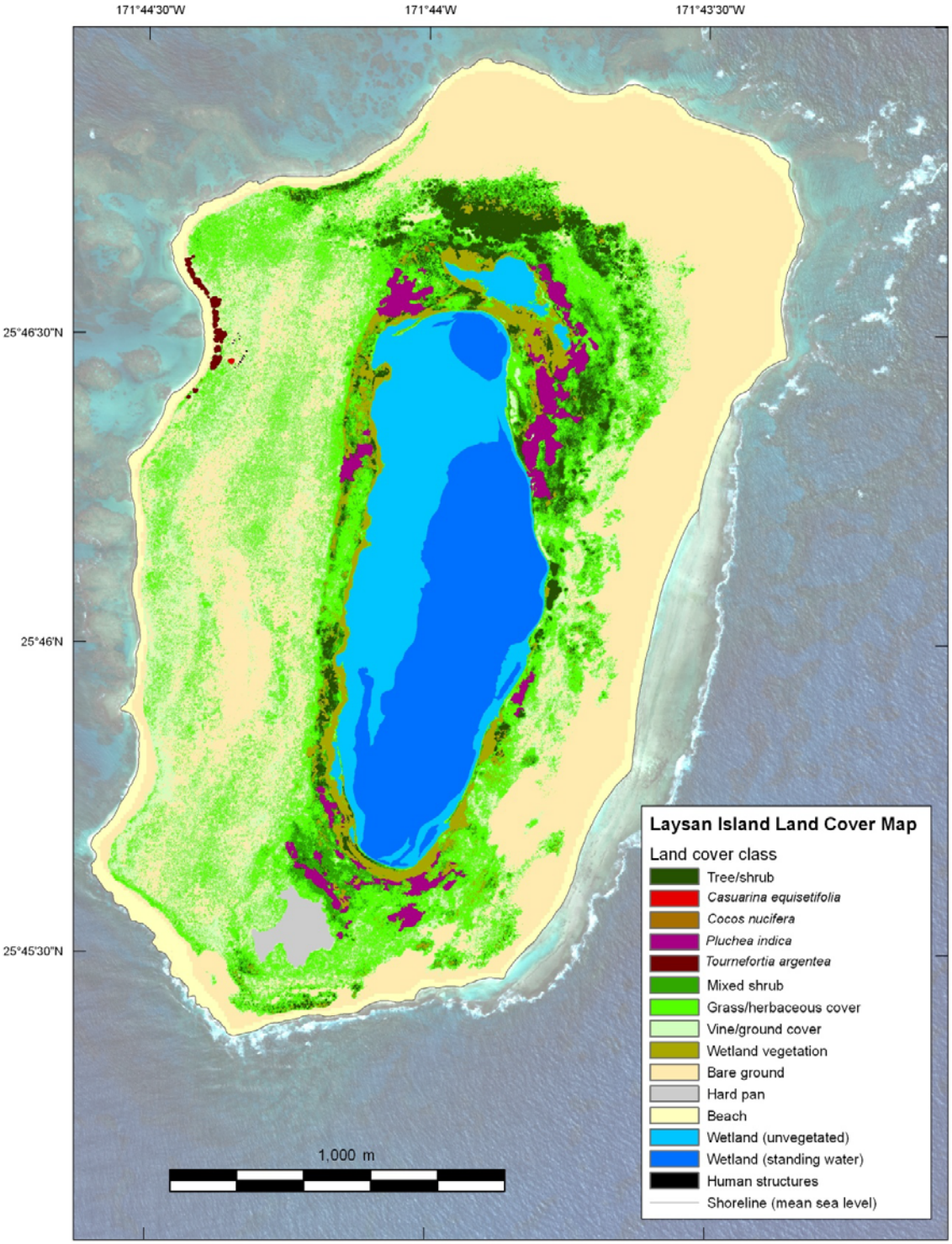

Appendix 3.4. Map of land cover classes on Laysan Island. Land cover classes (table 1) can exist on islands but not be visible in the land cover maps when the class covers an area less than 0.1 hectare.